Behaviour of Shear Critical RC Beams with Corroded Longitudinal Steel Reinforcement

by

Rizwan Azam

A thesis

presented to the University of Waterloo

in fulfillment of the

thesis requirement for the degree of

Master of Applied Science

in

Civil Engineering

Waterloo, Ontario, Canada, 2010

AUTHOR'S DECLARATION

I hereby declare that I am the sole author of this thesis. This is a true copy of the thesis, including any required final revisions, as accepted by my examiners.

I understand that my thesis may be made electronically available to the public.

Abstract

This thesis discusses the results of an experimental program designed to investigate the effect of corrosion on the behaviour of shear critical reinforced concrete (RC) beams. The results of twenty RC beams (ten deep beams and ten slender beams) are described and discussed. The test variables included: corrosion level (2.5%, 5% and 7.5%) and existence of stirrups (beams without stirrups and beams with stirrups). The feasibility of repairing the corroded shear critical RC beams with CFRP laminates was also investigated.

Sixteen specimens were corroded using an accelerated corrosion technique whereas four specimens acted as control un-corroded. Following the corrosion phase, all specimens were tested to failure under three point bending. Test results revealed that the corrosion does not adversely affect the behaviour of shear critical RC beams rather it improves their behaviour. It was found that corrosion changed the failure mode of the corroded beams. The control un-corroded deep beams (beams with and without stirrups) failed in shear-compression failure whereas corroded deep beams (beams with and without stirrups) failed by splitting of the compression strut. The control un-corroded slender beams (beams with and without stirrups) failed in diagonal tension failure whereas the corroded slender beams failed in anchorage failure (beams without stirrups) and flexural failure (beams with stirrups).

The analysis of the results showed that corrosion changed the load transfer mechanism and the change of failure mode was associated with the mechanism. The load transfer mechanism changed from a combination of beam and arch action in the control un-corroded deep beams to pure arch action in the corroded deep beams. The load transfer mechanism changed from pure beam action in the control un-corroded slender beams to pure arch action in the corroded slender beams.

Two strut and tie models are proposed: one for corroded deep beams and one for corroded slender beams. The ultimate loads of the corroded beams were predicted using these struts and tie models and compared with the experimental results. A very good correlation was found between predicted and experimental results.

Acknowledgements

I would like to express my deepest gratitude to my supervisor Dr. K.A. Soudki for his support, encouragement, guidance and valuable advice during my program of study.

I want to express my sincere thanks to Dr. A. El-Sayed, a post doctoral fellow at University of Waterloo, for his guidance and valuable advice at start of my research program.

I would like to thank Civil Engineering Laboratory technicians Richard Morrison, Doug Hirst, Robert Sluban, Ken Bowman and Terry Ridgeway for their help in my experimental work.

I would like to thank my colleagues, office mates and friends: N. Abdel-Wahab, A. Shihata, A. Al-Menoufy, S. Krem, M. Noël, L. Butler, M. Steenhof and A. du Tertre for their support in laboratory work and discussions.

I would like to thank my readers, Dr. J.S. West and Dr. S.L. Tighe for their comments.

Special thanks to my colleague R. Al-Hammoud for her help in the laboratory work.

I would like to acknowledge the financial support received from University of Engineering and Technology Lahore, Pakistan.

Dedication

To My Parents

Table of Contents

List of Figures

List of Tables

Chapter 1: Introduction

1.1 General

Corrosion of reinforcing steel is the most significant deterioration problem faced by reinforced concrete structures. In 2000, the US State Department spent an estimated $5 billion to remediate concrete bridges, which were directly affected by corrosion of reinforcing steel bars (Newman and Chow, 2003). Similar costs are spent in Europe and Canada to maintain their bridge infrastructure in service.

To efficiently rehabilitate corrosion-damaged reinforced concrete structures, the residual strength and failure mechanism of the deteriorated structure must be determined. For this purpose, a number of studies have been reported in the literature. The majority of the studies in the literature focused on flexural and bond strength of corroded beams Al-Sulaimani et al., 1990; Almusallam et al., 1996; Mangat and Elgarf, 1999). Models have been developed by many researchers to determine the residual flexural/bond strength of corroded beams (Wang and Liu, 2006; Bhargava et al., 2007; and Azad et al., 2007). However, there are only a few studies related to the shear strength of corroded beams.

At present, structures are facing corrosion problem after thirty to forty years of their service life. These structures were designed based on codes prevailing three to four decades ago. Recent studies on the size effect on shear strength of concrete members found that the shear strength of the members designed three to four decades ago was overestimated (Sneed, 2007 and Sherwood et al., 2006). There are structures in service without stirrups or with minimum stirrups, having a low margin of safety. For instance, the partial collapse of Viaduc de la Concorde overpass in Laval, Quebec in 2006 highlighted this problem. The collapsed portion of overpass was a thick cantilever slab which was constructed without stirrups and investigation of the failure indicated that the slab experienced the shear failure. Besides, a recent literature survey on the shear strength of members constructed without stirrups indicated that there are structures in service with higher probability of experiencing a shear failure (Collins et al., 2008).

Research is required to study the effect of corrosion of longitudinal reinforcement on behaviour of shear-critical reinforced concrete beams constructed without shear reinforcement or with

minimum shear reinforcement. This study has been designed to address this gap in our knowledge.

1.2 Research Objectives

The main objective of the study is to examine the effect of corrosion of longitudinal steel reinforcement on the shear behaviour of deep and slender reinforced concrete (RC) beams. Specific objectives are:

- Investigate the effect of corrosion on the shear behaviour of (RC) beams constructed without stirrups or with minimum shear reinforcement.
- Investigate the feasibility of FRP repair on corroded shear-critical RC beams.
- Develop a model to predict the ultimate strength of corroded shear critical RC beams.

1.3 Scope of the Work

This research program consists of experimental and analytical phases. The experimental phase comprises of testing twenty shear critical RC beams: ten deep beams and ten slender beams. The beams are divided into four series based on whether the beams are deep or slender and amount of shear reinforcement. Each series includes five beams: one control, three corroded (light (2.5%), medium (5%) and high (7.5%)) and one highly corroded (7.5%) and then repaired. The beams will be tested monotonically under a three-point bending regime.

The analytical work includes the analysis of the control un-corroded beams using the Canadian Reinforced Concrete Code, CSA A23.3-04. Two simple strut and tie models are also proposed to predict the capacity of corroded beams. The results predicted using proposed strut and tie models are compared with the experimental results.

1.4 Organization of Thesis

The thesis is divided into seven chapters as follows:

Chapter-1: This chapter describes the problem statement, objectives of the research program, scope of work and organization of the thesis.

Chapter-2: This chapter presents the background and literature review on shear strength of RC beams corrosion in reinforced concrete and effect of corrosion on reinforced concrete beams.

Chapter-3: This chapter describes the experimental program including the fabrication of test specimens, instrumentation, accelerated corrosion and test setup and procedure.

Chapter-4: This chapter presents the experimental results including accelerated corrosion results and monotonic test results.

Chapter-5: This chapter presents the discussion of experimental results including the effect of corrosion on behavior of shear critical RC beams and the effect of FRP repair on corroded shear critical RC beams.

Chapter-6: This chapter describes the proposed strut and tie model for predicting the shear capacity of RC beams with corroded longitudinal reinforcement along with a comparison of predicted and experimental results.

Chapter-7: This chapter presents the main conclusions from this study and recommendation for future research.

Chapter 2: Background and Literature Review

2.1 Shear Strength of Reinforced Concrete Beams

2.1.1 Mechanism of Shear Transfer

Shear in reinforced concrete beams is transferred by two load transfer mechanisms: beam action and arch action. The extent of the beam action and arch action depends on the shear span to depth ratio (a/d ratio). In general, beam action is the governing load transfer mechanism in slender beams (a/d ratio greater than 2.5) whereas arch action is the dominant load transfer mechanism in deep beams (a/d ratio less than 2.5). The two shear transfer mechanisms can be expressed mathematically as follows.

Consider a free body diagram of the portion of a reinforced concrete beam between two cracks as shown in Figure 2.1. The relationship between the shear force (V) and the tensile force in the bar (T) can be written as:

$$V = \frac{d}{dx}(TJd) \qquad Eq.(2.1)$$

$$\Rightarrow V = \frac{d(T)}{dx} + \frac{d(Jd)}{dx} \qquad Eq.(2.2)$$

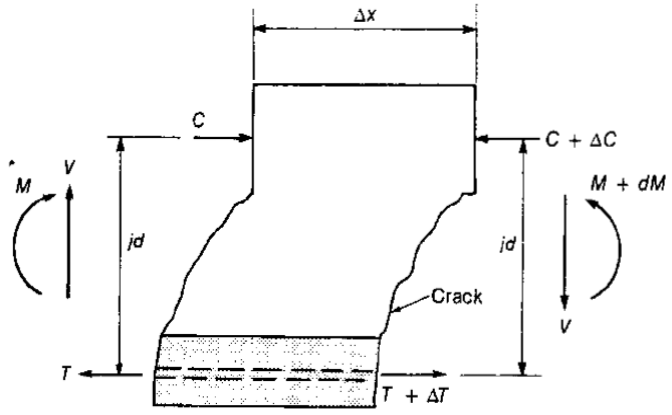

Figure 2.1 Free body diagram of beam between two cracks (MacGregor, 1997)

If the lever arm(Jd) remains constant as assumed in elastic beam theory, the shear force is transferred in beam action (V_b) as follows:

$$\frac{d(Jd)}{dx} = 0 \quad and \quad V = V_b = \frac{d(T)}{dx}$$

Where $V = \frac{d(T)}{dx}$ is the shear flow across any horizontal plane between the reinforcement and the compression zone. For beam action to exist shear flow must be present.

On the other hand if the shear flow, $\frac{d(T)}{dx}$, equals zero, then the shear force is transferred to arch action(V_a) as follows:

$$V = V_a = \frac{d(Jd)}{dx}$$

This happens when the reinforcing steel is unbonded and the shear flow cannot be transmitted, or when an inclined crack extend from the load point to the support preventing the transfer of shear flow. In such cases, shear is transferred by arch action instead of beam action (MacGregor, 1997).

2.1.2 Shear Strength Models

Several shear prediction models have been proposed since Ritter's original model in 1899 (Ritter, 1899). The majority of the theories and models developed over the course of the last century either satisfies equilibrium conditions or satisfies both equilibrium and compatibility conditions. The models satisfying only equilibrium conditions include; the 45˚ truss model, variable angle truss model, modified truss model and strut and tie model. The models satisfying both equilibrium and compatibility conditions include; compression field theory, modified compression field theory, rotating angle softened truss model and fixed angle softened truss model (El-Sayed, 2006).

The shear prediction models for deep and slender beams found in the North American codes are; strut and tie model (adopted by both American Concrete Institute, ACI 318M-08, and Canadian Standard Association, CSA A23.3-04, for deep beams) and modified compression field theory (adopted by CSA-A23.3-04 for slender beams) and the 45˚ truss model (adopted by ACI 318M-08 for slender beams with additional term for the concrete contribution). In the following sections, the strut and tie model and the modified compression field theory are presented in more detail as these methods are adopted in CSA A23.3-04.

2.1.2.1 Strut and Tie Model

The strut and tie model consists of three components; concrete compressive struts, reinforcing bar as tension ties and joints or nodal zones. A strut and tie model of a deep beam is shown in Figure 2.2.

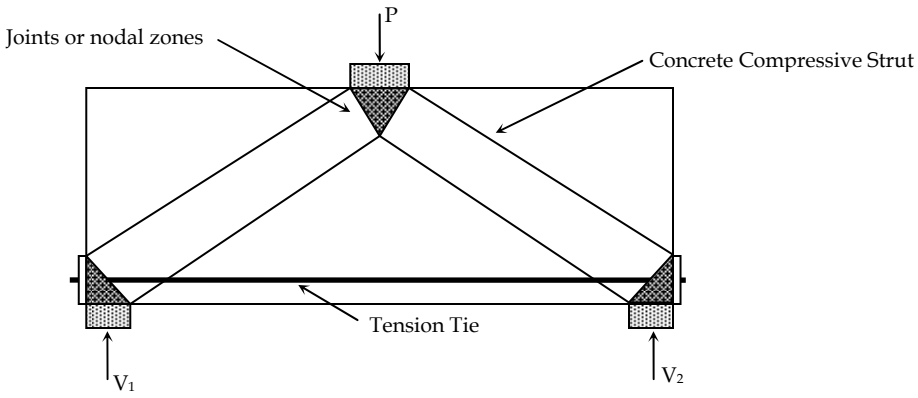

Figure 2.2: Strut and tie model of a deep beam

In the strut and tie model, the flow of internal forces is represented by a truss formed by concrete compressive struts and tension ties interconnected by nodal zones. The magnitude of the forces in the truss members is determined by satisfying the equilibrium conditions. Once the forces in the truss members are determined, the reinforcement is provided to resist the tension force in the tension tie and the compressive stress in the strut and nodal zones is limited to ensure the yielding of the tension tie. Special consideration is also given to properly anchor the reinforcement in the nodal zone. (Adebar and Zhou, 1993)

Strut and tie models are mainly used for deep beams, corbel, joists and members dominated by arch action. Stress limits on struts and nodal zones that need to be checked while proportioning the struts and ties, as required by CSA A23.3-04, are given in Table 2.1.

Table 2.1: Stress limits in strut and tie model (CSA A23.3-04)

Stress Limits in Concrete Strut	Stress Limits in Nodal Zone
$f_{cu} = \frac{f_c'}{0.80 + 170\epsilon_1} \leq 0.85 f_c'$ Where $\epsilon_1 = \epsilon_s + (\epsilon_s + 0.002)cot^2\theta_s$ f_{cu}= Limiting compressive stress in concrete Strut f_c'= Specified compressive strength of concrete ϵ_1= Principle tensile strain in cracked concrete ϵ_s= tensile strain in tension tie. θ_s = Smallest angle between strut and adjoining tie.	a) $0.85\varphi_c f_c'$ in node regions bounded by struts and bearing areas. b) $0.75\varphi_c f_c'$ in node regions anchoring a tie in only one direction. b) $0.65\varphi_c f_c'$ in node regions anchoring a ties in more than one direction. Where φ_c=resistance factor for concrete.

2.1.2.2 Modified Compression Field Theory

Modified compression field theory is a further development of compression field theory. Compression field theory is based on compatibility of displacements, equilibrium of forces and constitutive relationships of the concrete and steel reinforcement. In the compression field theory, cracked concrete is idealized as a series of compressive struts bounded by cracks and the concrete in between the cracks is assumed to behave as an orthotropic material with no tensile strength. The compression field theory has some weakness that it does not include the concrete shear contribution. This is overcome by the modified compression field theory which accounts for the tensile stresses in the concrete between cracks and the concrete shear contribution is assumed to be carried by these tensile stresses in the concrete.

The modified compression field theory is only applicable to slender beams as it based on sectional analysis and arch action is neglected in this theory.

The Canadian Standard Association, CSA A-23.3-04, uses modified compression field theory (MCFT) for shear design of reinforced concrete beams. The shear resistance of a reinforced concrete beam using CSA A23.3-04 is determined as follows:

$$V_r = V_c + V_s \qquad Eq.(2.3)$$

$$V_c = \phi_c \lambda \beta \sqrt{f_c'} b_w d_v \qquad Eq.(2.4)$$

$$V_s = \frac{\phi_s A_v f_y d_v \cot\theta}{s} \qquad Eq.(2.5)$$

Where, V_c is the concrete shear contribution; ϕ_c is the resistance factor for concrete; λ is the concrete density factor, f_c' is the specified concrete compressive strength, b_w is the beam web width and d_v is the moment arm between the compression and the tension in beam (d_v is taken greater of 0.72h or 0.9d). V_s is the steel stirrups shear contribution and ϕ_s, A_v and f_y are the resistance factor for steel, area of the stirrup and the yield strength of the steel stirrups, respectively. The CSA A23.3-04 recommends two methods to determine the values of β andθ; the simplified method for simple cases and the general method for detailed analysis. The general method for determining the values of β and θ is explained below.

The value of β and θ can be determined using equations 2.6 and 2.7 as follows:

$$\beta = \frac{0.4}{1 + 1500\epsilon_x} \cdot \frac{1300}{1000 + s_{ze}} \qquad Eq.(2.6)$$

$$\theta = 29 + 7000\epsilon_x \qquad Eq.(2.7)$$

The term ϵ_x in is the longitudinal strain at mid depth of the section and can be determined using equation 2.8.

$$\epsilon_x = \frac{\frac{M_f}{d_v} + V_f}{2E_s A_s} \qquad Eq.(2.8)$$

Where, $M_f, V_f, E_s \; and \; A_s$ are factored moment, factored shear force, modulus of elasticity of steel and area of the longitudinal steel, respectively.

For sections having at least minimum shear reinforcement, the factor s_{ze} shall be taken equal to 300. Otherwise, s_{ze} shall be computed using equation 2.9.

$$s_{ze} = \frac{35 s_z}{15 + a_g} \geq 0.85 s_z \qquad Eq.(2.9)$$

The crack spacing parameter s_z shall be taken as d_v or the maximum vertical distance between layers of distributed longitudinal reinforcement, whichever is less. Each layer of such reinforcement shall have an area at least equal to $0.003 b_w s_z$. Factor a_g is the maximum size of the coarse aggregate.

2.2 Corrosion in Reinforced Concrete

2.2.1 Effect of Corrosion

Corrosion effects the behaviour of reinforced concrete members by section loss of the reinforcing bar, cracking and spalling of concrete cover and loss of bond between steel bar and concrete. The pitting corrosion of the reinforcing bar leads to a reduction in the cross-sectional area of the bar resulting in a reduced load carrying capacity. The general corrosion of the reinforcing bar results in cracking and spalling of concrete cover, which causes the loss of bond between the reinforcing bar and the concrete and consequently a reduction in concrete section. Figure 2.3 summaries the effects of corrosion on reinforced concrete members.

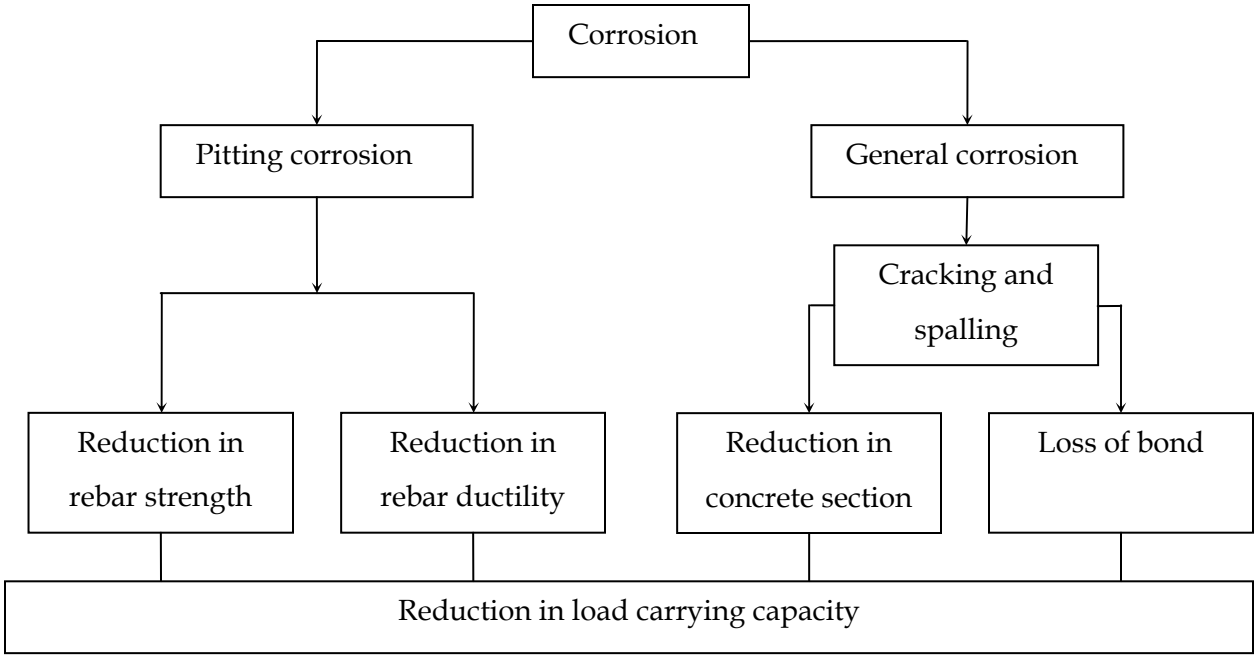

Figure 2.3: Effects of corrosion on reinforced concrete members

2.2.1 Mechanism of Corrosion in Reinforced Concrete

Concrete is an alkaline material under normal exposure conditions. The high alkalinity of concrete (pH > 13.0) allows formation of a passive oxide film on the surface of the embedded reinforcing steel bar, which protects it from corrosion. Once the protective layer around the reinforcing bar is disrupted either by lowering of pH due to carbonation or by ingress of chlorides, corrosion may start.

Corrosion is an electrochemical process. An electrochemical corrosion cell consisting of anode, cathode and an electrolyte must be formed for corrosion to occur. A moist reinforced concrete environment fulfills all the requirements to form an electrochemical cell by providing an electrolyte in the form of aqueous medium and the anode/cathode in the form of the steel reinforcement. During the corrosion process, anodic and cathodic reactions occur. At the anode, the iron is oxidized releasing two electrons, which are transferred to the cathode where these electrons along with water reduced the oxygen. Anodic and cathodic reactions are given in equations 2.10 and 2.11:

$$Fe \longrightarrow Fe^{2+} + 2e^{-} \qquad (Anodic\ reaction) \qquad Eq.(2.10)$$

$$2e^{-} + H_2O + \frac{1}{2}O_2 \longrightarrow 2(OH)^{-} \quad (Cathodic\ reaction) \qquad Eq.(2.11)$$

The hydroxyl ions formed during the cathodic reaction migrate to the anode through the aqueous medium/water (electrolyte) to complete the corrosion cell. Subsequently, a number of secondary reactions occur with the hydroxyl and iron ions to produce different types of hydroxides and oxides, depending on the amount of oxygen available. These secondary reactions are given in equations 2.12 to 2.20 (West, 1999).

$$Fe^{2+} + 2(OH)^{-} \longrightarrow Fe(OH)_2 \qquad Eq.(2.12)$$

$$Fe^{2+} + 2(OH)^{-} \longrightarrow FeO + H_2O \qquad Eq.(2.13)$$

$$2Fe(OH)_2 + 1/2O_2 \longrightarrow Fe_2O_3.H_2O + 2H_2O \qquad Eq.(2.14)$$

$$2Fe(OH)_2 + 1/2O_2 + H_2O \longrightarrow 2Fe(OH)_3 \qquad Eq.(2.15)$$

$$3Fe(OH)_2 + 1/2O_2 \longrightarrow 2Fe_3O_4 + 3H_2O \qquad Eq.(2.16)$$

$$2FeO + 1/2O_2 + H_2O \longrightarrow Fe_2O_3.H_2O \qquad Eq.(2.18)$$

$$2FeO + 1/2O_2 + H_2O \longrightarrow 2Fe(OH)_3 \qquad Eq.(2.19)$$

$$3FeO + 1/2O_2 \longrightarrow Fe_3O_4 \qquad Eq.(2.20)$$

The iron hydroxides and oxides (corrosion products) occupy more volume than the iron. The increase in volume depends on the type of iron hydroxide or oxide formed by secondary reactions. The volume of the different iron hydroxides or oxides formed compared to the volume of iron is shown in Figure 2.4. The increased volume of iron hydroxides or oxides exerts pressure on the surrounding concrete. Once the pressure exceeds the tensile strength of concrete, it cracks and the corrosion products reach the concrete surface making rust stains at crack locations.

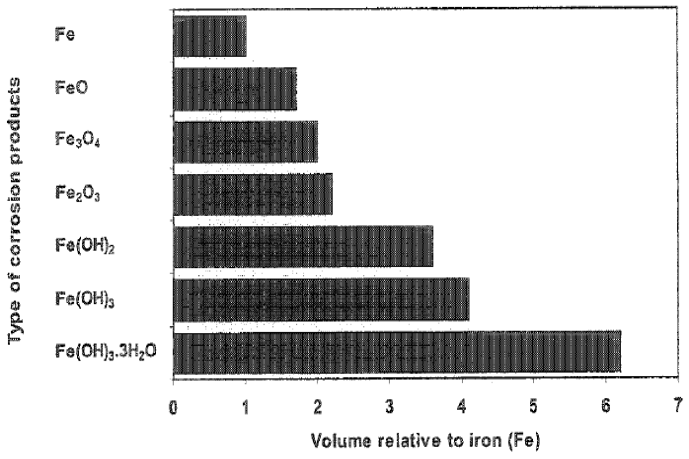

Figure 2.4: Relative volume of iron and iron oxides (Liu and Weyers (1998))

2.2.2 Types of Corrosion in Reinforced Concrete

2.2.2.1 General Corrosion

General corrosion is normally associated with both chloride ingress and carbonation of concrete. The iron oxide compound formed during general corrosion is usually known as brown rust. These compounds have relatively greater volume than the metal itself and exert expansive pressure onto the surrounding concrete. This leads to the cracking and spalling of the concrete cover around reinforcing bar before excessive loss of cross-sectional area of the reinforcing bars. Structures experiencing general corrosion of their reinforcing bar have reduced structural capacity due to reduction in bond strength between the reinforcing bar and surrounding concrete (fib, 2000).

2.2.2.2 Pitting Corrosion

Pitting corrosion is regarded as localized corrosion. Pitting corrosion is only associated with chloride ingress and not with carbonation induced corrosion. The compounds formed during pitting corrosion are different than those formed in general corrosion. These compounds have lesser volumetric expansion than the compounds formed during general corrosion. Consequently, there is less tendency of splitting of concrete cover due to pitting corrosion. On the other hand, excessive loss of cross section of the reinforcing bar may occur without any visible signs of deterioration on the surface of these members. Reinforced concrete structures experiencing pitting corrosion of their reinforcing bars exhibit reduced strength and ductility due to the reduction in the tensile strength of reinforcing bar (fib, 2000).

2.2.3 Accelerated Corrosion Technique

Accelerated corrosion technique is widely used to corrode reinforced concrete specimens in the laboratory. In the accelerated corrosion technique, corrosion process is activated by the chloride salts in the concrete and accelerated by electrical polarization of the reinforcing bar embedded in the concrete. Different methods have been used to incorporate salts in the concrete: some researchers added the salts in the concrete mix while others immersed the specimens in a salted solution. To electrically polarize the reinforcing bar, it is connected to an external power supply in such a way that a positive potential is created on the bar making it the anode in the corrosion cell. To complete the corrosion cell, an external or an internal cathode is used. Galvanized wire

mesh, copper or stainless steel plates are used as an external cathode while a stainless steel bar is used as an internal cathode.

Different current densities have been used in the literature ranging from as high as 10400μA/cm^2 to as low as 45μA/cm^2 while the highest corrosion rate recorded in field ranged between 10 and 25μA/cm^2 (El Maaddaway and Soudki, 2003). El Maaddaway and Soudki (2003) recommended that the current density in accelerated corrosion must not exceed 200μA/cm^2. This current density induces corrosion of steel reinforcement in reasonable time and produces corrosion products and cracking patterns similar to those found in the field.

2.3 Effect of Corrosion on Flexural and Bond Strength of Reinforced Concrete Members

2.3.1 Effect of Corrosion on Bond Strength of RC Members

The effect of corrosion of the reinforcing bar on the bond strength of reinforced concrete members has been investigated by many researchers and is relatively well understood. The majority of the studies reported that the bond strength increases initially with an increase in corrosion level until concrete cracks and then the bond strength starts decreasing with further increase in the corrosion level (Al-Sulaimani et al., 1990; Almusallam et al., 1996; Bharava et al., 2007 and Ouglova et al., 2008). Figure 2.5 shows the typical change in bond strength with increase in corrosion level. It is also reported in the literature that the bond strength of unconfined steel bar is significantly lower than confined steel bar at the same corrosion level (Fang et al., 2006).

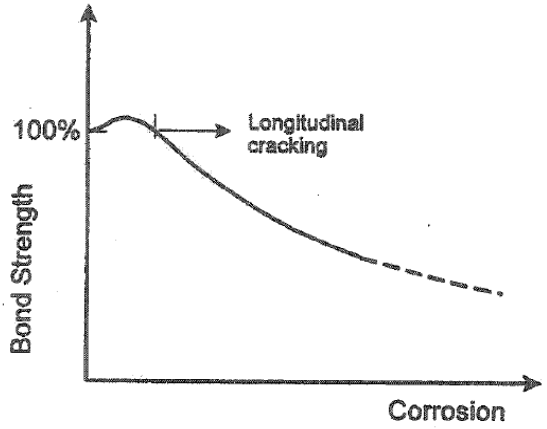

Figure 2.5: Effect of corrosion on bond strength (fib, 2000)

Models have been developed to predict the residual bond strength of RC members (Wand and Liu, 2006; Bharava et al., 2007).

2.3.2 Effect of Corrosion on Flexural Strength of RC Members

A large number of studies have been conducted to investigate the effect of corrosion on bond strength of RC members. The effect of corrosion on flexural strength of RC members is also well understood. A few of the studies conducted in this area are presented in the following.

Al-Sulaimani et al. (1990) investigated experimentally the effect of corrosion on the flexural strength of RC beams. It was observed that up to 1.5% corrosion level, there was no reduction in ultimate flexural strength, however; there was a reduction in flexural strength with further increase in corrosion levels (12% reduction at 5% corrosion level).

Almusallam et al., (1996) carried out an experimental investigation to determine the effect of corrosion on the behaviour of corroded slabs. It was observed that corrosion changed the failure mode from flexure in the control slabs to bond-shear failure in the corroded slabs. Reduction in the ultimate flexural strength was also observed; 25% and 60% reduction in ultimate strength for 5% and 25% corrosion level, respectively.

Mangat and Elgarf (1999) investigated the effect of corrosion on flexural strength of RC beams. A significant reduction in the ultimate flexural strength was noticed (75% reduction in flexural strength for 10 % corrosion level).

A number of models have been developed to predict the residual flexural strength of RC members (Azad et al., 2007; Xiao-Hui and Xia-La, 2008).

2.4 Effect of Corrosion on Shear Strength of Reinforced Concrete Beams

2.4.1 General

The effect of corrosion on shear strength of RC members is not as well understood as the bond strength or flexural strength and models need to be developed in this area.

A number of studies have been reported in the literature to investigate the effect of corrosion on shear strength of reinforced concrete beams. The majority of these studies did not incorporate actual corrosion instead corrosion effects were simulated in different ways. A review of these

studies is presented in the following sections with a critical evaluation of their applicability to corrosion effects on shear strength of reinforced concrete beams.

2.4.2 Is the Effect of Corrosion on Shear Strength of RC Beams Significant?

Rodriguez et al. (1997) carried out an extensive research work to investigate the effect of corrosion on the load carrying capacity of reinforced concrete beams. The beam specimens used in this study were 200 mm deep, 150 mm wide and 2300 mm in length. The test variables included the level of corrosion, reinforcement details (ratio of tensile reinforcement (2-10mm or 2-12mm or 4-12 mm bars), ratio of compression reinforcement (2-8mm or 4-8mm bars), spacing of stirrups (6mm stirrups at 85mm or 150mm or 170mm c/c) and anchorage condition) and the interaction between the corrosion and loading. After corroding the reinforcement (only the flexural or both the flexural and shear reinforcement) by an accelerated corrosion technique, the beams were tested in four-point bending with a shear span to height ratio of 4.0. It was concluded that the mode of failure changes from bending to shear after the corrosion of the reinforcement in beams with usual reinforcement and that pitting corrosion of the shear stirrups was the most influencing factor in the reduction of the load carrying capacity of corroded beams.

Val (2007) conducted reliability analysis to investigate the effect of general and pitting corrosion on the flexural and shear behaviour of reinforced concrete beams. Different corrosion rates were considered in the reliability analysis. The results of the analysis showed that higher corrosion rates ($\geq 1\mu A/cm^2$) had a significant effect on the behaviour of corroded beams and that at these corrosion rates pitting corrosion (especially pitting corrosion of stirrups) had a more pronounced effect on the behaviour of the test beams as compared to those with general corrosion. The results also showed that, in case of pitting corrosion, at higher corrosion rates the shear failure becomes the dominant type of failure.

The above two studies investigated the effect of general and pitting corrosion on the flexural and shear behaviour of reinforced concrete beams. The results of these studies indicated that the reduction in shear capacity is higher as compared to reduction in flexural capacity under induced or simulated corrosion effects (especially pitting corrosion effects) as the beams that were designed to fail in flexure, failed in shear when subjected to corrosion effects.

2.4.3 Shear Strength of RC Beams with Exposed or Corroded Longitudinal Reinforcement:

Cairns (1995) carried out an analytical and experimental research work to study the shear strength of reinforced concrete beams with exposed reinforcement. The variables studied included the beam size and shape and the portion of the span over which the tensile reinforcement is exposed. A total of ten beams designed to fail in shear were tested. The test beams were divided into three series: A, B and C. Series A and B had three beams: one control beam with fully bonded reinforcement (A1 and B1) and two beams with one of the two longitudinal bars exposed (A2, A3, B2 and B3). In specimens A2 and B2, the reinforcement was exposed over 83% of the whole span and in specimens A3 and B3; reinforcement was exposed only within the shear span (69% and 77% of the shear span, respectively). Series C had four beams: one control with fully bonded reinforcement and three with exposed reinforcement. The reinforcement was only exposed within shear span (C1: 87% of the shear span, C2 and C3: 43% of the shear span, the exposed section being close to the load point in C3 and close to the support in C4). The beams were tested in four-point bending with a shear span to depth ratio of approximately 3.0. It was concluded that properly anchored reinforcement significantly contributed to strength of reinforced concrete even if it was exposed over the span and that the shear strength of the beams increased with exposed reinforcement. The author also proposed a method to calculate the shear strength of beams with portion of the reinforcement exposed.

Raoof and Lin (1997) carried out an extensive experimental work consisting of 44 small-scale beams and 88 large-scale beams to study the behaviour of reinforced concrete beams with exposed tensile reinforcement. Several variables were examined including the extent of removal of steel-concrete bond, the distance of damage from the support, load position relative to the support, the percentage of tensile reinforcement, the depth of concrete removal, the ratio of compression reinforcement, the effect of stirrups and loading arrangement. The tests conducted on the small-scale beams with exposed reinforcement revealed that beams with a/d less than 3.0 have little increase in their ultimate strength while beams with a/d greater than 3.0 have reductions in their ultimate strength with a maximum reduction at a/d between 3.0 and 4.0. Similar results were observed in the large scale beams with exposed reinforcement. It was also observed that loss in ultimate strength in beams with exposed reinforcement (in absence of

shear stirrups) increases with increase in the percentage of longitudinal reinforcement at a/d between 3.0 and 4.0.

Jeppsson and Thelandersson (2003) carried out an experimental study to investigate the reduction in shear capacity of reinforced concrete beams with unbonded longitudinal reinforcement. To create a loss of bond, the longitudinal reinforcements were placed within plastic tubes close to support. A total of six beams, all designed to fail in shear, were tested: one without stirrups and five with stirrups. Two beams (one beam without stirrups and one beam with stirrups) acted as control with full bond. In the remaining four beams (with stirrups), the length of the longitudinal reinforcement with no bond was varied from one stirrup spacing to four stirrup spacings. It was observed that there is a moderate reduction in shear capacity with a significant loss of bond: 33% reduction in load carrying capacity with 80% loss of bond. The author concluded that loss of bond over longitudinal reinforcement is partially compensated by the increased utilization of the stirrups which results in relatively higher residual strengths. The stirrups are very important in beams where longitudinal reinforcement is unbonded because the bond forces redistribute to forces in the stirrups.

Toongoenthong and Maekawa (2004) studied the effect of pre-induced damage on the shear capacity of reinforced concrete beams without stirrups. Six different damage conditions were examined. Series 1 consisted of four beam specimens: one control specimen and three specimens subjected to accelerated corrosion causing cracks at three different local locations (case 1-3). Series 2 consisted of two beam specimens: one control specimen and one specimen with horizontal crack planes produced by inserting a 1mm thick paper plate simultaneously at the three locations studied in series 1 simulating extreme corrosion conditions (case 4). Series 3 (case 5) and series 4 (case 6) were similar to series 2 except for the damage locations: in series 3 the damage was extended to the anchorage zone whereas in series 4 damage was induced over the whole shear span leaving the anchorage zone undamaged. The details of the specimens showing the damage type and location are given in Figure: 2.6. All beam specimens were tested in three-point bending with a shear span to depth ratio of 3.2.

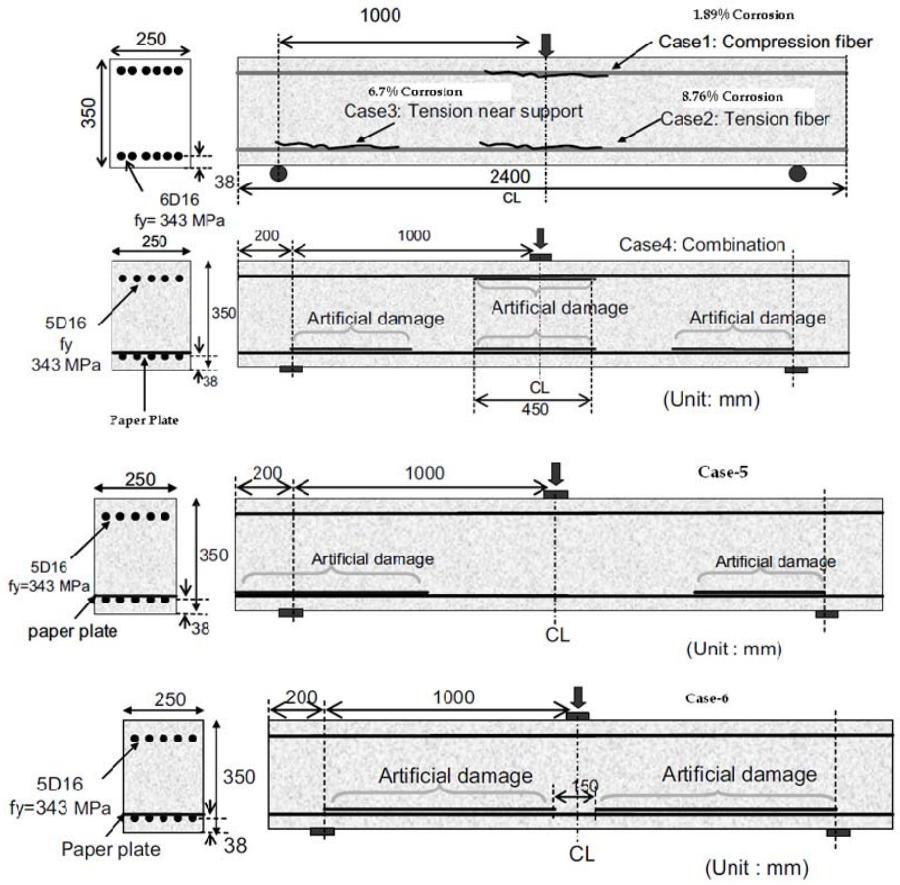

Figure: 2.6: Details of specimens (Toongoenthong and Maekawa, 2004)

The test results showed that a small reduction in shear capacity of beams with local corrosion damage (case 1-3) and a large reduction in shear capacity under extreme simulated corrosion conditions (case 4-5). The reduction in shear capacity under extreme corrosion conditions ranged between 20% (case 4) to 60% (case 5) depending on whether the damage is extended to anchorage zone or not. The load deflection curves of case-4 and case-5 are shown in Figure 2.7 and Figure 2.8, respectively. The author concluded that special attention should be given to the condition of anchorage while assessing the performance of such beams under extreme simulated corrosion conditions.

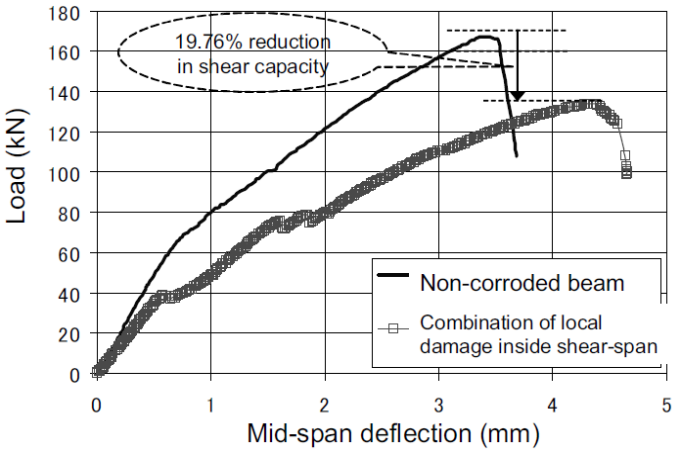

Figure 2.7: Load vs. deflection curve of case-4 (Toongoenthong and Maekawa, 2004)

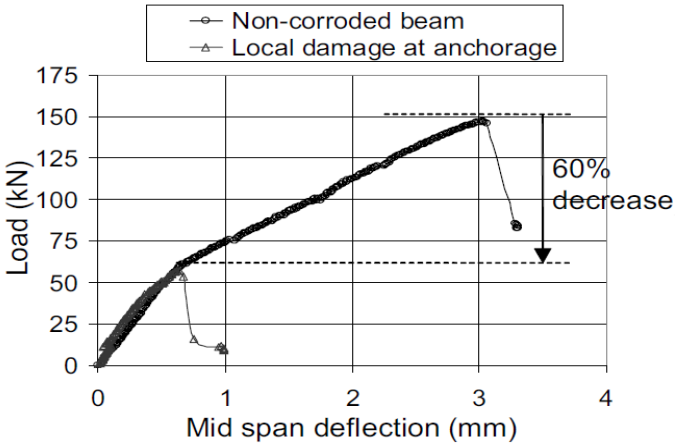

Figure 2.8: Load vs. deflection curve of case-5 (Toongoenthong and Maekawa , 2004)

None of these studies have considered the effects of different levels of corrosion, whereas the corrosion induced degradation is directly associated with the corrosion levels. The findings were contradictory: Cairns (1995) found that shear strength increases with loss of bond between the longitudinal reinforcement and concrete while Jeppsson and Thelandersson (2003) found that shear strength decreases with loss of bond between the longitudinal reinforcement and concrete. This is possibly because of the different methods used to create the loss of bond in the longitudinal reinforcement. Raoof and Lin (1997) revealed that the increase or decrease in shear strength due to corrosion of the longitudinal reinforcement mainly depend on the a/d ratio of the beams.

From the above it is evident that further research must be done to investigate the effect of corrosion on the shear behavior of RC beams with different a/d ratios at different corrosion

levels and that this should be done by actually inducing corrosion in the reinforcement instead of simulating its effects.

2.4.4 Shear Strength of RC Beams with Damaged or Corroded Stirrups

Regan and Kennedy (2004) investigated the effect of corrosion on the shear strength of reinforced concrete beams. The effect of corrosion was simulated by damage of the stirrups and delamination of the concrete cover. The damage of the stirrups was simulated by removing the end anchorage of the stirrups and using two straight vertical pins except in one beam where U shaped stirrups were used. The delamination of the concrete cover was simulated by exposing the main steel reinforcement during casting of the beam specimens. A total of fourteen beams were tested: ten beams were 400 mm deep, 150 mm wide, and 3000 mm in length and four beams were 200 mm deep, 150 mm wide, and 2000 mm in length. These beams were simply supported over a clear span of 2.5 m and 2m, respectively. The tensile reinforcement consisted of 4-20mm or 4-25mm deformed bars and the compression reinforcement consisted of 2-20mm or 2-25mm deformed bars. The shear stirrups were 6mm diameter stirrups at 75mm c/c or 6mm diameter at 150mm c/c or 8mm diameter stirrups at 150mm c/c. The specimens were tested in three-point bending with a varied shear span to depth ratio of 3.5 to 3.66. The reduction in shear strength was recorded as 14-33% for 65-75% loss of stirrup end anchorage. The authors concluded that the stirrups lacking end anchorage can still contribute to the shear resistance of RC beams.

Toongoenthong and Maekawa (2005) investigated the effect of fractured stirrups on the shear strength of reinforced concrete beams. The beam specimens were 350 mm deep, 250 mm wide, and 3000 mm in length and were simply supported over a clear span of 2.0 m. Figure 2.9 shows the specimen setup, dimension and reinforcement details. The tension and compression reinforcement consisted of 4-19mm high strength deformed bars. The shear stirrups were 6mm U shaped spaced at 100mm c/c. The fractured stirrups were considered the replicas of stirrups damaged by corrosion or alkali-aggregate reaction of concrete. The fractured stirrups were simulated by removing the bond near the edges of stirrup legs. A 50 mm strip of vinyl tape was used to eliminate the bond near the edges of the stirrup legs. The beam specimens were tested in three-point bending with a shear span to depth ratio of 3.2.

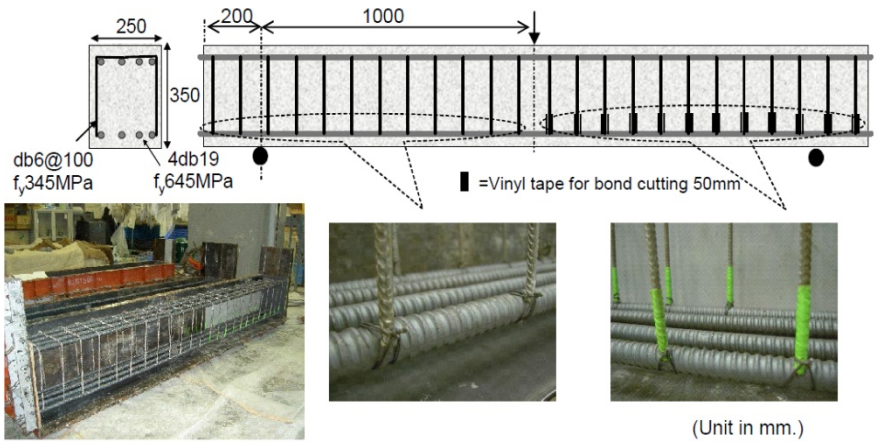

Figure 2.9: Details of Specimens (Toongoenthong and Maekawa, 2005)

Figure 2.10 shows the load deflection curves of the damaged beam with the fractured stirrups and the undamaged reference beam. The results showed that the damaged beam experienced 37% reduction in shear capacity compared to the undamaged beam. It was also observed that beams having stirrups without proper anchorage experienced longitudinal cracking along the main reinforcement before inclined cracking, which leads to the ineffectiveness of stirrups. The load carrying mechanism was changed from a truss mechanism to a tied-arch action leading to anchorage failure of the main reinforcement.

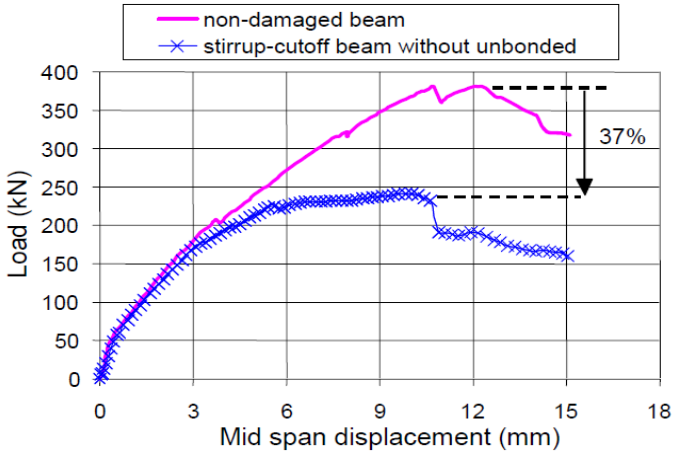

Figure 2.10: Load ~ Deflection Curve (Toongoenthong and Maekawa, 2005)

Higgins and Farrow (2006) carried out an experimental work to investigate the shear capacity of conventionally reinforced concrete beams with corrosion damaged stirrups. Figure 2.11 shows the details of the beam specimens tested. A total of fourteen beam specimens were tested; eight rectangular beam specimens that were 610 mm deep, 254 mm wide, and six T beam specimens (Three T and Three inverted T) that were 610 mm deep with a flange width of 610 mm, a web

width of 254 mm and a flange depth of 102mm. All beam specimens were 3050 mm long and were simply supported over a clear span of 2440mm. The main variables examined in this study were the spacing of the stirrups (203 mm, 252 mm, and 305mm) and the level of corrosion (none (A), light (B), moderate(C) and severe (D)). After corroding the stirrups in the beam specimens by accelerated corrosion technique, the specimens were tested in four-point bending with a shear span to depth ratio of 2.04. The authors observed that the lightly corroded and control beam specimens failed by shear-compression while the moderate to severely corroded beam specimens failed by fracture of the stirrups. It was also observed that maximum strength loss occurred when the location of pitting corrosion coincided with the location of a diagonal crack. The maximum strength reductions for the rectangular, T and inverted T beam specimens were 30, 26 and 42 % respectively.

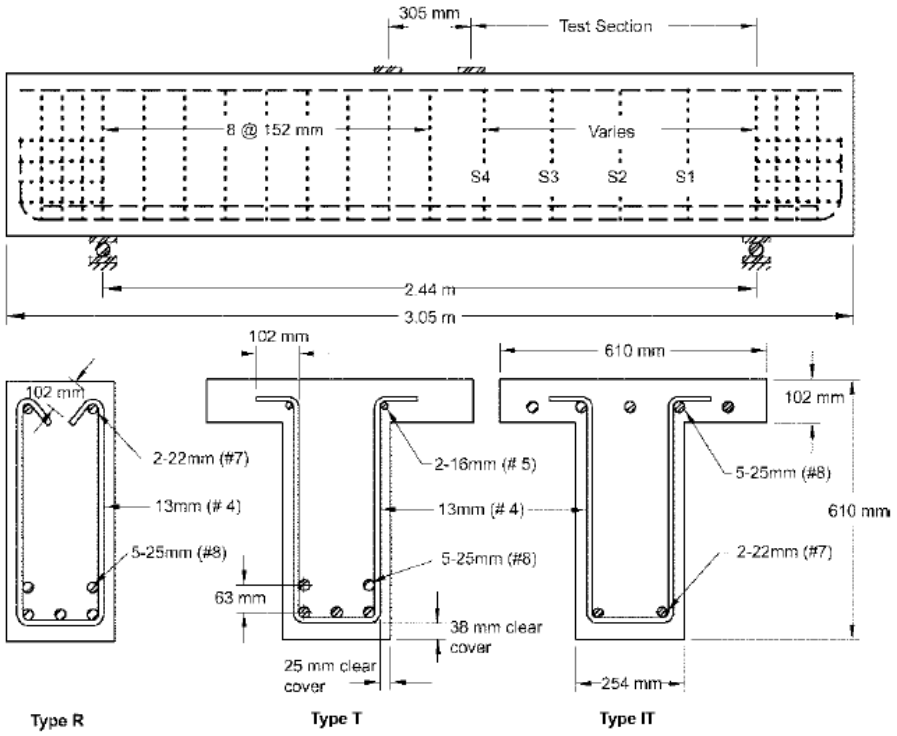

Figure 2.11 : Details of specimens (Higgins and Farrow, 2006)

The authors concluded that the inspection of corrosion damaged structures in high shear regions should not be focused on visual distress instead it should be focused on identification of sequential stirrups with reduced stirrup cross sections and that the conventionally reinforced concrete girders with severely corroded stirrups will behave like girders without stirrups.

Suffern (2008) investigated the shear behaviour of reinforced concrete deep beams with corroded stirrups. A total of fifteen beams were tested. All beam specimens were 350 mm deep, 125 mm wide, and 1850 mm in length and were simply supported over a clear span of 1500 mm. The tension and compression reinforcement consisted of 2-25M bars and 2-10M bars, respectively. The stirrups were 10M U shaped spaced at 150mm c/c .The test variables included the shear span to depth ratio (1.0, 1.5, and 2.0), presence of stirrups (without stirrups and with stirrups) and corrosion levels (21 days exposure, 60 days exposure and 120 days exposure). After corroding the stirrups by the accelerated corrosion technique, the specimens were tested in three-point bending with a varied shear span to depth ratio of 1.0, 1.5 and 2.0. A reduction in strength was observed in most corroded beams; 26% reduction with low corrosion level, 18-53% reduction with medium corrosion level and 41% reduction with high corrosion level which was approximately uniform for all a/d ratios. Stiffness of the corroded beams was also reduced: 30%, 38% and 34% reduction in beams with shear span to depth ratio of 1.0, 1.5 and 2.0, respectively.

Zhao et al. (2009) reviewed the existing studies conducted on shear strength of corroded reinforced concrete beams. He reported that shear strength of corroded reinforced concrete beams increases at low corrosion level (up to 10% sectional loss of stirrups) and decreases at higher corrosion levels (when sectional loss of stirrups exceeds 10%). The effect of reduced stirrup cross section on the shear strength is more significant at higher a/d ratios.

Zhao et al. (2009) proposed an empirical equation to estimate the residual shear strength of corroded reinforced concrete beams, presented in equation 2.21.

$$V_u = P_v V_{uo} \qquad Eq.(2.21)$$

The V_u is shear strength of RC beams with corroded stirrups; V_{uo} is the shear strength of the same type of RC beam not subjected to any corrosion and P_v is the degradation parameter of shear strength due to corrosion of stirrups. The value of P_v is expressed as a function of the ratio of the average section loss of the stirrup (η_v). The value of P_v can be determined using equation 2.22.

$$P_v = \begin{cases} 1.0 & \eta_v \leq 10\% \\ 1.17 - 1.17\eta_v & \eta_v > 10\% \end{cases} \qquad Eq.(2.22)$$

In summary, the studies by Regan and Kennedy (2004) and Toongoenthong and Maekawa (2005) simulated the effect of severely corroded stirrups by removing the anchorage of the

stirrups. This assumption is applicable for very extreme corrosion conditions. Higgins and Farrow (2006) and Suffern (2008) investigated the effect of corroded stirrups on shear strength of RC beam with shear span to depth ratios less than 2.0. These studies are only applicable to deep beams. There is no study in the literature that investigated the behaviour of reinforced concrete slender beams with corroded stirrups. Further research is required to investigate the behavior of slender beams with corroded stirrups.

2.4.5 Shear strength of RC beams with corroded Longitudinal Steel and Stirrups

Only one study was found in the literature on the effects of corrosion of longitudinal steel and stirrups on shear strength of RC beams.

Xu and Niu (2003) carried out an experimental study to investigate the shear behaviour of corroded reinforced concrete beams. A total of twenty one beam specimens were tested: eighteen corroded and three un-corroded. The beam specimens used in this study were 150 mm deep, 120 mm wide and 1400 mm in length. The test variables included the level of corrosion and shear span to depth ratio. The beams were tested in four-point bending with a varied span to depth ratio of 1-2. It was observed that for a given corrosion level, there is a larger reduction in ultimate shear capacity at higher a/d ratios: the reduction in ultimate shear capacity was 10% at a/d=1 and 20 % at a/d=2.0 for specimens with 20% corrosion.

This study was conducted on very small scale beams and this has a significant influence the on the shear strength. Size effect must be considered on any future study on shear strength. Further research is needed to investigate the shear strength of full-scale RC beams subjected to corrosion of both stirrups and longitudinal reinforcement.

2.5 Summary

The basics about the mechanism of shear transfer in RC beams, mechanism of corrosion in reinforced concrete and the effects of corrosion on reinforced concrete members are presented in this chapter. The effects of corrosion on the shear strength of RC beams are also discussed in detail in this chapter.

A number of studies have been reported in the literature to investigate the effects of corrosion on shear strength of RC beams, but due to complex nature of shear behaviour of RC beams still a lot of work is required in this area. The literature review revealed that there are still a lot of

gaps in the state-of-knowledge on the shear strength of corroded beams. As discussed in section 2.4, to the author's knowledge, there is not a single study conducted to investigate the effect of corrosion on the shear strength of RC beams with induced corrosion of the longitudinal bars. The studies conducted in the literature with simulated corrosion effects had contradictory results. The effect of corrosion of longitudinal reinforcement on the shear strength of RC beams with different shear span to depth ratios is not understood. The current study attempts to increase our understanding in this area.

Chapter 3:Experimental Program

3.1 Introduction

The experimental program is designed to investigate the effect of corrosion of the longitudinal reinforcement on the behaviour of shear-critical reinforced concrete (RC) beams. The details of the experimental program including the design of the test specimens, the accelerated corrosion process, instrumentation, test setup and test procedure are presented in the following sections.

3.2 Test Program

A total of twenty reinforced concrete beams were tested: ten deep and ten slender beams. The test matrix is given in Table 3.1. The test variables included the shear span to depth ratio (a/d=1.63 and 3.25), the corrosion level (none, light, medium and high), presence or absence of stirrups and FRP repair.

Table 3.1: The test matrix

Specimen	Corrosion Level	Shear span to depth ratio (a/d)			
		a/d = 1.63		a/d = 3.25	
		Without	With Stirrups	Without	With Stirrups
Evaluation	None	1	1	1	1
	Light (2.5%)	1	1	1	1
	Medium (5%)	1	1	1	1
	High (7.5%)	1	1	1	1
Repair	High (7.5%)	1	1	1	1

3.2.1 Test Specimens

The details of the test specimens are presented in Table 3.2. The test beams were divided into two series: series-A (deep beams) and series B (slender beams). Test series A consisted of ten reinforced concrete deep beams: five beams without stirrups and five beams with stirrups (Figure 3.1and Figure 3.2). Test series B consisted of ten reinforced concrete slender beams: five beams without stirrups and five beams with stirrups (Figure 3.3 and Figure 3.4). Each sub-series had one control un-corroded beam, three corroded beams and one corroded FRP repaired beam.

Table 3.2: Details of test specimens

Specimen		Target fc′ (MPa)	Longitudinal Reinforcement					Shear Reinforcement
			Amount of Reinforcement	ρ , %	ρ_b , %	ρ/ ρ_b	Corrosion level	
Series- A (Deep Beams)	1.63-L-0%	40	2-M25 Bars	2.17	4.37	0.50	None	-
	1.63-L-2.5%	40	2-M25 Bars	2.17	4.37	0.50	Light	-
	1.63-L-5%	40	2-M25 Bars	2.17	4.37	0.50	Medium	-
	1.63-L-7.5%	40	2-M25 Bars	2.17	4.37	0.50	High	-
	1.63-L-7.5%-R	40	2-M25 Bars	2.17	4.37	0.50	High	-
	1.63-LS-0%	40	2-M25 Bars	2.17	4.37	0.50	None	6mm@215mmc/c
	1.63-LS-2.5%	40	2-M25 Bars	2.17	4.37	0.50	Light	6mm@215mmc/c
	1.63-LS-5%	40	2-M25 Bars	2.17	4.37	0.50	Medium	6mm@215mmc/c
	1.63-LS-7.5%	40	2-M25 Bars	2.17	4.37	0.50	High	6mm@215mmc/c
	1.63-LS-75%-R	40	2-M25 Bars	2.17	4.37	0.50	High	6mm@215mmc/c
Series- B (Slender Beams)	3.25-L-0%	40	2-M25 Bars	2.17	4.37	0.50	None	-
	3.25-L-2.5%	40	2-M25 Bars	2.17	4.37	0.50	Light	-
	3.25-L-5%	40	2-M25 Bars	2.17	4.37	0.50	Medium	-
	3.25-L-7.5%	40	2-M25 Bars	2.17	4.37	0.50	High	-
	3.25-L-7.5%-R	40	2-M25 Bars	2.17	4.37	0.50	High	-
	3.25-LS-0%	40	2-M25 Bars	2.17	4.37	0.50	None	6mm@215mmc/c
	3.25-LS-2.5%	40	2-M25 Bars	2.17	4.37	0.50	Light	6mm@215mmc/c
	3.25-LS-5%	40	2-M25 Bars	2.17	4.37	0.50	Medium	6mm@215mmc/c
	3.25-LS-7.5%	40	2-M25 Bars	2.17	4.37	0.50	High	6mm@215mmc/c
	3.25-LS-7.5%-R	40	2-M25 Bars	2.17	4.37	0.50	High	6mm@215mmc/c

The beam designation was as follows: XX-YY-ZZ with XX= shear span to depth ratio, YY = beam reinforcement and ZZ= corrosion level. The shear to depth ratio is specified as 1.63 and 3.25; beam reinforcement is specified as L (only longitudinal reinforcement) and LS (longitudinal and transverse reinforcement); and the corrosion level is specified as 0%(none), 2.5%(Light), 5%(medium), and 7.5 %(high). FRP repair is specified with an additional letter "R" in the beam designation.

All beams had the same cross section (150 mm width and 350 mm depth) but had two different lengths of 1400 mm and 2400 mm for deep and slender beams, respectively. The longitudinal tensile reinforcements in all the beams were 2-25M bottom bars with standard 90˚ hooks. The side and vertical covers to the tension reinforcement were kept at 30 mm for all beams. The

stirrups used were 6mm smooth bars at 215 mm spacing with three additional stirrups provided in the anchorage zone. The corroded beams were divided into two zones: a corroded zone and an un-corroded zone. Typical corroded and un-corroded zones in a corroded beam (1.63-L-2.5%) are shown in Figure 3.1 with the dotted area representing the corroded zone and the remaining area as un-corroded zone. The longitudinal tensile reinforcements were corroded in the corroded zone and the stirrups in the corroded zone were epoxy coated to prevent them from corrosion. A 15 mm diameter stainless steel hollow tube was placed at 125mm from the bottom of beams. The stainless steel tube acted as a cathode in the accelerated corrosion process. During specimen fabrication, dividers were used to contain the salted concrete within the corroded zone.

3.2.2 Material Properties

3.2.2.1 Concrete

The concrete used for construction of the test beams was supplied by Hogg ready-mix concrete. Two concrete trucks were ordered: one truck for the salted concrete and one truck for the unsalted concrete. The concrete was batched with Type-10 Portland cement with a maximum coarse aggregate size of 19 mm. The concrete was batched at a water cementing material ratio of 0.45. Water containing salt was added to one truck for the salted concrete. The amount of water added was calculated to adjust the water cementing ratio from 0.45 to 0.55 and the amount of salt added was calculated to have 2.3% chlorides by mass of cement. Water was added to the second truck to adjust its water cementing material ratio from 0.45 to 0.55 for the unsalted concrete.

A total of twenty concrete cylinders (100mm x 200mm) were also cast from the same concrete batch (ten cylinders for salted concrete and ten cylinders for unsalted concrete). At the time of beam testing, the average compressive strength of the salted and unsalted concrete was 51.7 ± 5.12 MPa and 47.3 ± 0.68 MPa, respectively.

3.2.2.2 Reinforcing Steel

Grade 400 reinforcing steel bars were used as longitudinal reinforcement in the concrete beams: 25M bars as tensile reinforcement and 10M bars as compression reinforcement. The 6 mm smooth bars with nominal yield strength of 384 MPa were used as stirrups. A stainless steel tube with an outside diameter of 15 mm and a wall thickness of 0.89 mm was used as a cathode.

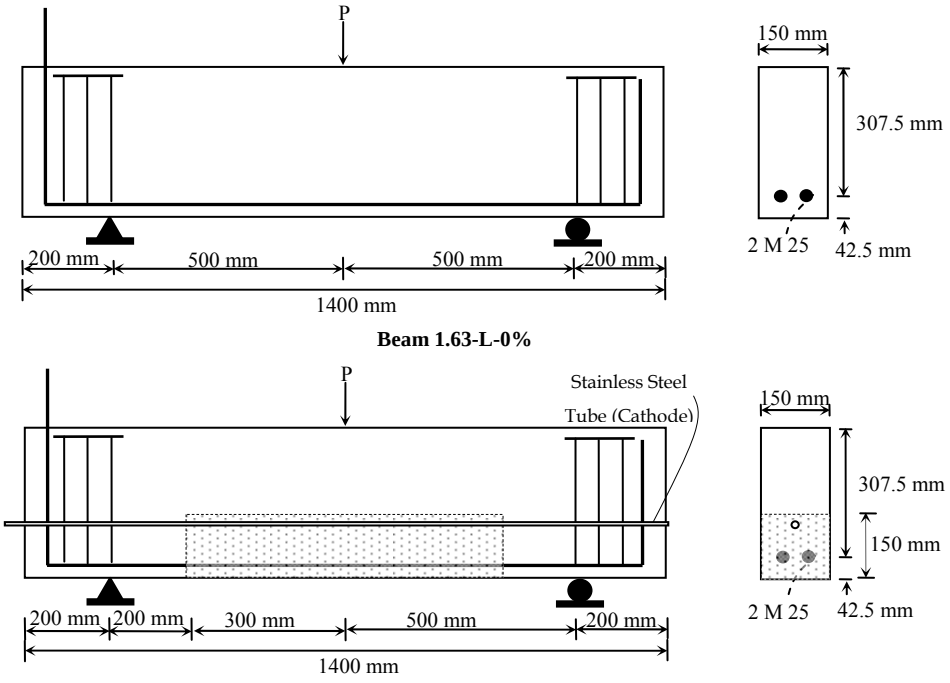

Figure 3.1: Deep beams without stirrups

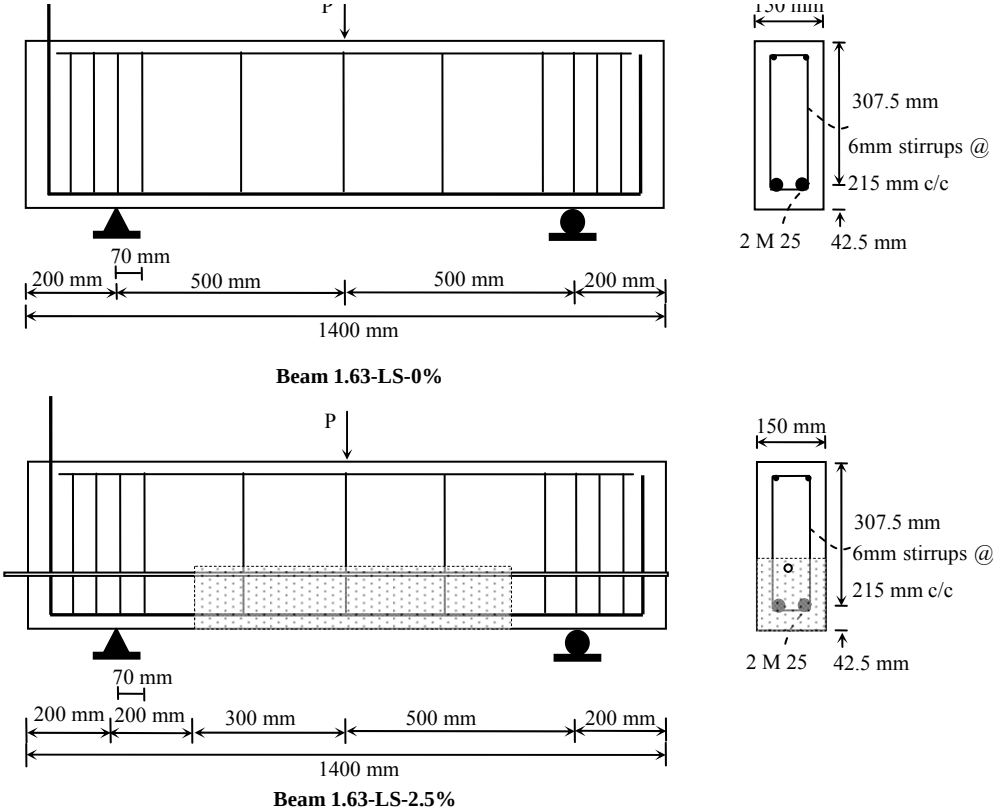

Figure 3.2: Deep beams with stirrups

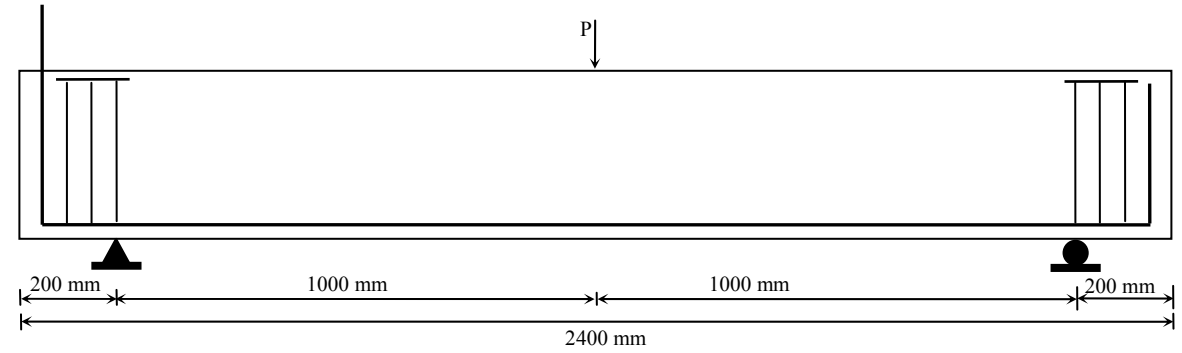

Beam 3.25-L-0%

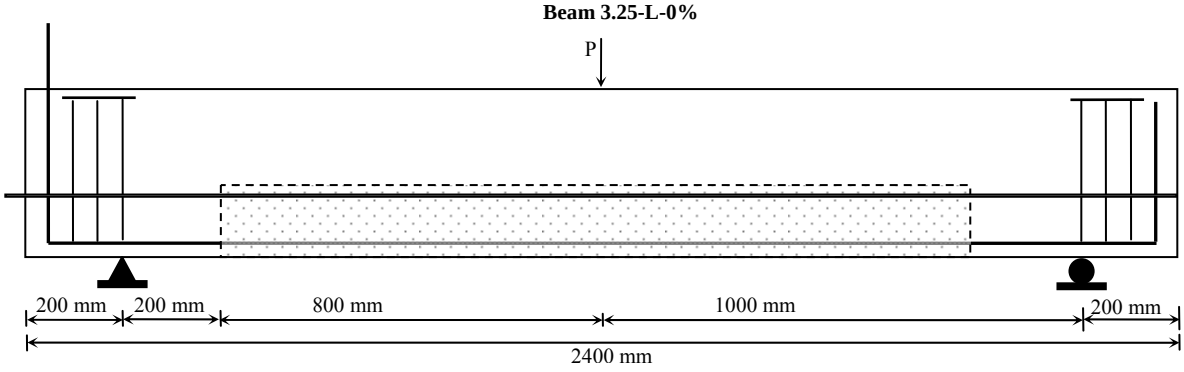

Beam 3.25-L-2.5%

Figure 3.3: Slender beams wihout stirrups

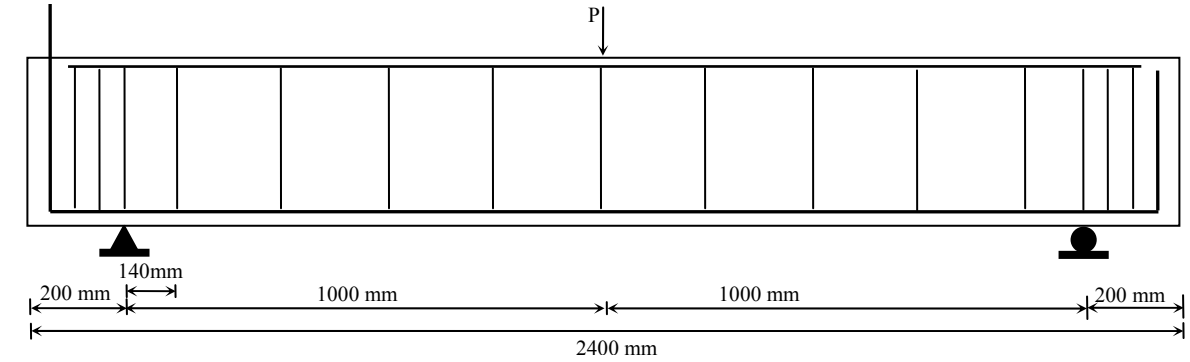

Beam 3.25-LS-0%

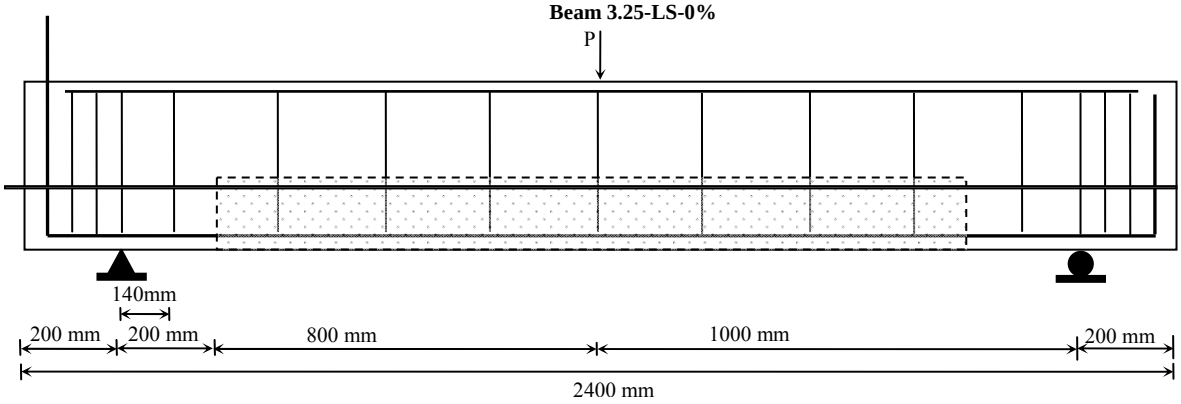

Beam 3.25-LS-2.5%

Figure 3.4: Slender beams with stirrups

3.2.3 Fabrication of Test Specimens

The beams were cast in formwork that consisted of a steel base and wooden sides as shown in Figure 3.5. The formwork was lubricated before casting the concrete for ease of stripping the beams. The reinforcement cages were hung from the top of the formwork in order to provide cover to the main longitudinal reinforcement. All twenty specimens were cast from the same concrete batch. Immediately after casting, the specimens were covered with plastic sheets to avoid moisture loss. Subsequently, the specimens were covered with wet burlap and plastic sheets for curing up to fourteen days and then the beams were stripped from the formwork and stored in the laboratory.

Figure 3.5: Formwork with cages

3.3 Accelerated Corrosion

Sixteen beams, four beams from each series, were subjected to accelerated corrosion by impressing a direct current into the longitudinal bars using a separate power supply for each series. The longitudinal reinforcing bars acted as an anode and the stainless steel tube acted as a cathode in this artificial corrosion cell. A schematic diagram showing the details of the connection between the longitudinal reinforcing bars, the stainless steel tube and the power supply is shown in Figure 3.6.

The direct current was impressed through the reinforcing bars at a constant current density of 150μA/cm². This value was selected, based on a study by El Maaddawy and Soudki (2004), to produce corrosion cracking similar to those found in the field while corroding the beams in a reasonable time period.

To disrupt the passive layer around the reinforcing bar embedded in the concrete, salt was mixed in the concrete during casting of the beams. The moisture and oxygen required for the corrosion reactions, was provided by a mist nozzle. The nozzle was connected to a water tap and pressurized air tap. To maintain the humid environment around the beams, they were placed on steel frames and covered with plastic sheets to make a full enclosure.

The time required to corrode the reinforcing steel bars was calculated based on Faraday's law. Faraday's law along with sample impressed current calculation is presented in Appendix-A. After reaching the light and medium corrosion levels (2.5% and 5%, respectively) eight beams were removed from the corrosion chamber. The remaining eight beams remained in the chamber until reaching the theoretically corrosion level of 7.5%.

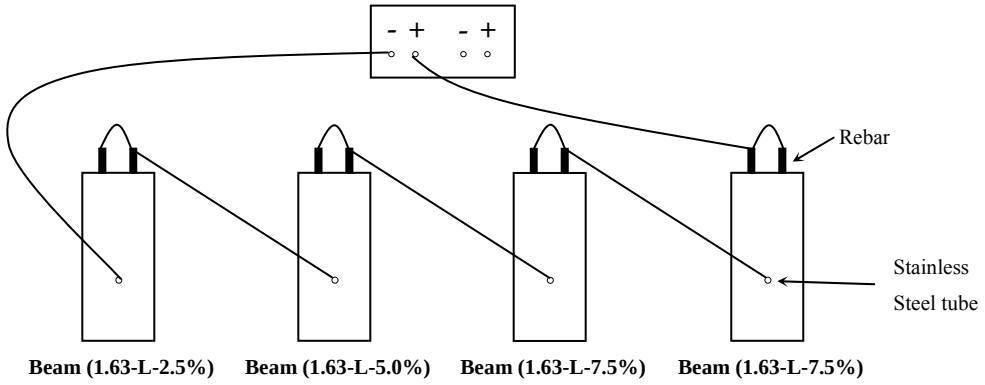

Figure 3.6: Schematic diagram of accelerated corrosion circuit

3.4 FRP Repair

Four corroded beams (7.5% corrosion level), one from each series, were repaired with carbon fibre reinforced polymer (CFRP) sheets. FRPs with their high strength to weight ratio and corrosion resistant properties have been successfully used in repair and rehabilitation of concrete structures (ACI 440, 2006 and ISIS Manual No. 4, 2007). Two different widths of intermittent U-wraps were used: 150 mm wide U-wraps in the shear span and 300 mm wide U-wrap under point load. The spacing of U-wrap was kept constant at 100mm. Deep and slender beams had same repair scheme. Detail of the wrapping is shown schematically in Figure 3.7.

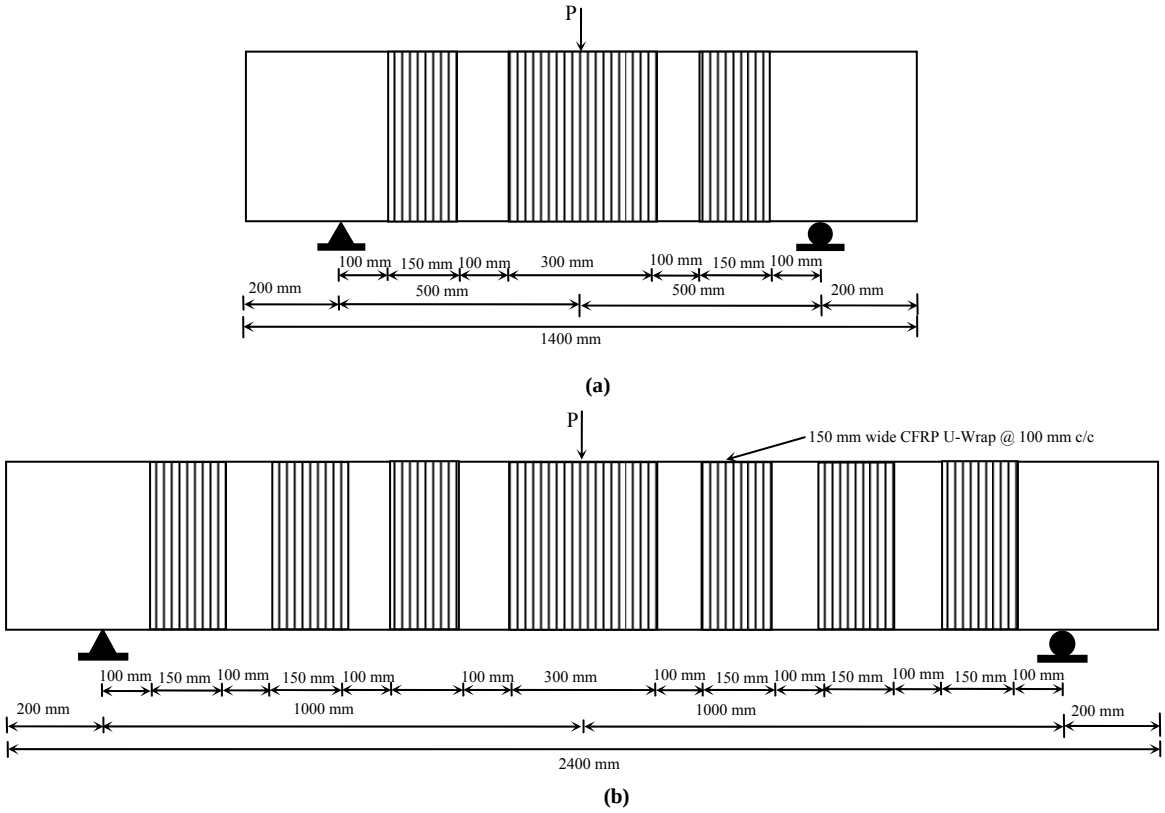

Figure 3.7: FRP repair scheme (a) deep beam (b) slender beam

The CFRP sheets used in the study were Sika Wrap 230C and the epoxy resin used was Sikadur 330. Sikadur 330 had two components A and B that were mixed in 4:1 ratio by weight. The concrete surfaces were ground and cleaned to get rid of the corrosion staining on the surface and to expose the aggregates for proper application of CFRP sheet. The edges of the beam cross section were rounded. Once the concrete surfaces were prepared, Sikadur 330 epoxy resin was placed on the concrete surface. Then the CFRP sheet was placed using a steel roller. The pressure was applied by the roller on the CFRP sheet to ensure CFRP sheet is impregnated with epoxy. After applying the U-wraps, beams were left for seven days to allow curing of the CFRP system.

3.5 Instrumentation

Electrical resistance strain gauges, with a gauge length of 5mm and a resistance of 120Ω, were attached to the longitudinal steel bars before casting the beams to measure the strain at different locations in the longitudinal bar in control specimens. Note that strain gauges were not installed on the reinforcement in the corroded beams as strain gauges would be destroyed during the

accelerated corrosion process. Strain gauges were mounted on two longitudinal steel bars in such a way that each bar had strain gauges attached over half the rebar length between the support and mid-span of the beam. Strain gauges, with a gauge length of 60mm and resistance of 120Ω, were also installed in the control beams to measure the strain in the concrete. The details and layout of the strain gauges, used to monitor the behavior of deep and slender beams, are shown in Figure 3.8 and Figure 3.9, respectively.

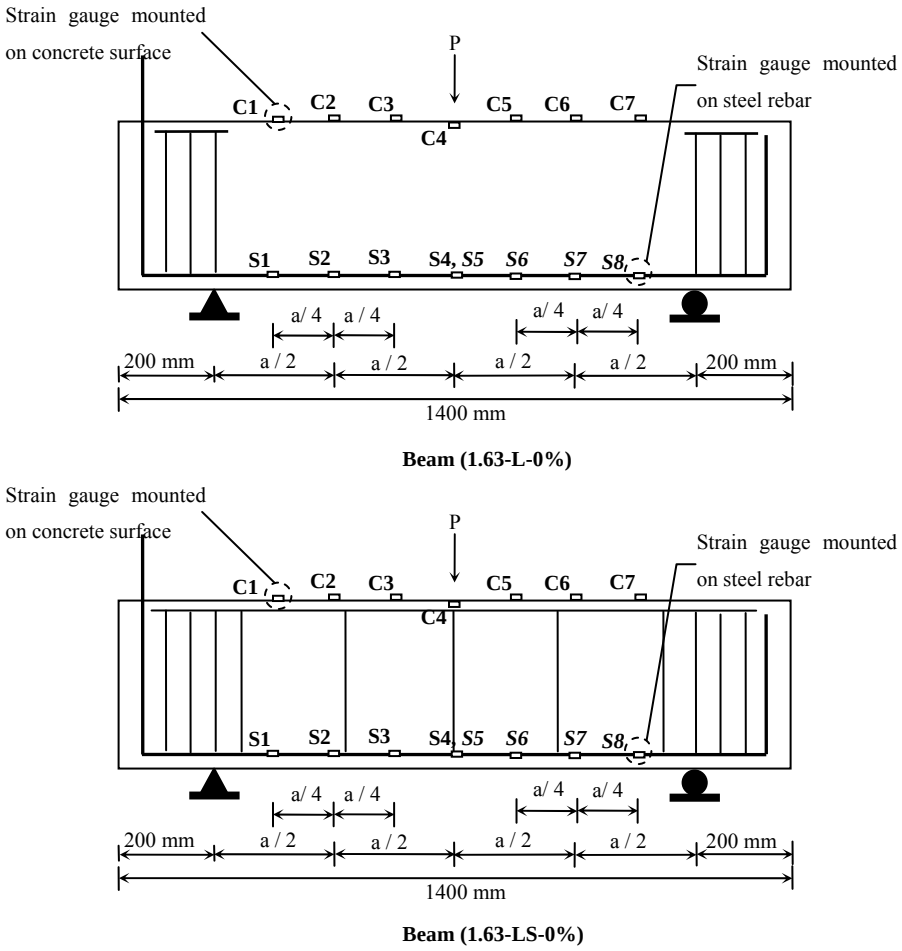

Figure 3.8: Details of strain gauges in deep beams

Two linear variable differential transducers (LVDTs) one at each side of the beam, with a range of 0-25mm, were placed at mid-span to measure the deflection of the beam. The arrangement used to support the LVDT at mid-span is shown in Figure 3.10.

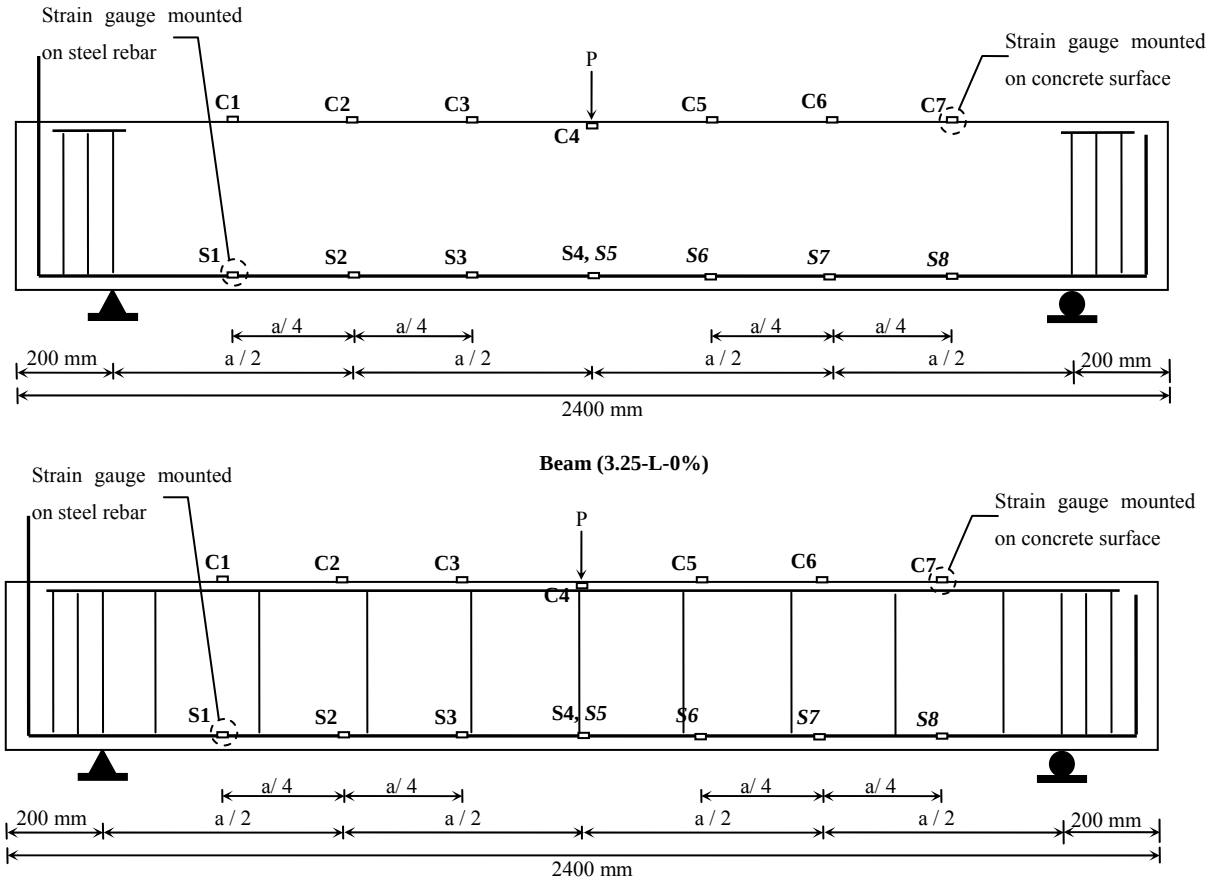

Figure 3.9 : Details of strain gauges in slender beams

3.6 Test Setup and Procedure

The beams were tested in three-point bending using a closed-loop hydraulic MTS actuator with a 500 KN capacity load cell mounted on a Uniroyal test frame. The beams were simply supported over a clear span of 2000 mm and 1000 mm for the slender and deep beams, respectively and loaded with one concentrated load at mid-span as shown in Figure 3.10. The load was applied at a stroke rate of 0.05 mm/min and 0.2 mm/sec for the deep and slender beams, respectively. The load was transferred from the actuator to the beam through a single point loading as shown in Figure 3.10. The loading plate was 100 mm x 150 mm. To uniformly distribute the load, the loading plate was potted to the beam using hydro-stone. The roller and hinge support system used for beams is shown in Figure 3.10.

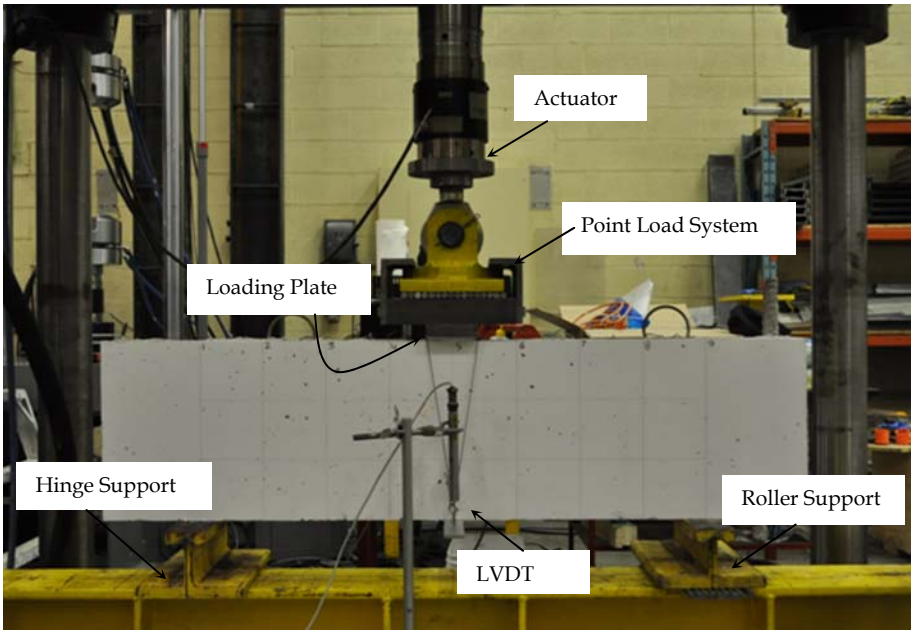

Figure 3.10: Test Setup

The test procedure was as follows: first each beam was placed over supports, leveled and centered under the point load system. Once the beam was leveled and centered, LVDT's were mounted at mid-span under the point load. Then, the instrumentation (LVDT's and strain gauges) was connected to data acquisition system. The data acquisition system started gathering data before the application of load. The load was increased monotonically using a ramp function applied until failure of beam. During the test, the initiation and progression progress of cracks was monitored in order to understand the behaviour of the tested beams.

Chapter 4: Experimental Results

4.1 General

The experimental program consisted of testing twenty shear critical RC beams; ten deep beams and ten slender beams. Test variables studied were corrosion level (0%, 2.5%, 5% and 7.5%), existence of stirrups, and FRP repair. This chapter presents the results of the experimental program.

4.2 Accelerated Corrosion Results

4.2.1 Corrosion Crack Widths and Cracking Pattern

Crack patterns and crack widths, produced by the expansion of the corrosion products were monitored for all corroded beams at final stages of corrosion. To observe the crack width, the beam was divided into a number of zones and crack width measurements were taken from each zone. A CTL crack comparator, which can measure a crack width of at least 0.15mm, was used. The cracking patterns and crack widths of deep beams without stirrups, deep beams with stirrups, slender beams without stirrups and slender beam with stirrups are shown in Figure 4.1, Figure 4.2, Figure 4.3 and Figure 4.4, respectively.

Different types of crack patterns were observed: some beams had two longitudinal cracks, both at the bottom soffit of the beams running parallel to the longitudinal reinforcement; some beams had one crack at the bottom soffit and another crack on the side of the beam; some beams had both the cracks on the sides of the beam (one crack on one side and a second crack on other side of beam); some beams had irregular cracks (cracks starting from the bottom soffit of the beam that moved to the side of the beam). All beams had equal horizontal and vertical cover to the longitudinal reinforcement of 30 mm but the placement of the cage within the formwork may have caused a shift in the cover which may explain the different cracking patterns observed. Another possible reason is that the corrosion products may not have been uniformly distributed around the cross section of the bar, which may explain both the observed side and bottom cracking.

The maximum crack widths in the deep beams without stirrups were 1.0 mm, 1.25 mm and 1.5 mm at 2.5%, 5% and 7.5% theoretical corrosion level, respectively. The maximum crack widths

in the deep beams with stirrups were 0.6 mm, 1.0 mm and 1.5 mm at 2.5%, 5% and 7.5% theoretical corrosion level, respectively. The maximum crack widths in the slender beams without stirrups were 1.0 mm, 1.25 mm and >1.5 mm at 2.5%, 5% and 7.5% theoretical corrosion level, respectively. The maximum crack widths in the slender beams with stirrups were 0.6 mm, 1.25 mm and >1.5 mm at 2.5%, 5% and 7.5% theoretical corrosion level, respectively.

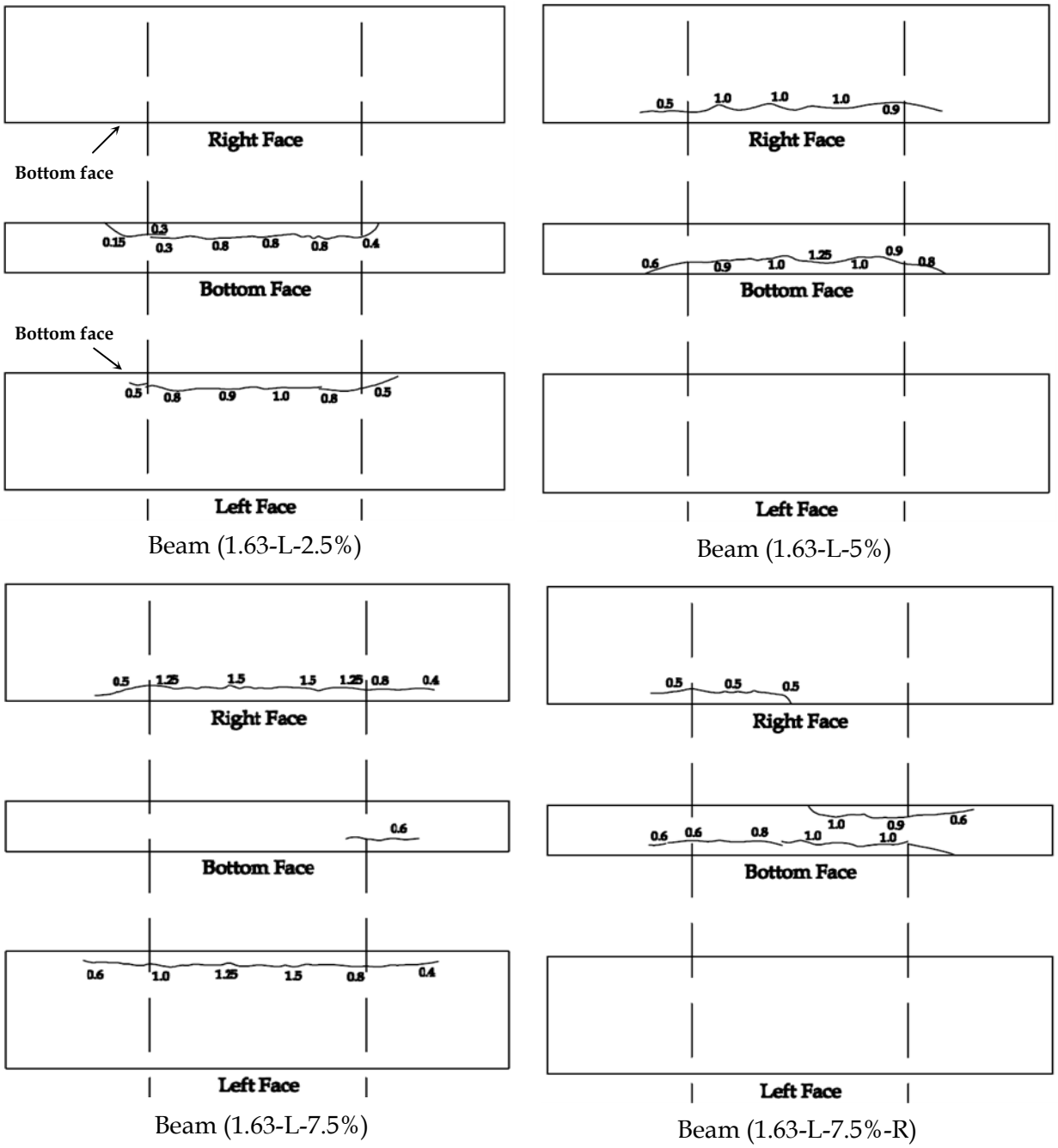

Figure 4.1: Corrosion crack patterns and crack widths of deep beams without stirrups

It is evident that the presence of stirrups reduces the crack widths at low and medium corrosion levels for both slender and deep beams.

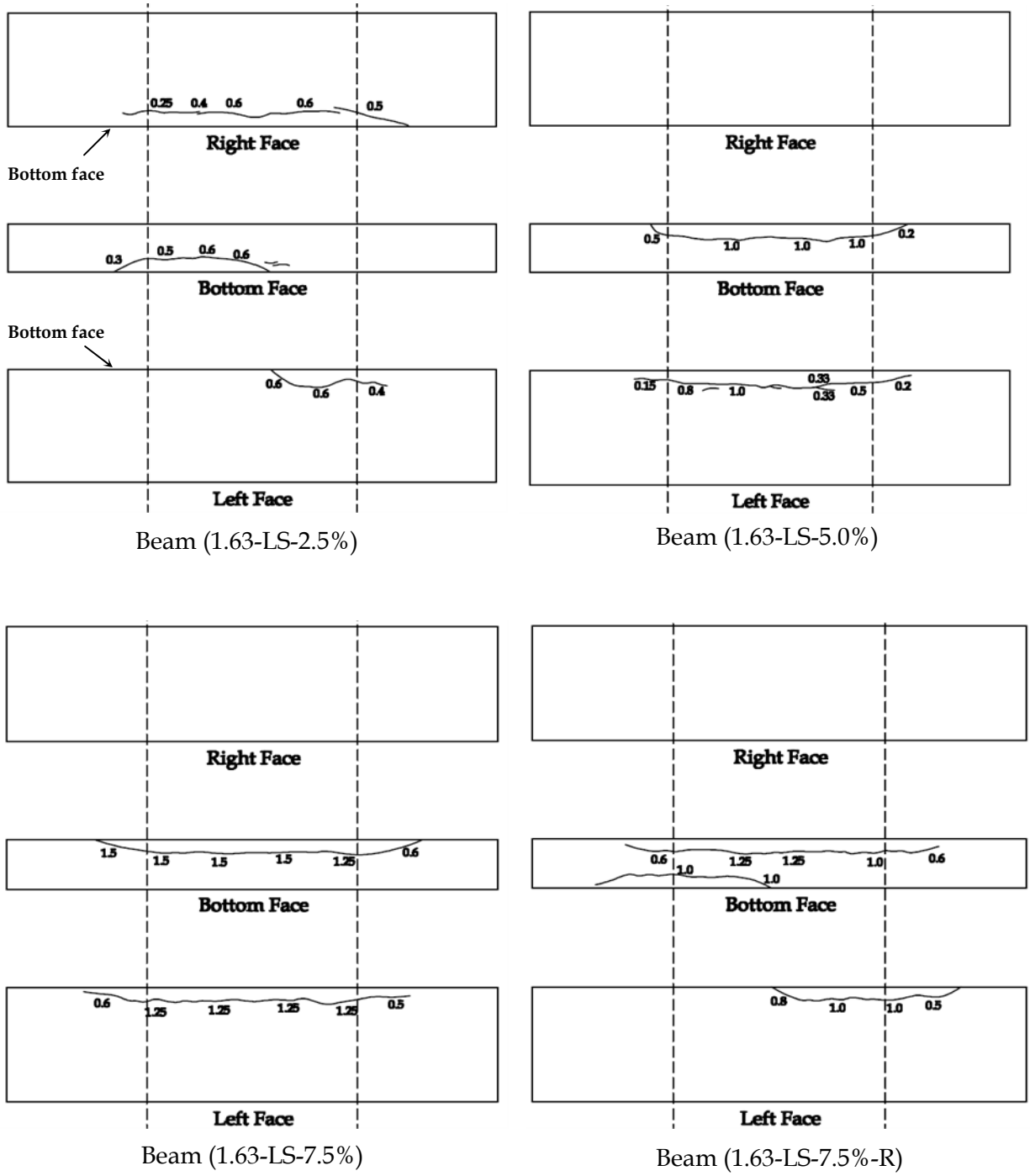

Figure 4.2: Corrosion crack patterns and crack widths of deep beams with stirrups

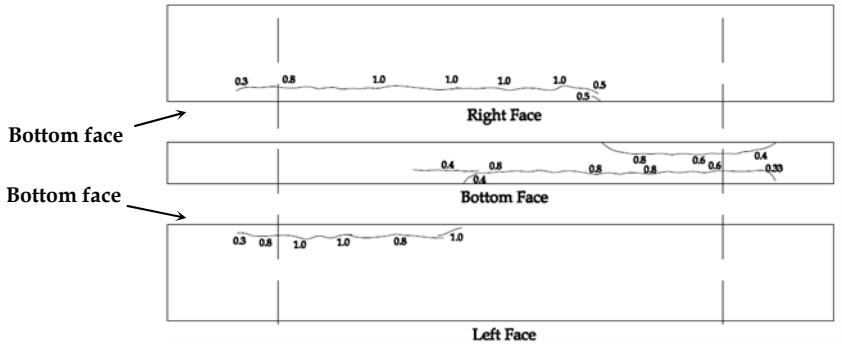

Beam (3.25-L-2.5%)

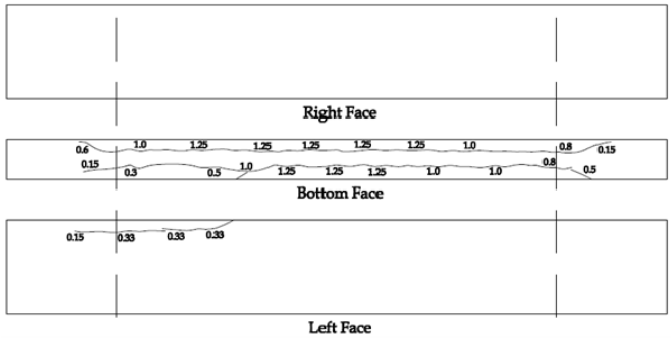

Beam (3.25-L-5.0%)

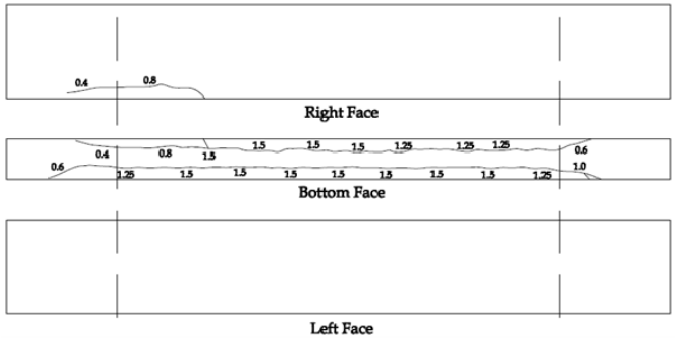

Beam (3.25-L-7.5%)

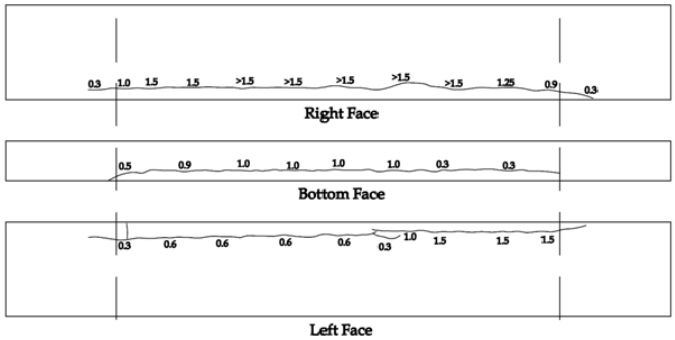

Beam (3.25-L-7.5%-R)

Figure 4.3: Corrosion crack patterns and crack widths of slender beams without stirrups

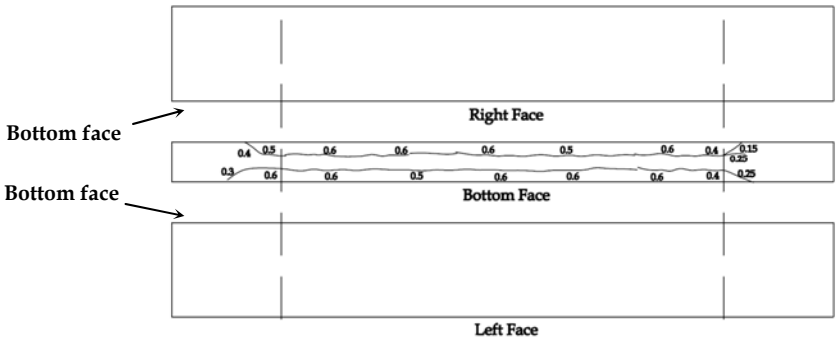

Beam (3.25-LS-2.5%)

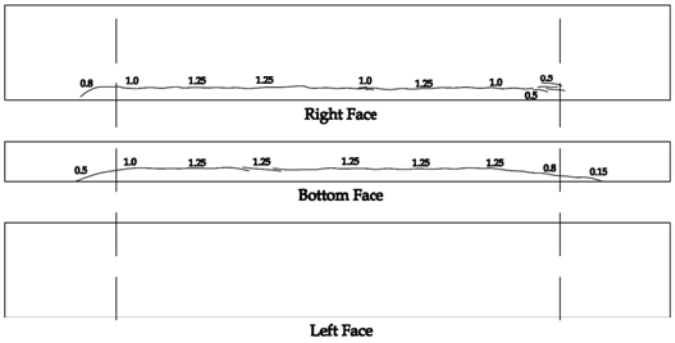

Beam (3.25-LS-5.0%)

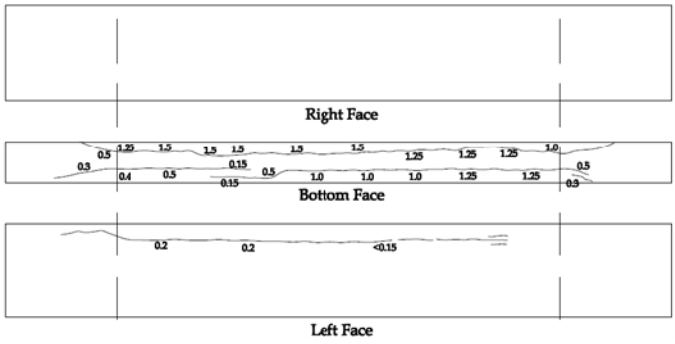

Beam (3.25-LS-7.5%)

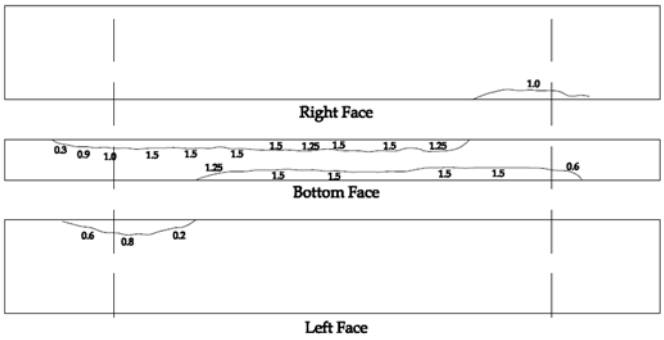

Beam (3.25-LS-7.5%-R)

Figure 4.4: Corrosion crack patterns and crack widths of slender beams with stirrups

4.2.2 Reinforcing Steel Moss Loss

To determine the actual mass loss due to steel reinforcement corrosion, bars were carefully extracted from the corroded beams following the load testing phase. The procedure given in ASTM standard GI, designation C.3.5 was used for the mass loss analysis. Six coupons, three from each bar, of 300 mm length were taken from all corroded slender beams and four coupons, two from each bar, of the 300 mm length were taken from all corroded deep beams. Coupons from the control beams were used as a reference. Figure 4.5 shows the coupons taken from the control bar, the corroded bar and the corroded bar coupon after moss loss analysis.

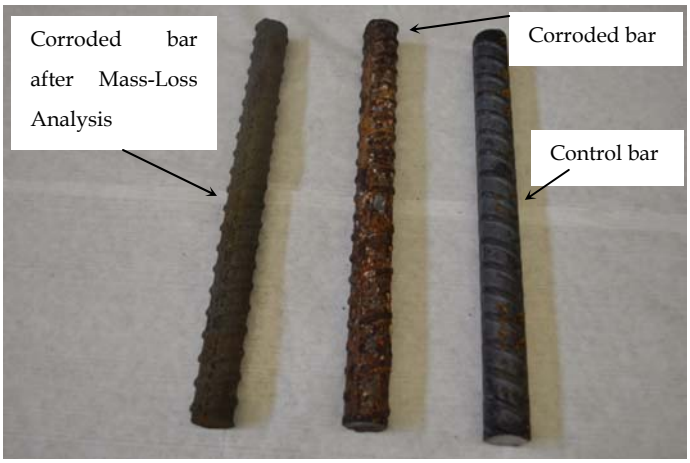

Figure 4.5: Coupons for mass loss analysis

Figure 4.6 shows the average mass loss results for beams with and without stirrups at all three corrosion levels (2.5%, 5.0% and 7.5%). It can be observed from the curve that for lower mass losses, Faraday's law underestimates the mass losses; whereas for higher mass losses it overestimates the steel mass loss due to corrosion. This is explained in the following: at early stages of corrosion (lower corrosion level), the cracks are opened and oxygen and water can easily reach the bar to accelerate the corrosion, whereas at later stages of corrosion (higher corrosion level), the corrosion products build up around the bar and fill the cracks, thus reducing the concentration of oxygen and water around the bar, which ultimately slows down the corrosion rate.

It can also be seen from the curve that the beams with stirrups have relatively lower mass loss compared to beam without stirrups. This is possibly because of larger steel area (longitudinal steel plus stirrups) being polarized, which resulted in lower current density in longitudinal bars. The lower current density might have caused lower steel mass loss in these beams.

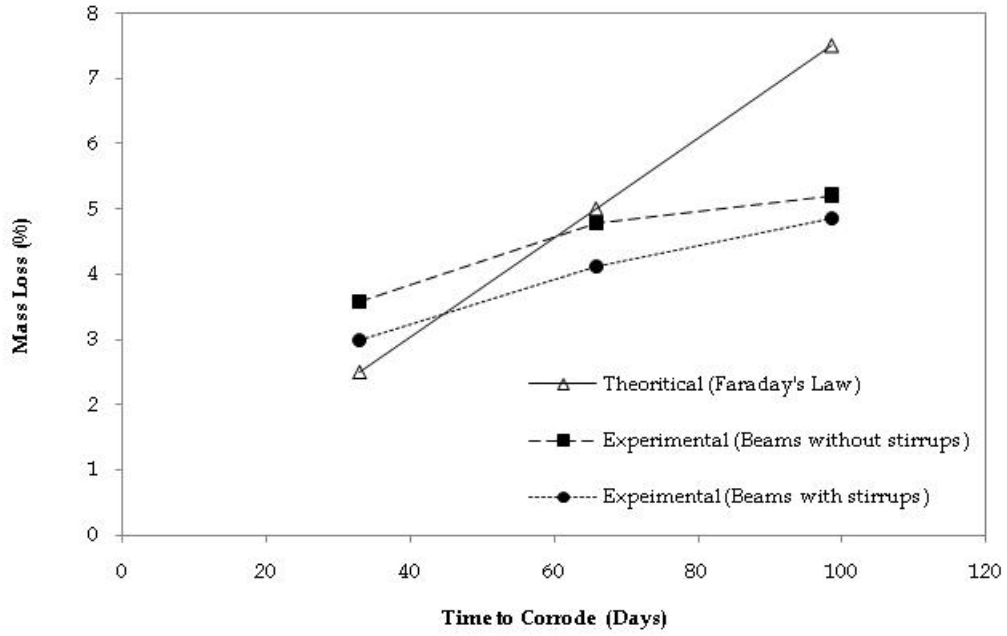

Figure 4.6: Average mass loss vs. time relationship

The average measured mass loss for all beams was 3.3%, 4.5% and 5.1% for 2.5%, 5.0% and 7.5% theoretical mass loss. It is evident that the 7.5% mass loss was not achieved in this study possibly due to the length of exposure which was based on Faraday's law. The comparison of the theoretical and experimental mass losses along with the attack penetration depth is given in Table 4.1. The corrosion mass loss results were consistent with findings of El Maaddawy (2004) and Al-Hammoud (2006).

Table 4.1 : Theoretical and experimental mass loss along with corrosion attack penetration depth

Beam designation	Theoretical moss loss (%)	Experimental moss loss (%)	Corrosion attack penetration depth(mm)
1.63-L-2.5%	2.5%	3.15 ± 0.29	0.20
1.63-L-5.0%	5.0%	4.38 ± 0.40	0.27
1.63-L-7.5%	7.5%	4.64 ± 0.20	0.29
1.63-L-7.5%(R)	7.5%	2.45 ± 0.23	0.15
1.63-LS-2.5%	2.5%	2.69 ± 0.08	0.17
1.63-LS-5.0%	5.0%	3.85 ± 0.45	0.24
1.63-LS-7.5%	7.5%	4.49 ± 0.42	0.28
1.63-LS-7.5%(R)	7.5%	4.47 ± 0.39	0.28
3.25-L-2.5%	2.5%	4.0 ± 0.18	0.25
3.25-L-5.0%	5.0%	5.18 ± 0.41	0.32
3.25-L-7.5%	7.5%	5.78 ± 0.18	0.36
3.25-L-7.5%(R)	7.5%	5.79 ± 0.22	0.36
3.25-LS-2.5%	2.5%	3.28 ± 0.10	0.21
3.25-LS-5.0%	5.0%	4.39 ± 0.26	0.27
3.25-LS-7.5%	7.5%	5.22 ± 0.56	0.33
3.25-LS-7.5%(R)	7.5%	5.38 ± 0.35	0.34

4.3 Monotonic Test Results of Deep Beams

A total of ten shear critical reinforced concrete deep beams, five beams without stirrups and five beams with stirrups were tested monotonically in three-point bending to failure. The ten beams were divided into two series, series A-1: deep beams without stirrups and series A-2: deep beams with stirrups. Each series included five beams: one control, three corroded to 2.5% (light), 5.0% (medium) and 7.5% (high) mass loss and one repaired corroded (7.5% mass loss) beam. The longitudinal reinforcement in the beam was properly anchored with standard 90˚ hook at the support. The reinforcement was only corroded within the span with no corrosion

induced in the anchorage zone. Corrosion was induced only in the longitudinal steel bars. The stirrups in the corroded zone were epoxy coated to prevent their corrosion.

4.3.1 Deep Beams without Stirrups (Series A-1)

4.3.1.1 Control Beam

The load deflection response of the control un-corroded beam (1.63-L-0%) is shown in Figure 4.7. Two distinct stages in the response are evident; the first stage represents the behaviour of the beam before inclined/shear cracking and the second stage represents the behaviour of the beam after inclined/shear cracking up to failure.

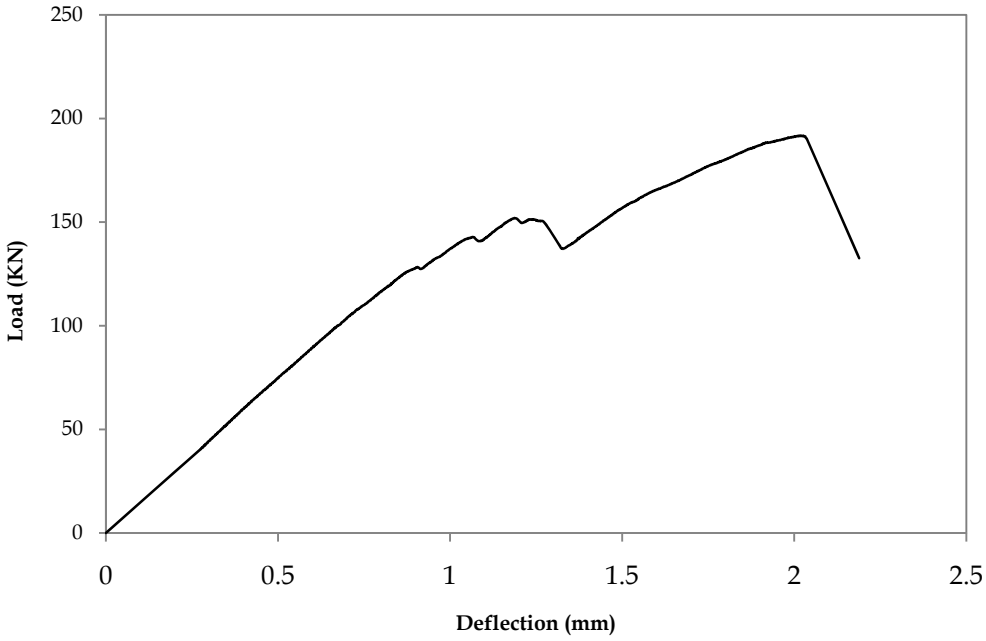

Figure 4.7: Load vs. deflection curve of control beam (series A-1)

The failure mode of the control beam is shown in Figure 4.8. The control beam failed abruptly in shear indicating the brittle nature of this type of failure. The cracking in the control beam was initiated with the appearance of flexural cracks at mid-span under the concentrated load. The load at flexural cracking was 95 kN. As the load increased, an inclined crack appeared in the right shear span at 127 kN accompanied with a slight drop in the load and another inclined crack appeared in the left shear span at 151 kN with a higher drop in the load. After the appearance of the inclined cracks, the beam continued to carry the load until concrete crushing

at the tip of the inclined crack that caused shear-compression failure at a load of 191.6 kN and a mid-span deflection of 2.0 mm.

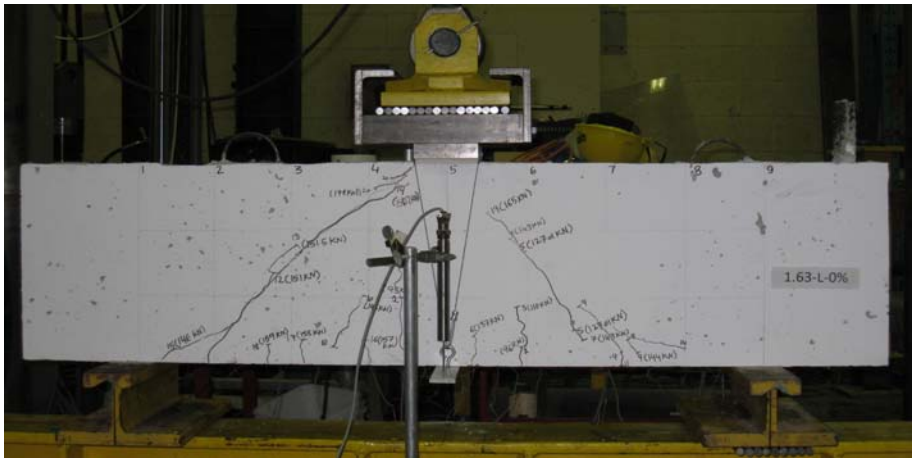

Figure 4.8: Failure mode of control beam (series A-1)

The measured strain profiles in the longitudinal steel reinforcement and on the top concrete surface of the beam are shown in Figure 4.9 and Figure 4.10, respectively. The strain gauge readings are presented for ten loading stages (0.1P to P). Figure 4.9 shows that the strain values in the longitudinal bar varied linearly at early stages of loading (0.1P to 0.7P), as expected according to elementary beam theory. At higher load levels (0.8P to P), the strains in the longitudinal bar were almost constant over the entire clear span of the beam or slightly higher near the supports. This provided evidence of arch action in the beam. At failure, the strain values in steel were below the yield strain and that the strain in concrete was below crushing strain. It is important to note that the inclined crack appeared at 151 kN (0.78P) which changed the load transfer mechanism and the beam started carrying load by arch action.

The strains values in concrete at the top surface of the beam showed a similar trend as shown by the strain values in the reinforcing bar. At early stages of the loading (up to 70% load), the beam behaved according to elementary beam theory. Once, the inclined crack appeared, the beam starting behaving as a tied arch. At higher load level, the longitudinal steel tried to straighten the 90˚ hook on the end of the longitudinal bar in the anchorage zone, which caused tension in the concrete at the top surface of the beam near the support as shown in Figure 4.10.

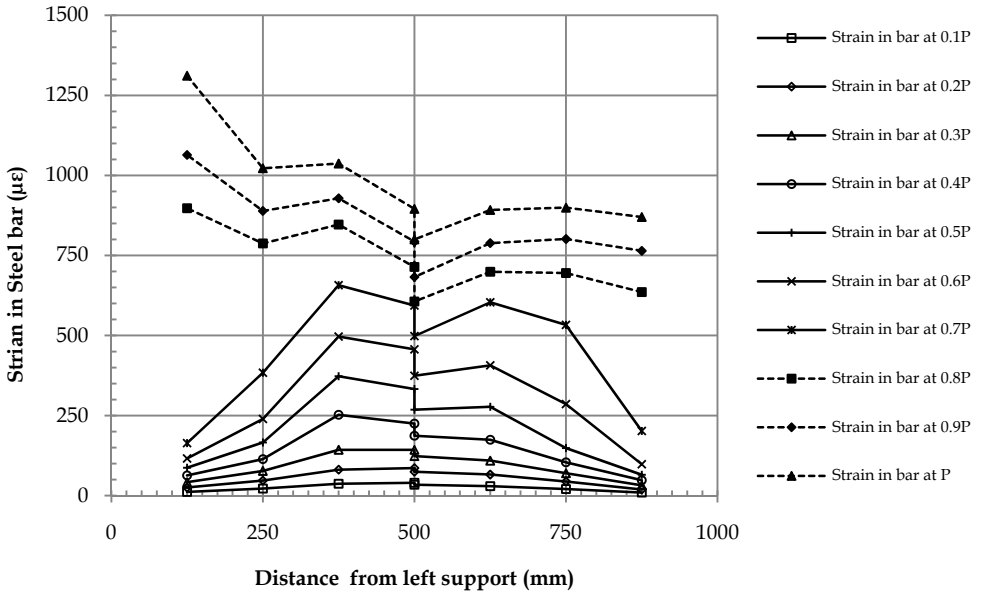

Figure 4.9: Strain profile in the longitudinal bars of control beam (series A-1)

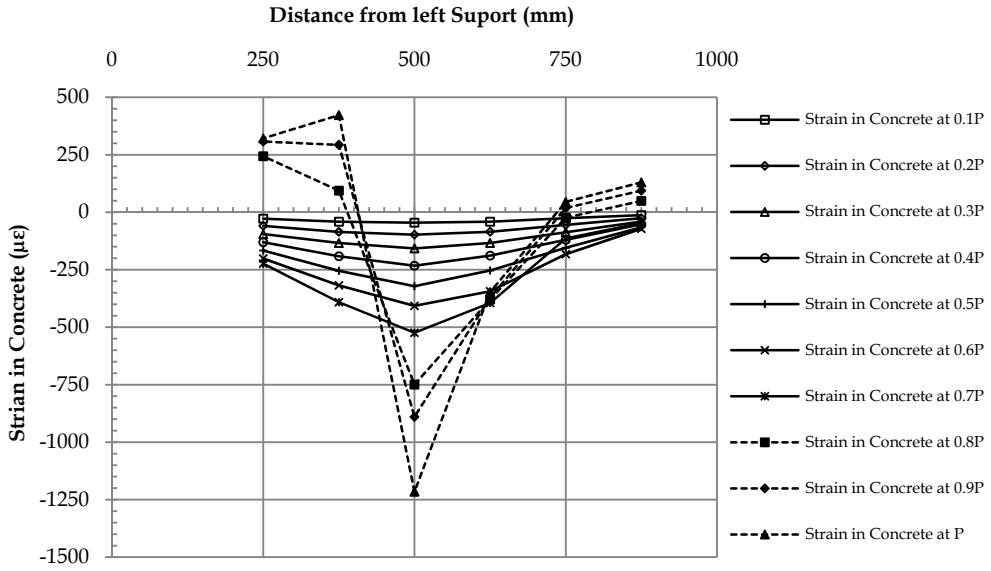

Figure 4.10: Strain profile at top surface of concrete in control beam (series A-1)

4.3.1.2 Corroded Beams

The load deflection curves of all corroded beams (1.63-L-2.5%, 1.63-L-5.0% and 1.63-L-7.5%) are shown in Figure 4.11. The load deflection response of the corroded beams can be expressed by two distinct stages; the first stage represents the behaviour of the beam before flexural cracking and the second stage represents the behaviour of the beam after flexural cracking until failure.

The stiffness reduction in corroded beams occurred at onset of flexural cracking while the stiffness reduction in the control beams occurred at the onset of inclined/shear cracking.

The failure modes of the corroded beams are shown in Figure 4.12. All corroded beams failed suddenly by the formation of a shear crack between the load point and the support. Cracking initiated as flexural cracks at mid-span under the concentrated load. The flexural cracking load for the corroded beams ranged from 94 to 96 kN.

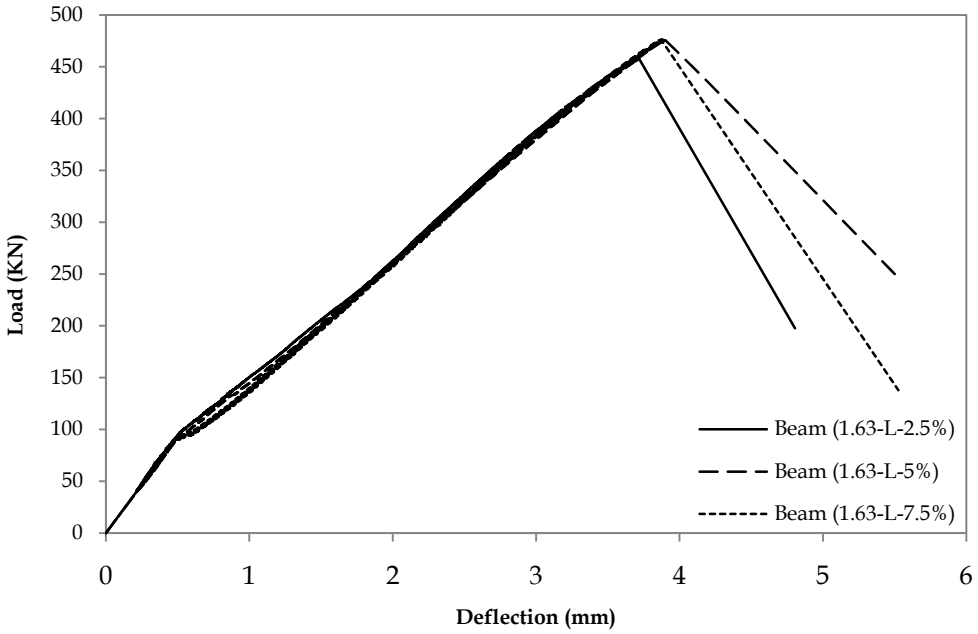

Figure 4.11: Load vs. deflection curves of corroded beams (series-A-1)

The beam with a low corrosion level (1.63-L-2.5%) had two main flexural cracks at mid-span, which progressed towards the compression zone as the load increased. After a load of 260 kN, these cracks stopped progressing towards the compression zone and no additional cracks appeared. Widening of the horizontal cracks due to corrosion was observed. The beam failed suddenly in shear with a diagonal crack starting from the load point to the support at a load of 459.3 kN and a mid-span deflection of 3.7 mm.

(a)

(b)

(c)

Figure 4.12: Failure mode of corroded beams (a) (1.63-L-2.5%), (b) (1.63-L-5.0%) and (c) (1.63-L-7.5%)

The beam with medium corrosion level (1.63-L-5.0%) had one main flexural crack that progressed towards the compression zone as the load increased and simultaneously horizontal

cracks appeared which progressed towards the support. This beam had corrosion cracks on the soffit and back face and no corrosion cracks on the beam face. The horizontal cracks reached the support at a load of 210 kN but the flexural crack kept progressing towards the compression zone until it reached the same height as in the beam with the low corrosion level at a load of 222 kN. After a load of 222 kN, no further crack appeared and widening of horizontal cracks was observed. The beam failed suddenly in shear with the formation of a diagonal crack starting from the load point to the support at a load of 476.4 kN and a deflection of 3.9 mm.

The beam with high corrosion level (1.63-L-7.5%) also had one main flexural crack that progressed towards the compression zone as the load increased. The flexural crack reached the same height as the beams with low and medium corrosion levels at a load of 191 kN and the flexural crack stopped progressing towards the compression zone. After 191 kN no further cracks appeared except a horizontal crack which appeared above an existing horizontal crack due to corrosion and progressed from the mid-span to the support at a load of 320 kN. The beam failed suddenly in shear with the formation of a diagonal crack starting from the load point to the support at a load of 476.2KN and a mid-span deflection of 3.88 mm.

4.3.1.3 FRP Repaired Corroded Beam

The load deflection response and failure mode of the FRP repaired corroded beam (1.63-L-7.5 %- R) is shown in Figure 4.13 and Figure 4.14 respectively. Two distinct stages are evident from the load deflection curve shown in Figure 4.13; the first stage represents the behaviour of the beam before flexural cracking and the second stage represents the behaviour the beam after flexural cracking up to failure. The FRP-repaired beam failed in a similar manner as the corroded beams except that due to the confinement provided by the FRP U-wrap, the failure crack was delayed and the FRP repaired corroded beam exhibited a slight increase in ultimate failure load. The beam failed at a load of 497 kN and a mid-span deflection of 3.4 mm.

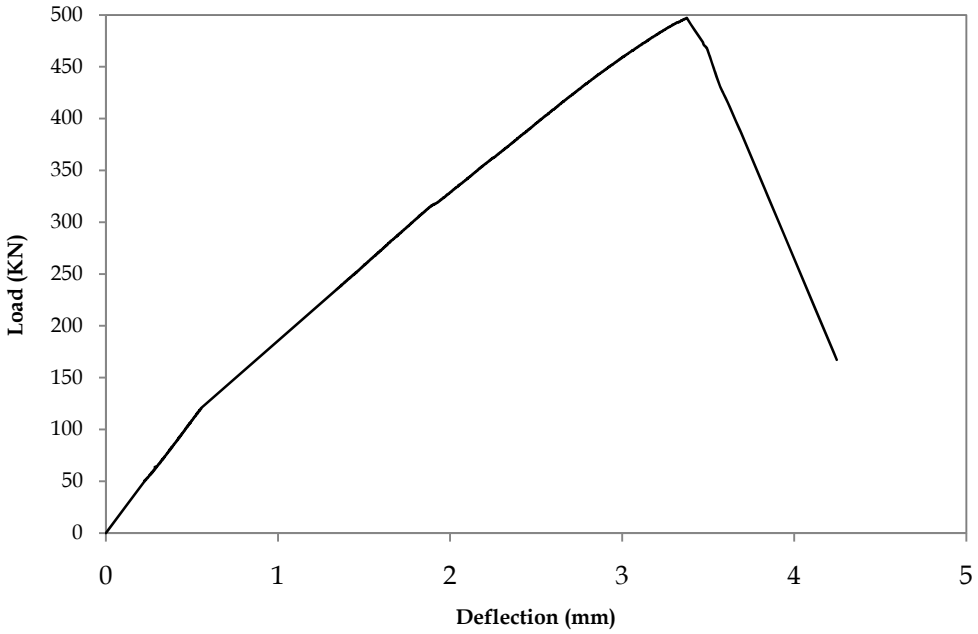

Figure 4.13: Load vs. deflection curve of repaired corroded beam (series A-1)

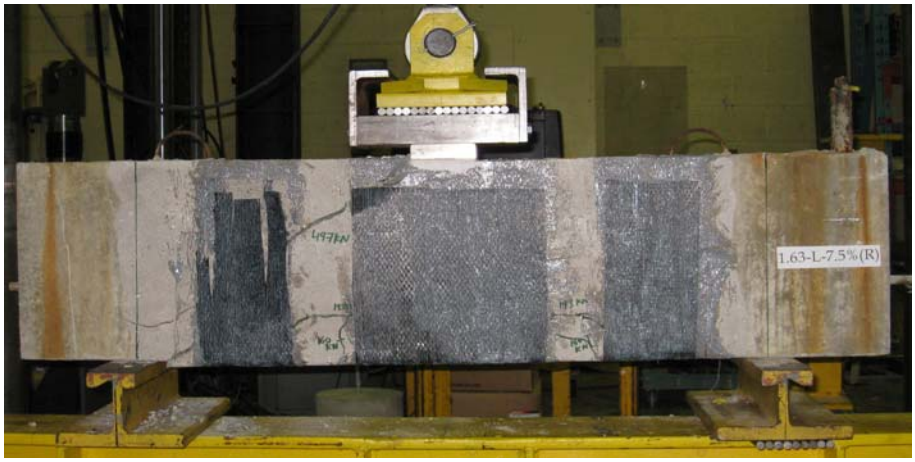

Figure 4.14: Failure mode of FRP repaired corroded beam (1.63-L-7.5%-R)

4.3.2 Deep Beams with Stirrups (Series A-2)

4.3.2.1 Control Beam

The load deflection response of the control un-corroded beam (1.63-LS-0%) is shown in Figure 4.15. Two distinct stages are evident; the first stage represents the behaviour of the beam before inclined/shear cracking and the second stage represents the behaviour of the beam after inclined/shear cracking up to failure.

The failure mode of the control beam is shown in Figure 4.16. The control beam failed abruptly in shear indicating the brittle nature of this type of failure. The cracking in the control beam was initiated with the appearance of flexural cracks at mid-span under the concentrated load. The flexural cracking load was 92 kN. As the load increased, an inclined crack appeared in the right shear span at a load of 124 kN and another inclined crack appeared in the left shear span at a load of 146 kN. There was a slight drop in the measured load upon the appearance of these inclined cracks. Both inclined cracks kept progressing towards the load point as well as the support. Inclined cracks reached the supports at a load of 187 kN but kept progressing towards the load point until a load of 205 kN. After 205 kN, no additional cracks appeared and the beam kept carrying the load until concrete crushing occurred at the tip of the inclined crack which caused shear-compression failure at a load of 418.4 kN and a mid-span deflection of 3.9 mm.

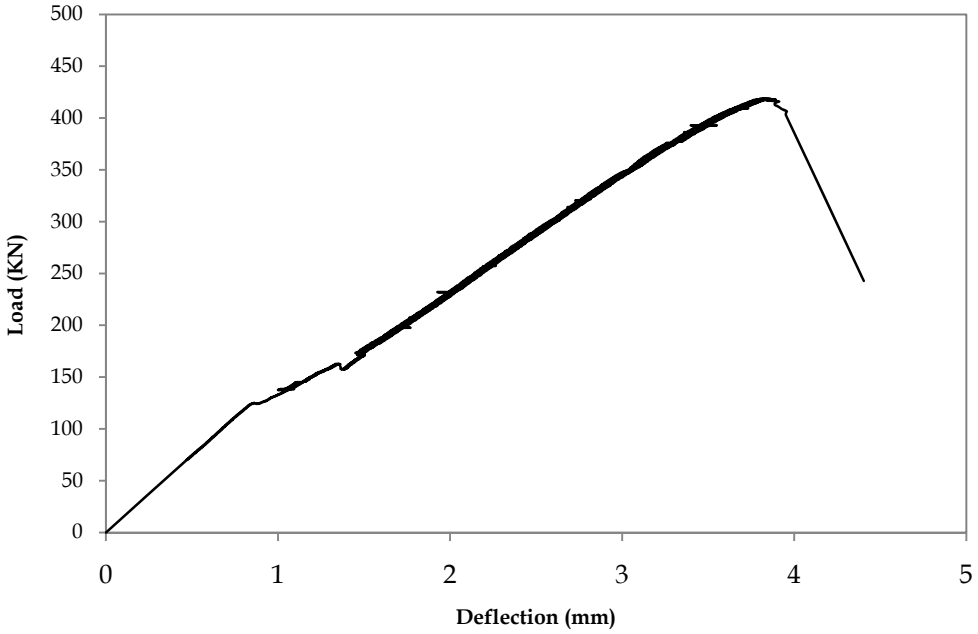

Figure 4.15: Load vs. deflection curve of control beam (series A-2)

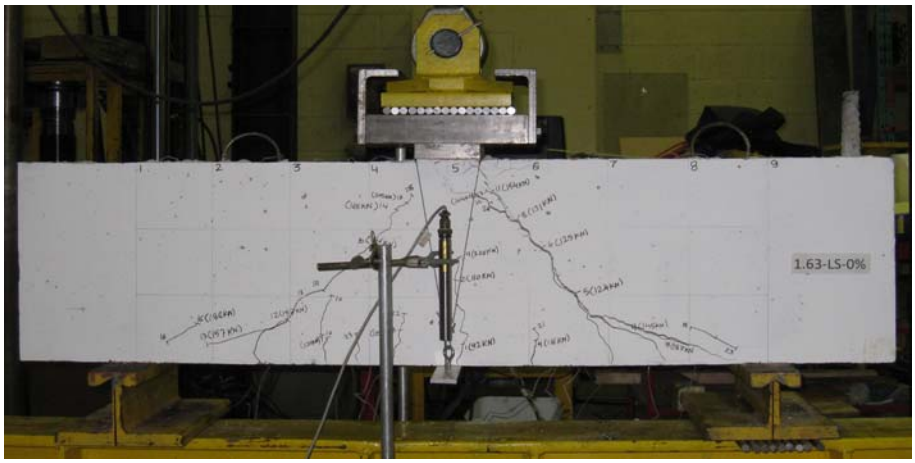

Figure 4.16: Failure mode of control beam (series A-2)

Figure 4.17 and Figure 4.18 shows the measured strain profiles in longitudinal steel reinforcement and on the top concrete surface of the beam. The strain gauge readings are presented for ten loading stages (0.1P to P). The strain values in the longitudinal bar varied linearly as expected according to elementary beam theory until the inclined cracks appeared at 146 kN (0.35P) as shown in Figure 4.17. After the appearance of inclined cracks, the strains in the longitudinal bars were almost constant over the entire clear span of the beam or slightly higher near support. This provided the evidence of the arch action in the beam. At failure, the strain values in steel were close to the yield strain and the strain in concrete at mid-span was close to the crushing strain.

The strain values in the concrete at the top surface of the beam showed a similar trend as shown by the strain values in the reinforcing bar. At lower load levels (up to 30% load), the beam behaved according to elementary beam theory. Once, the inclined crack appeared, the beam behaved as a tied arch. At higher load levels, the longitudinal steel tried to straighten the 90˚ hook on the end of the end of the longitudinal bar, which caused tension in the top surface of concrete near the support as shown in Figure 4.18.

The strain gauge data indicate that in control deep beams (with and without stirrups), the load transfer mechanism changed from beam action to arch action at onset of inclined cracking (the inclined cracking loads for both control deep beams with and without stirrups are approximately the same at 146 kN and 151 kN, respectively). However, after cracking, the contribution of arch action in control deep beam with stirrups is higher (65 % of the total load) as compared to control deep beam without stirrups (22% of the total load).

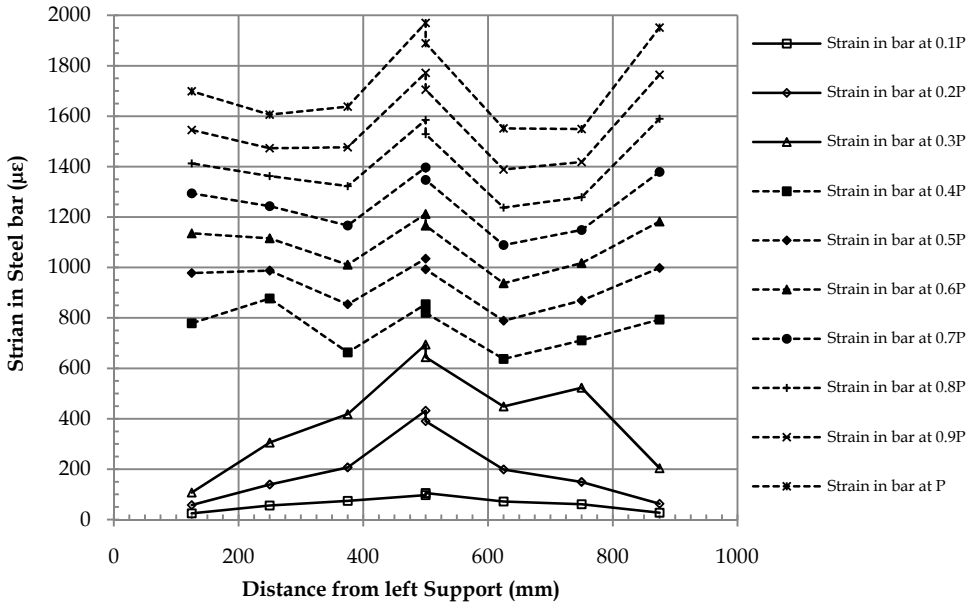

Figure 4.17: Strain profile in the longitudinal bars of control beam (series A-2)

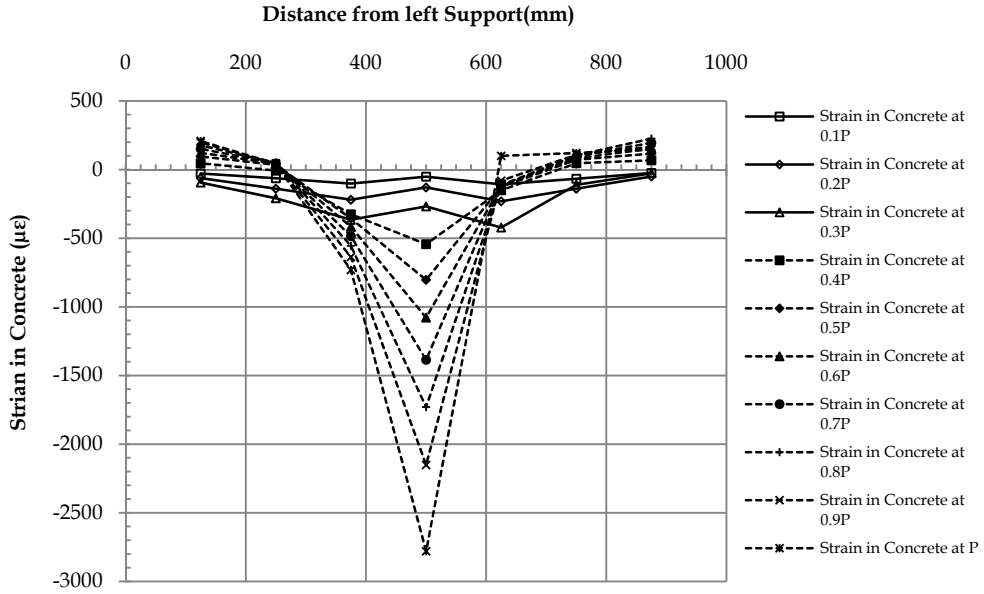

Figure 4.18: Strain profile at top surface of concrete in control beam (series A-2)

4.3.2.2 Corroded Beams

The load deflection curves of the corroded beams with medium and high corrosion level (1.63-LS-5.0% and 1.63-LS-7.5%) are shown in Figure 4.19. The beam with a low corrosion level (1.63-LS-2.5%) had an anomaly response due to problems possibly during casting which resulted in

corrosion over part of the shear span and hence, the results of this beam are not presented in this section.

Two distinct stages are evident from the load-deflection curves shown in Figure 4.19 ; the first stage represents the behaviour of the beam before flexural cracking and the second stage represents the behaviour of the beam after flexural cracking up to failure. The stiffness reduction in the corroded beams occurred at the onset of flexural cracking, while, the stiffness reduction in the control beam occurred at the onset of inclined/shear cracking. The failure modes of the corroded beams are shown in Figure 4.20. Corroded beams failed suddenly with the appearance of a diagonal crack starting from the load point to the support. The cracking in the corroded beams was initiated as flexural cracks at mid-span under the concentrated load. The flexural cracking loads for beam (1.63-LS-5.0%) and beam (1.63-LS-7.5%) were 90 kN and 94 kN, respectively.

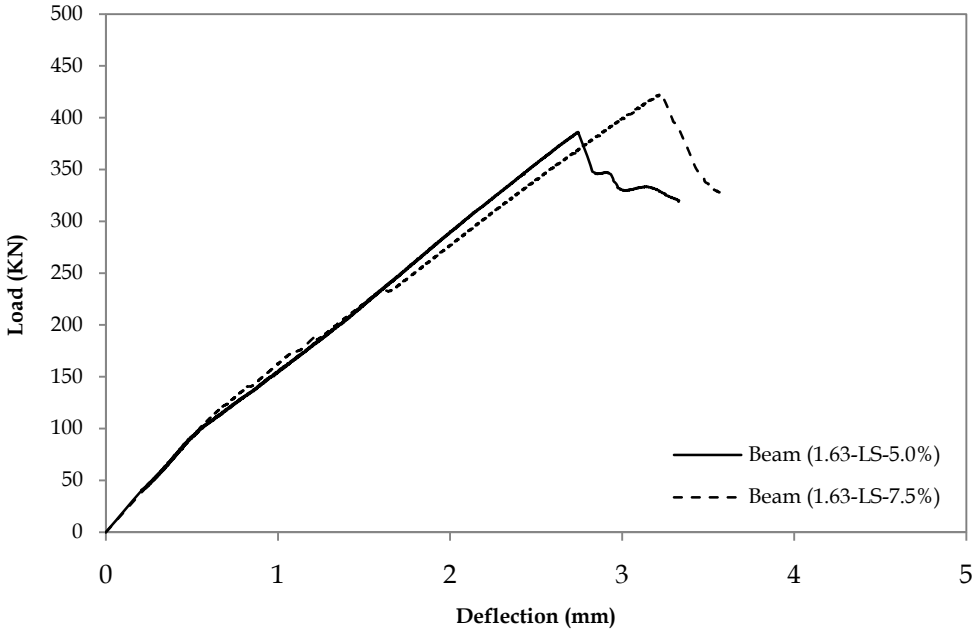

Figure 4.19: Load vs. deflection curves of corroded beams (series-A-2)

The beam with medium corrosion level (1.63-LS-5.0%) had two main flexural cracks that progressed towards the compression zone as the load increased and simultaneously the horizontal corrosion cracks increased in width (this beam had corrosion cracks on beam face). After reaching a load level of 300 kN, flexural cracks stopped progressing towards the compression zone. After 300 kN, no additional cracks were observed. The beam failed suddenly

in shear with the appearance of a diagonal crack that started from the load point to the support at a load of 386 kN load and a deflection of 2.7 mm.

The beam with high corrosion level (1.63-LS-7.5%) had one main flexural crack that progressed towards the compression zone as the load increased. After reaching a load level of 155 KN, the flexural crack stopped progressing toward the compression zone. At a load of 186 KN, a shear crack appeared in the left shear span and at a load of 238 KN a shear crack appeared in the right shear span. These two shear cracks kept progressing towards the compression zone until a load of 380 KN. At a load of 400 KN, horizontal cracks appeared in the right span extending the shear crack to the support. After a load of 400KN no additional cracks appeared. The beam failed suddenly in shear with the appearance of a diagonal crack starting from the load point to the support at a load of 423 KN load and a deflection of 3.2 mm.

(a)

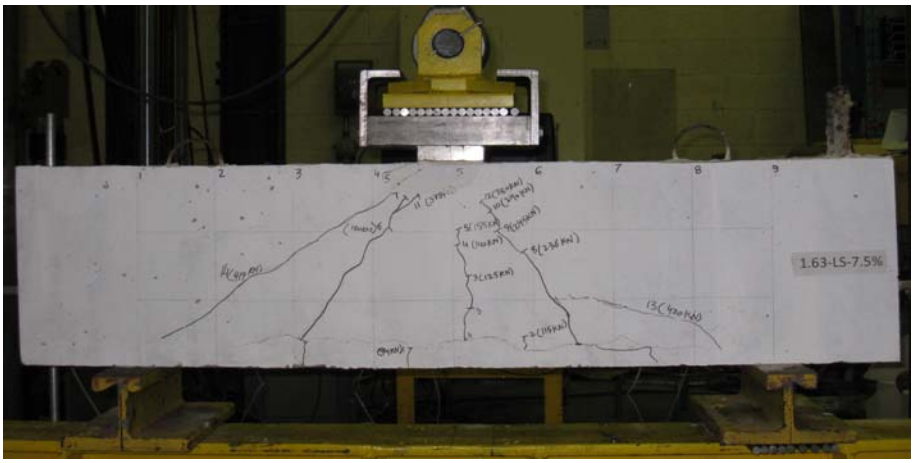

(b)

Figure 4.20: Failure modes of corroded beams (a) (1.63-LS-5.0%), (b) (1.63-LS-7.5%)

4.3.2.3 FRP Repaired Beam

The load deflection response and failure mode of FRP repaired beam (1.63-LS-7.5 %-R) is shown in Figure 4.21 and Figure 4.22 respectively. Two distinct stages are evident from the load deflection curve shown in Figure 4.21; the first stage represents the behaviour of the beam before flexural cracking and the second stage represents the behaviour of the beam after flexural cracking until failure. The FRP-repaired corroded beam failed in a similar manner as the corroded beams; however, due to the confining effect of the FRP U-wrap, the failure crack was delayed and the beam exhibited a slight increase in ultimate failure load. The first drop in the load deflection curve indicates splitting of the strut and the second drop indicates the debonding of the FRP wrap. The beam failed at a load of 447 kN and a deflection of 3.5 mm.

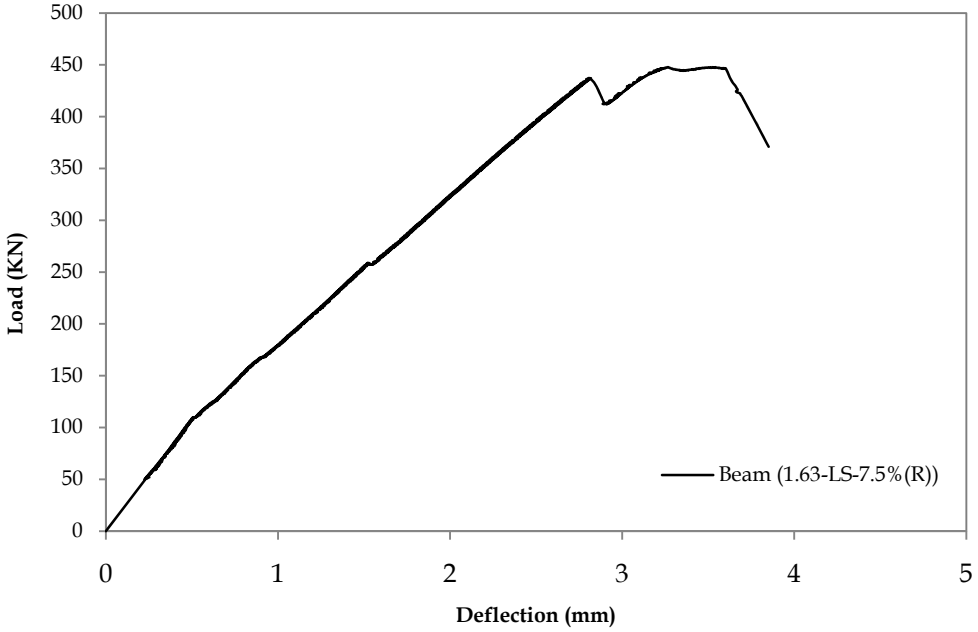

Figure 4.21: Load vs. deflection curve of FRP repaired corroded beam (series A-1)

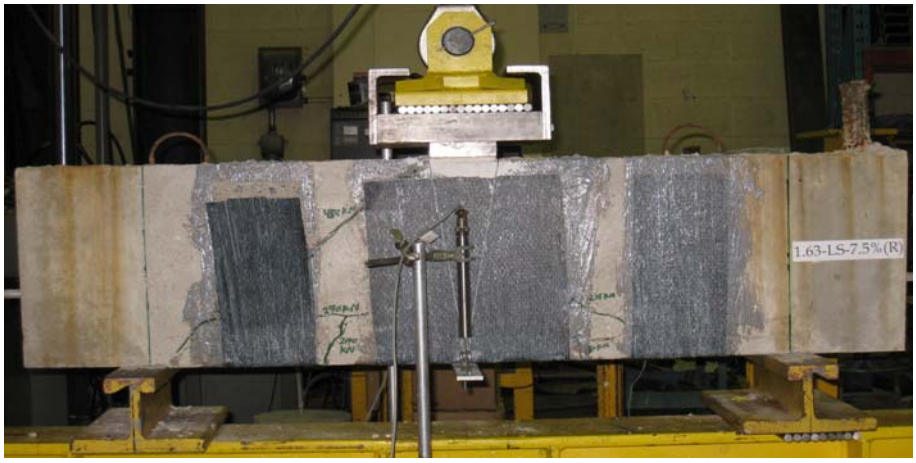

Figure 4.22: Failure Mode of FRP Repaired Beam (1.63-LS-7.5 %- R)

4.4 Monotonic Test Results of Slender Beams

A total of ten shear critical reinforced concrete slender beams were tested to failure. The ten beams were divided into two series, series B-1: slender beams without stirrups and series B-2: slender beams with stirrups. Each series included five beams: one control, three corroded three corroded to 2.5% (light), 5.0% (medium) and 7.5% (high) mass loss and one repaired corroded (7.5% mass loss) beam. The longitudinal reinforcement in the beam was properly anchored with a standard 90˚ hook at the support. The reinforcement was only corroded within the span and no corrosion was induced in the anchorage zone. Corrosion was induced only in longitudinal bars. The stirrups in the corroded zone were epoxy coated to prevent their corrosion.

4.4.1 Slender Beams without Stirrups (Series B-1)

4.4.1.1 Control Beam

The load deflection response of the control beam (3.25-L-0%) is shown in Figure 4.23. The load deflection response of the control beam exhibited fairly linear behaviour from zero-load up until failure by inclined cracking.

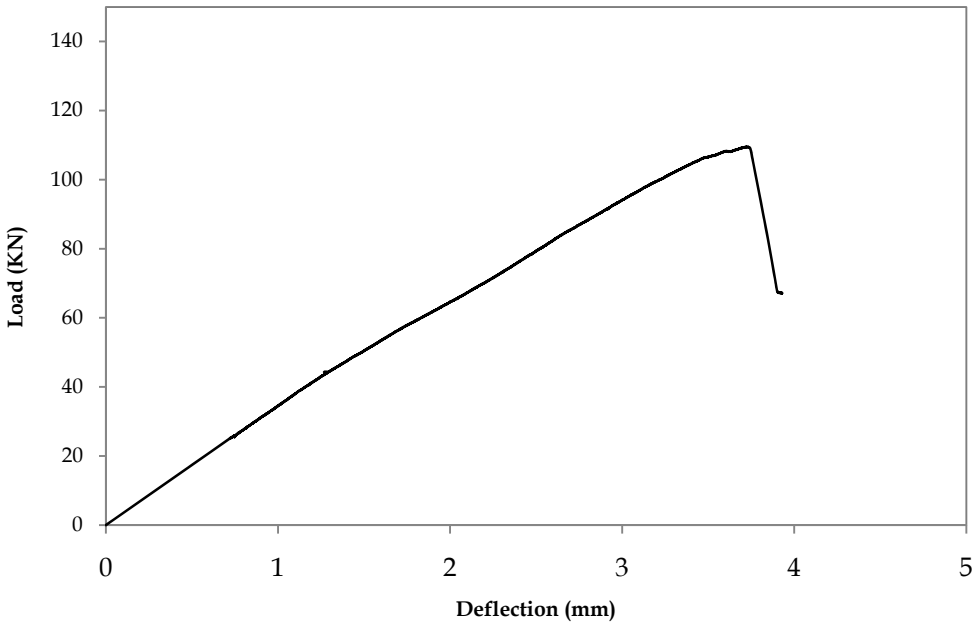

Figure 4.23: Load vs. deflection curve of control beam (series B-1)

The failure mode of the control beam is shown in Figure 4.24. The control beam failed abruptly in shear indicating the brittle nature of this type of failure. The cracking in the control beams was initiated with the appearance of flexural cracks at mid-span under the concentrated load. The flexural cracking load was 46 kN. As the load increased, an inclined crack appeared in the shear span which progressed towards the load point and the support, leading to a diagonal tension failure at a load of 109 kN and a deflection of 3.7 mm.

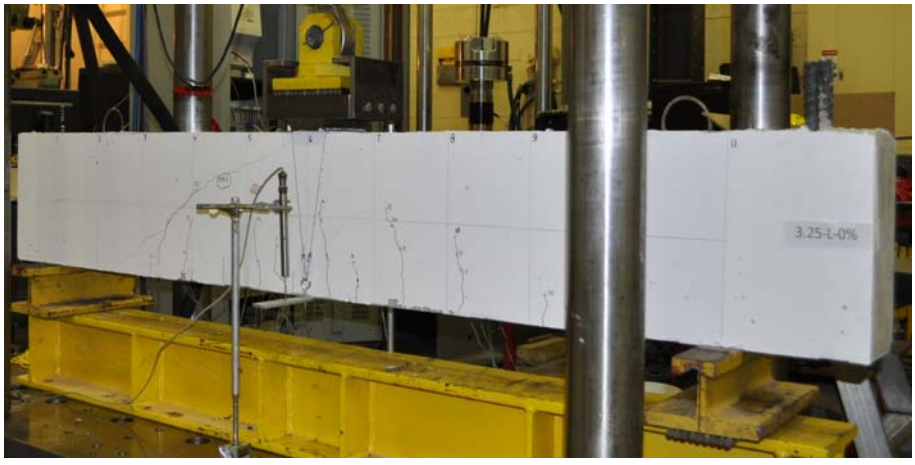

Figure 4.24: Failure mode of control beam (series B-1)

The strain profiles in longitudinal steel and on top concrete surface of the beam measured during test are shown in Figure 4.25 and Figure 4.26.

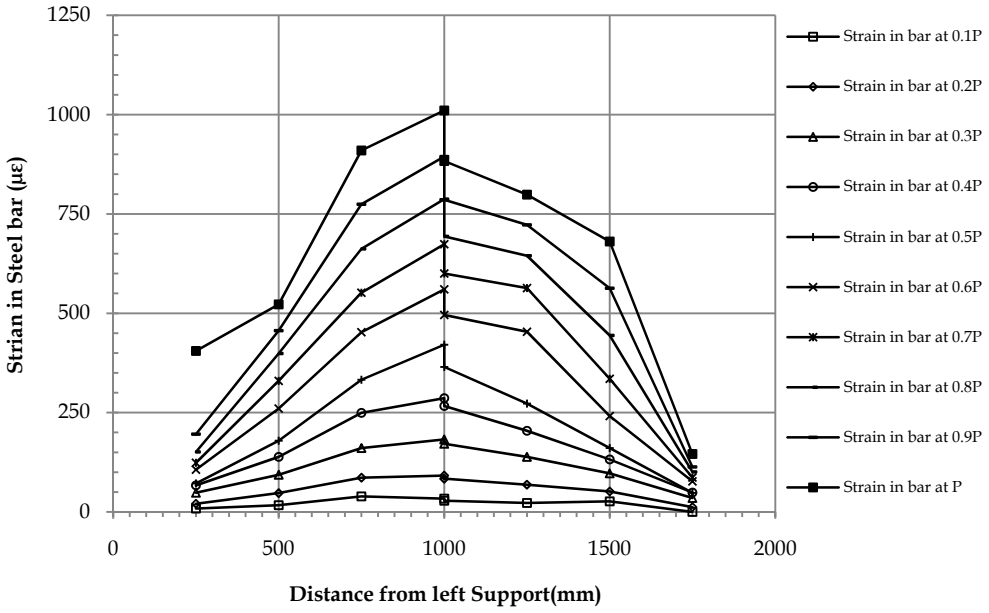

Figure 4.25: Strain profile in the longitudinal bars of control beam (series B-1)

The values of the strains in the longitudinal bar and the concrete indicated that beam theory was valid up to the failure load for slender beams as the strains were higher in the middle of the beam and lower near the supports. The strains in the tension steel were lower than the yield strain and strains in the concrete were lower than the crushing strain. The strain gauge data indicate that the slender beam carried 100% load by beam action.

Strain gauges were mounted on two longitudinal steel bars in such a way that each bar had strain gauges attached over half the rebar length between the support and mid-span of the beam. The variation in the strain gauge data in the left span as compared to right span may be due to different cracking patterns between the two faces of the beam.

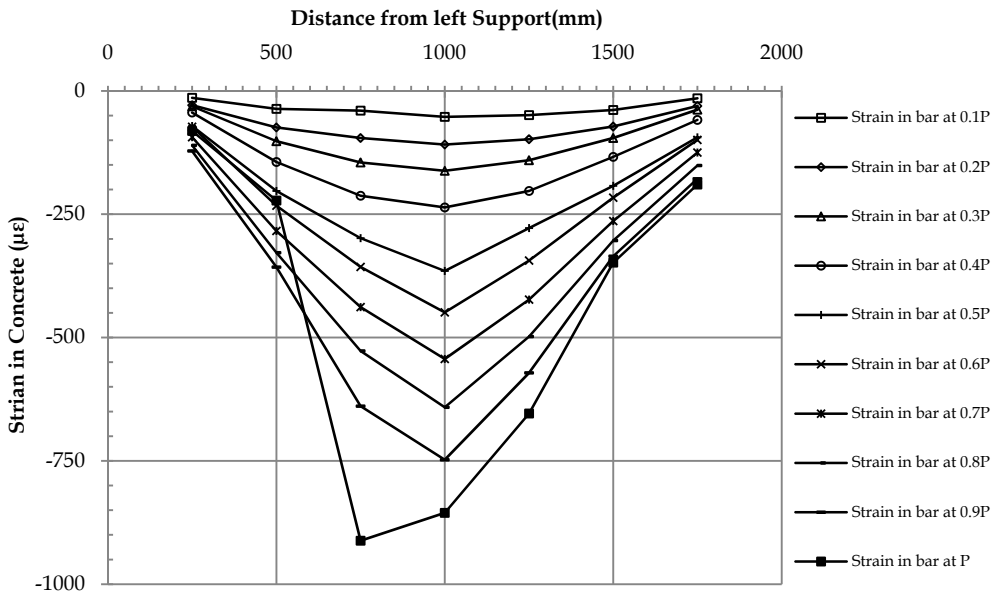

Figure 4.26: Strain profile at top surface of concrete in control beam (series B-1)

4.4.1.2 Corroded Beams

The load deflection curves of the corroded beams (3.25-L-2.5%, 3.25-L-5.0% and 3.25-L-7.5%) are shown in Figure 4.27. Two distinct stages are evident from the load-deflection curves shown in Figure 4.19 ; the first stage represents the behaviour of the beam before flexural cracking and the second stage represents the behaviour of the beam after flexural cracking until failure. The stiffness reduction in the corroded beams occurred at the onset of flexural cracking while there was no stiffness reduction in the control beams at the onset of flexural cracking.

The failure modes of the corroded beams are shown in Figure 4.28. All corroded beams failed similarly by a sudden appearance of a vertical crack near the support causing an anchorage failure. The cracking in the corroded beams was initiated as flexural cracks at mid-span under the concentrated load. The flexural cracking load for all corroded beams ranged between 42 to 45 kN.

The beam with low corrosion level (3.25-L-2.5%) had two main flexural-shear cracks near mid-span, which progressed towards the compression zone and towards the support as the load increased. When the cracks reached the support a sudden vertical crack appeared at the top surface of the beam near the support at a load of 172 kN. The beam continued to carry the load until the vertical crack propagated into the support region causing an anchorage failure at a load of 206 kN and a deflection of 12 mm.

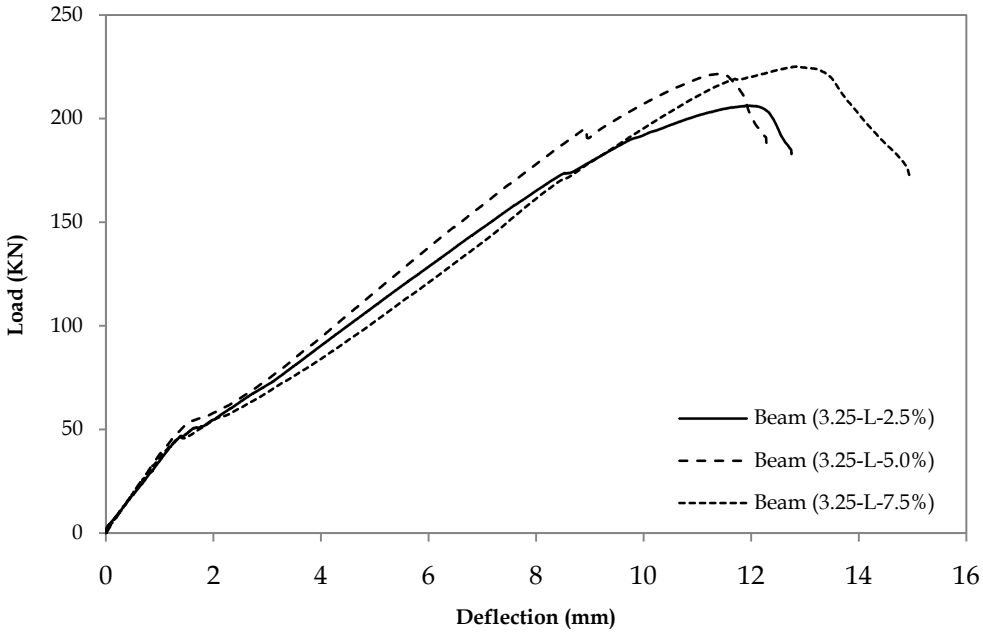

Figure 4.27: Load vs. deflection curves of corroded beam (series B-1)

The beam with medium corrosion level (1.63-L-5.0%) also had two main flexural-shear cracks near the mid-span, which progressed upwards towards the compression zone, and laterally towards the supports with increasing load. At a load level of 161 kN, the cracks stopped progressing towards the compression zone but kept moving towards the support. When the cracks reached the support, a sudden vertical crack appeared at the top surface of the beam near the support at a load of 190 kN. The beam continued taking load until the vertical crack propagated into the support region causing anchorage failure at a load of 222 kN and a deflection of 11.4 mm.

The beam with high corrosion level (1.63-L-7.5%) had one main flexural crack, which progressed upward into the compression zone with increasing load. Simultaneously, horizontal cracks appeared which started progressing towards the support with increasing load. At a load of 135 KN, the flexural crack stopped progressing towards the compression zone but the horizontal cracks kept moving towards the support. When the horizontal cracks just reached the support, a vertical crack appeared at the top surface of the beam near the support at a load of 170 kN. The beam continued taking load until the vertical crack propagated into the support zone causing anchorage failure at a load of 225 kN and a deflection of 12.9 mm.

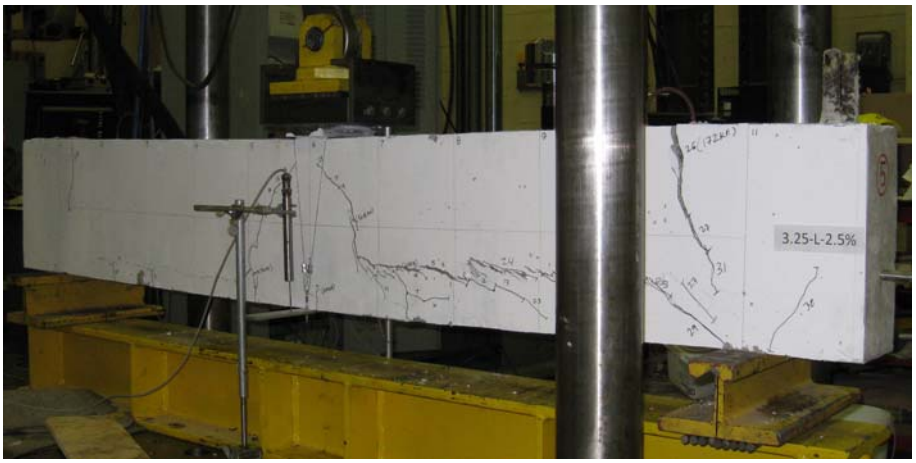

(a)

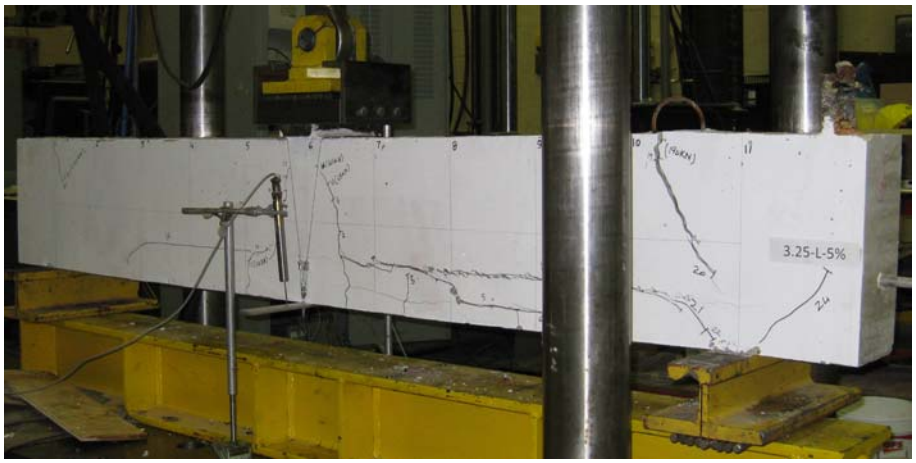

(b)

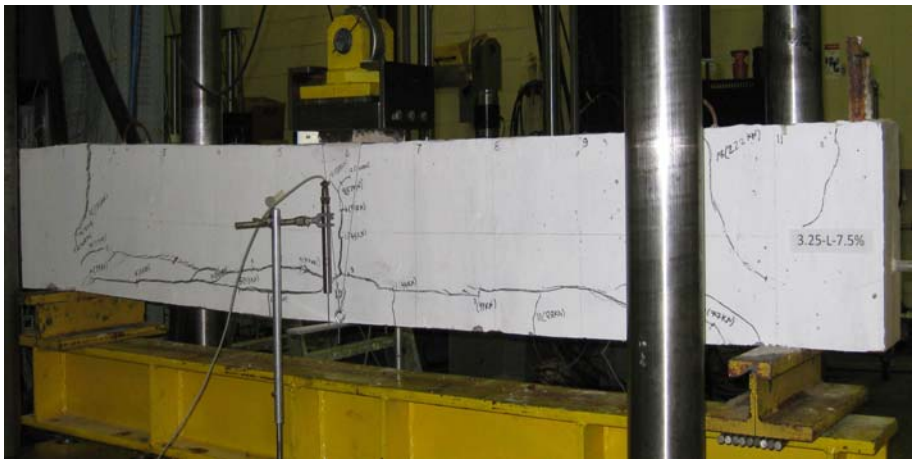

(c)

Figure 4.28: Failure modes of corroded beams (a) (3.25-L-2.5%), (b) (3.25-L-5.0%) and (c) (3.25-L-7.5%)

4.4.1.3 FRP Repaired Beam

The load-deflection response and failure mode of the FRP-repaired corroded beam (3.25-L-7.5 %- R) is shown in Figure 4.29 and Figure 4.30 respectively. Figure 4.29 shows three distinct stages in the load deflection curve; behaviour of the beam before flexural cracking, behaviour of the beam after flexural cracking until yielding and the behaviour of the beam after yielding until failure by crushing of the concrete.

The failure mode of the FRP-repaired corroded beam was changed as the repaired beam failed by yielding and then crushing of the concrete instead of experiencing an anchorage failure as in the case of corroded beams. The yield load was 236 kN at a deflection of 9.4 mm. The load at concrete crushing was 224.4 kN at a deflection of 12.4 mm.

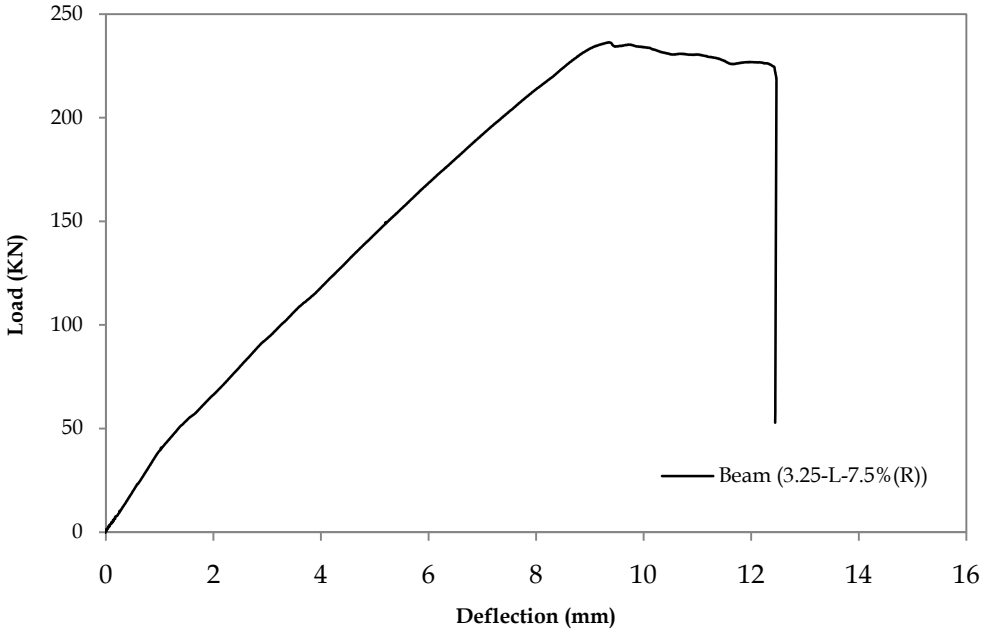

Figure 4.29: Load vs. deflection curve of FRP repaired corroded beam (series A-1)

Figure 4.30: Failure mode of FRP repaired corroded beam (3.25-L-7.5%- R)

4.4.2 Slender Beams with Stirrups (Series B-2)

4.4.2.1 Control Beam

Two beams with stirrups were tested: beam 1 was cast with the specimens and beam 2 was cast separately to verify observed behaviour of beam 1. The load deflection response of the beam 1 (3.25-LS-0%) is shown in Figure 4.31. The load deflection response of the control beam exhibited fairly linear behaviour from zero-load up until failure by inclined cracking.

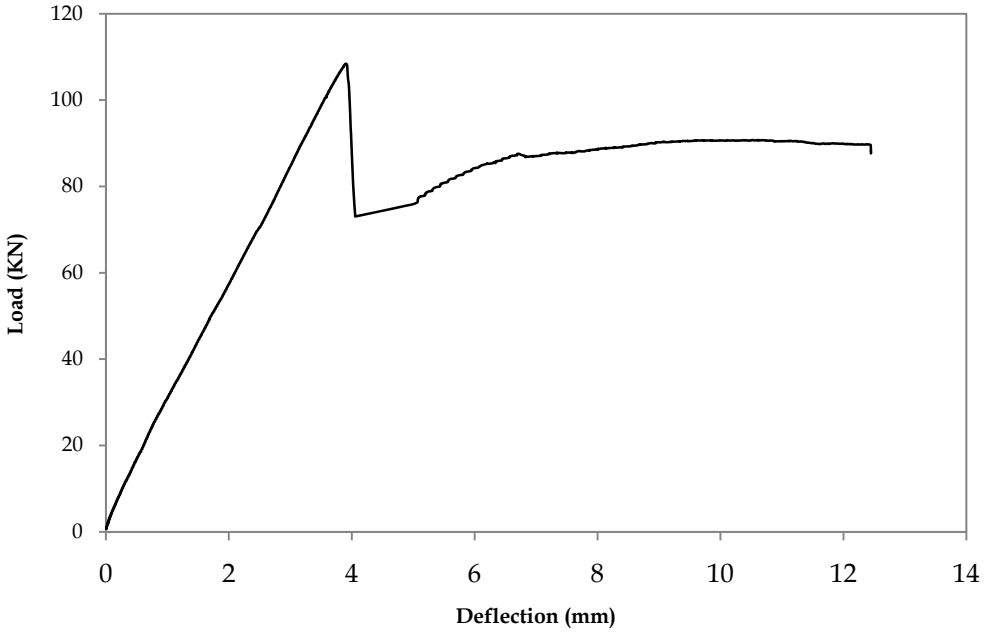

Figure 4.31: Load vs. deflection curves of control beam 1 (series B-2)

The control beam failed abruptly as shown in Figure 4.32. The cracking in the control beams was initiated upon the appearance of flexural cracks at the mid-span under a concentrated load of 46 kN. As the load increased, an inclined crack appeared in the shear span which progressed towards the load point and the support, leading to a diagonal tension failure at a load of 108 kN and a deflection of 3.9 mm. This beam failed at the same load as the control beam without stirrups.

Figure 4.32: Failure mode of control beam 1 (series B-2)

The strain profiles in the longitudinal steel and top concrete surface measured during test are shown in Figure 4.33 and Figure 4.34. The strain gauge readings in the longitudinal bar indicated that beam theory was valid up to the failure load.

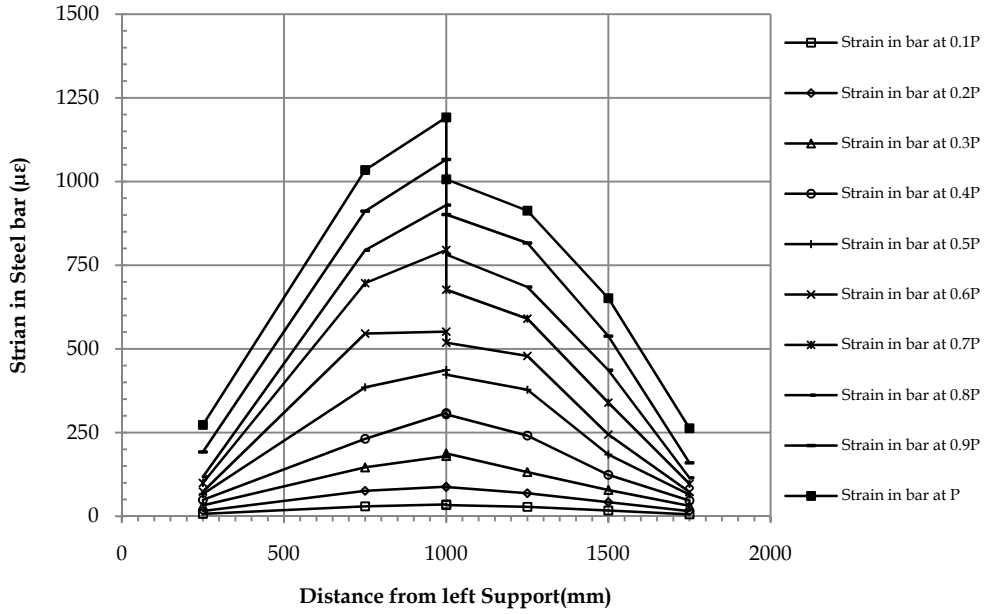

Figure 4.33: Strain profile in the longitudinal bars of control beam 1 (series B-2)

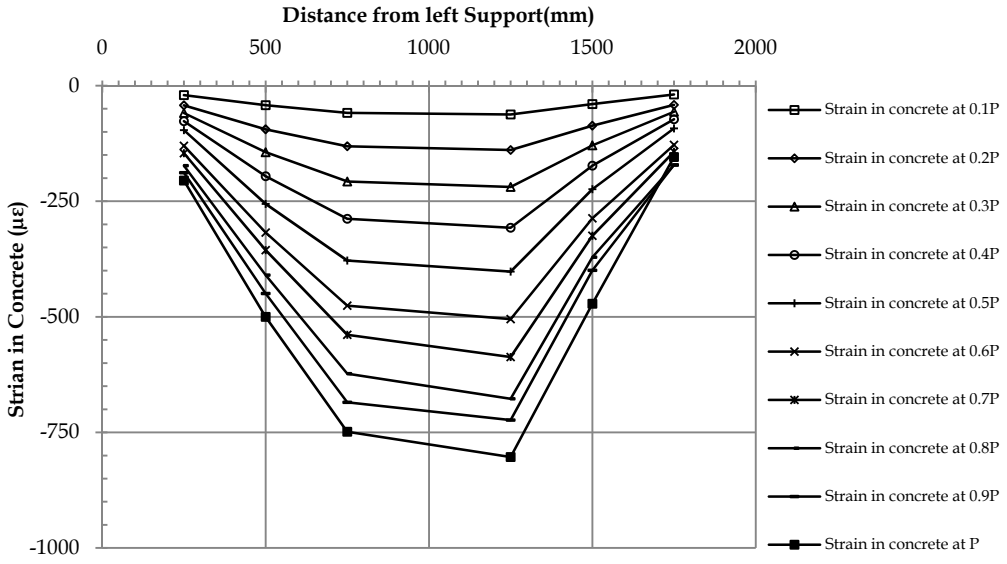

Figure 4.34: Strain gauge reading at top surface of concrete in control beam 1 (series B-2)

The results of the control beam 1 illustrated that the existence of stirrups had almost no effect on the behaviour of the control beam 1. The beam 1 failed suddenly after appearance of inclined crack causing diagonal tension failure. The beam 1 with stirrups was expected to carry higher load and behave in a more ductile fashion. The reason for this behaviour may be due to the

spacing of stirrups that was provided as per the maximum spacing provided in CSA A23.3-94, which may not be adequate.

Therefore, in order to confirm the behaviour of slender beam with stirrups in this study, it was decided to cast an additional control beam (control beam 2). The results from this beam are presented in the following.

The load deflection response and the failure mode of the control beam 2 are shown in Figure 4.35 and Figure 4.36, respectively. The control beam 2 showed relatively ductile behaviour, however, ultimately the beam failed abruptly in shear. The cracking in the control beams was initiated with the appearance of flexural cracks at mid-span under the concentrated load. The flexural cracking load was 45 kN. As the load increased, the flexural crack became flexural-shear cracks in the right shear span. The flexural-shear cracks kept progressing towards the load point with increasing load. At a load of 128 kN, an inclined shear crack appeared in the left shear span, which marked the first drop in the load deflection curve as shown in Figure 4.35. After the appearance of the inclined shear crack the beam kept carrying load until the beam failed in diagonal tension at a load of 132 kN and a deflection of 6.6 mm.

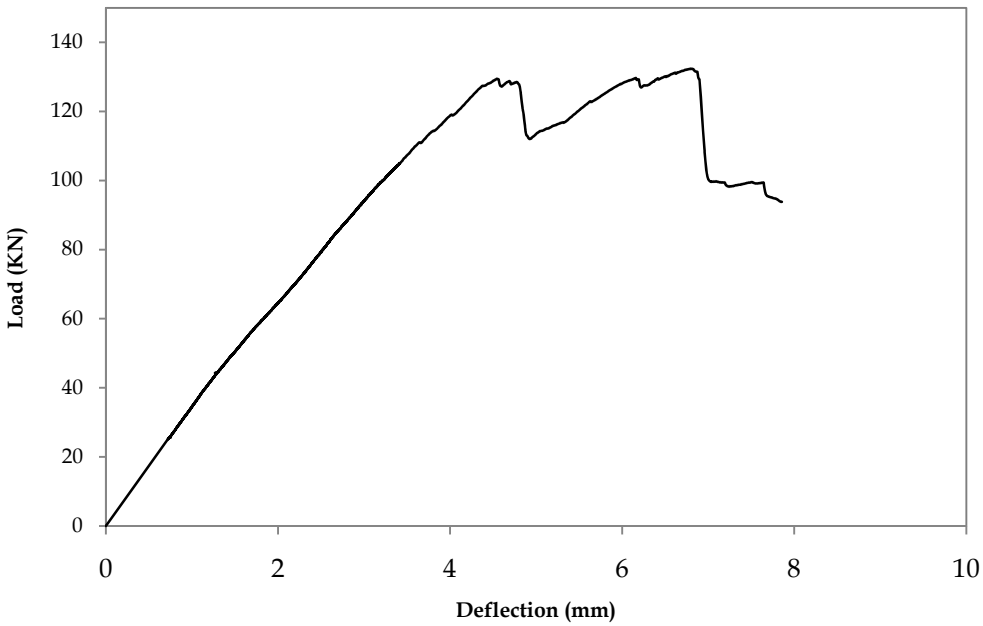

Figure 4.35: Load vs. deflection curve of control beam 2 (series B-2)

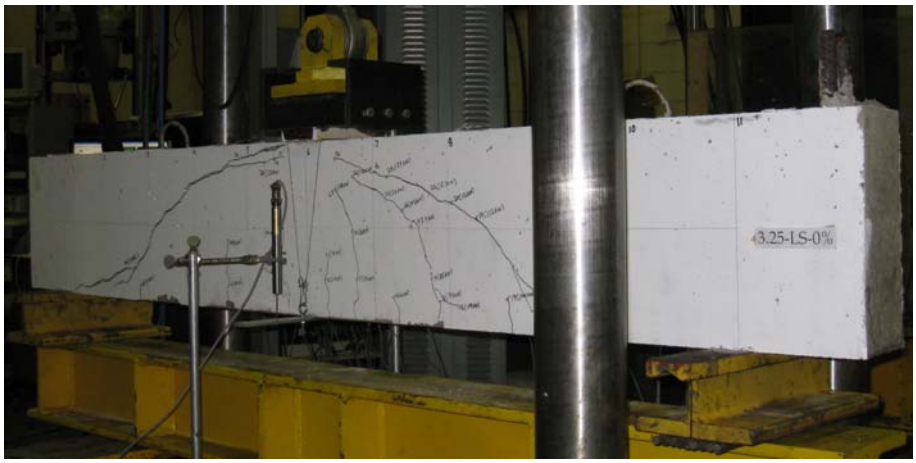

Figure 4.36: Failure mode of control beam 2 (series B-2)

For this beam strain gauges were mounted on reinforcing bar in the right shear span at a distance of 250 mm, 500 mm and 1000 mm (mid-span) from support. Strain gauges were also mounted on the concrete at the top surface of the beam. The strain profiles in the longitudinal steel and top concrete surface measured during the test are shown in Figure 4.37 and Figure 4.38, respectively. The strain values in the longitudinal reinforcement indicated that beam theory was valid up to failure load and the beam carried 100% load by beam action.

Strain gauges were also mounted on the stirrups in this beam to check the effectiveness of stirrups. Figure 4.39 shows the load strain curves along with locations of strain gauges on stirrups in the beam. It can be seen that the maximum strain in the stirrups was less than the yield strain of 2000με, which clearly shows that the smooth stirrups, even though fully anchored, were not effective in controlling the crack width of the shear crack at the maximum stirrup spacing provided as per CSA A23.3-94.

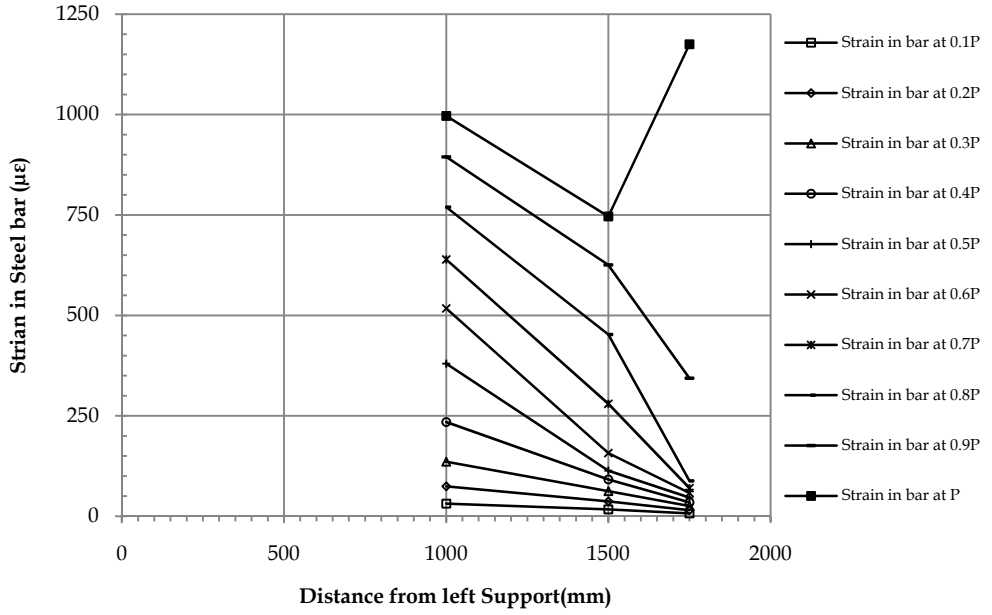

Figure 4.37: Strain profile in the longitudinal bars of control beam 2 (series B-2)

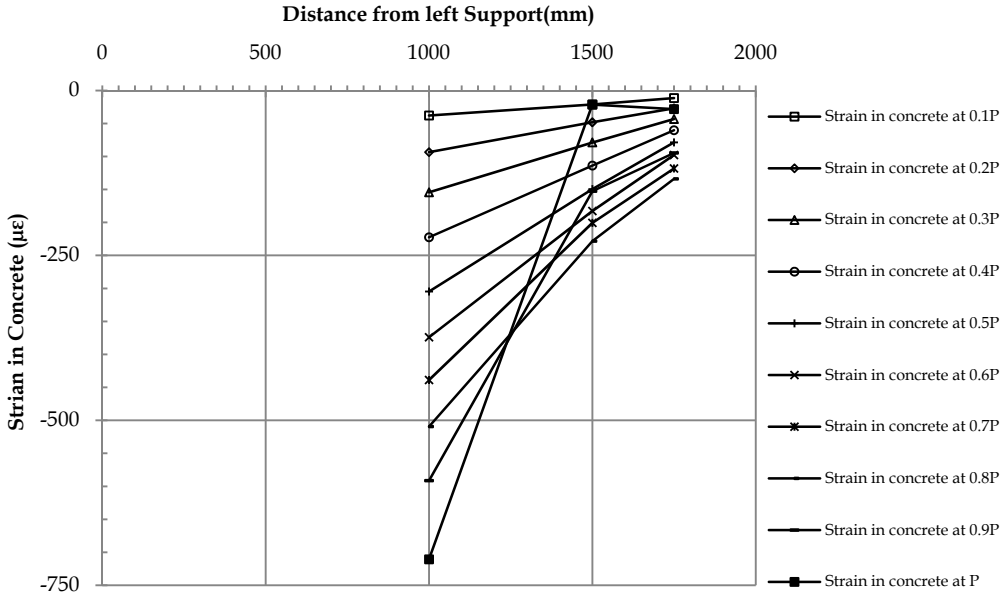

Figure 4.38: Strain profile at top surface of concrete in control beam 2 (series B-2)

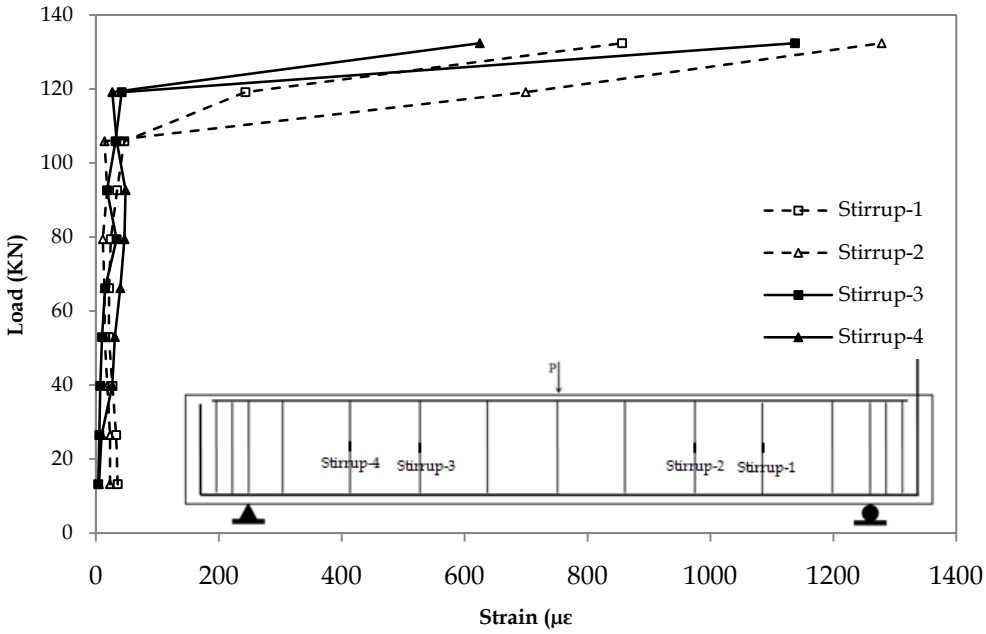

Figure 4.39: Load vs. strain in stirrups of control beam 2 (series A-2)

4.4.2.2 Corroded beams

The load deflection curves of all corroded beams (3.25-LS-2.5%, 3.25-LS-5.0% and 3.25-LS-7.5%) are shown in Figure 4.40. The load-deflection response of all corroded beams can be described by three distinct stages; the first stage represents the behaviour of the beam before flexural cracking, the second stage represents the behaviour of the beam after flexural cracking until yielding and the third stage represents the behaviour of the beam after yielding until failure by crushing of concrete.

The failure modes of the corroded beams are shown in Figure 4.41. All corroded beams failed similarly by yielding of the longitudinal steel and then crushing of the concrete. The cracking in the control beam began with the appearance of cracks at mid-span. The cracking load for all corroded beam ranged between 44 to 46 kN.

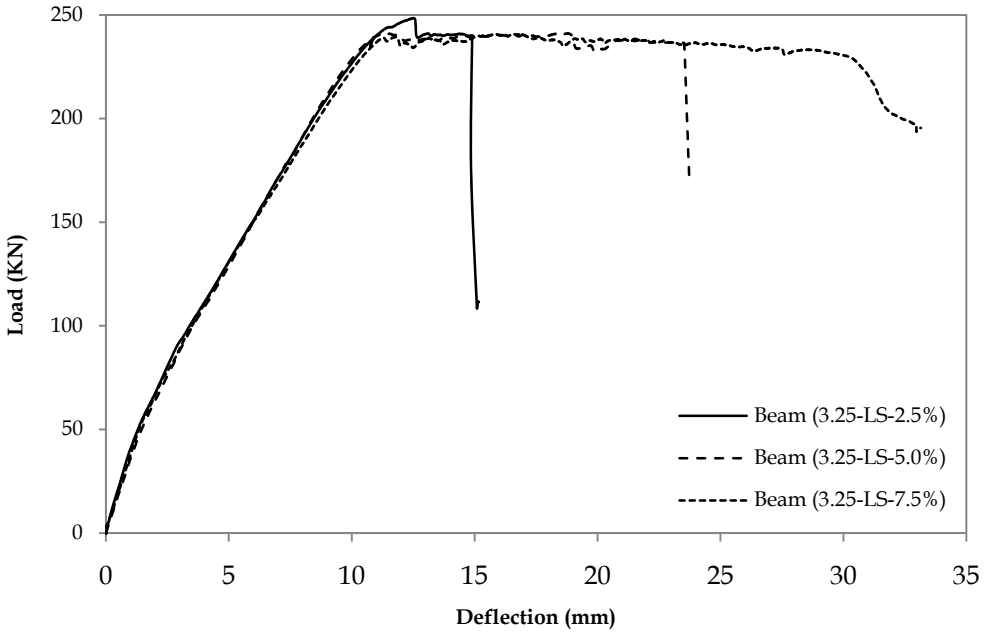

Figure 4.40: Load vs. deflection curves of corroded beams (series B-2)

The beam with a low corrosion level (3.25-LS-2.5%) had two main flexural-shear cracks near mid span, which progressed upwards towards the compression zone and laterally towards the support with increasing load. The beam continued to carry load until yielding of the longitudinal bar at a load of 248 KN load and a deflection of 12.5 mm. After yielding of the longitudinal bar, load was maintained approximately constant but the deflection continued to increase until crushing of the concrete occurred at a load of 238 kN and a deflection of 15 mm.

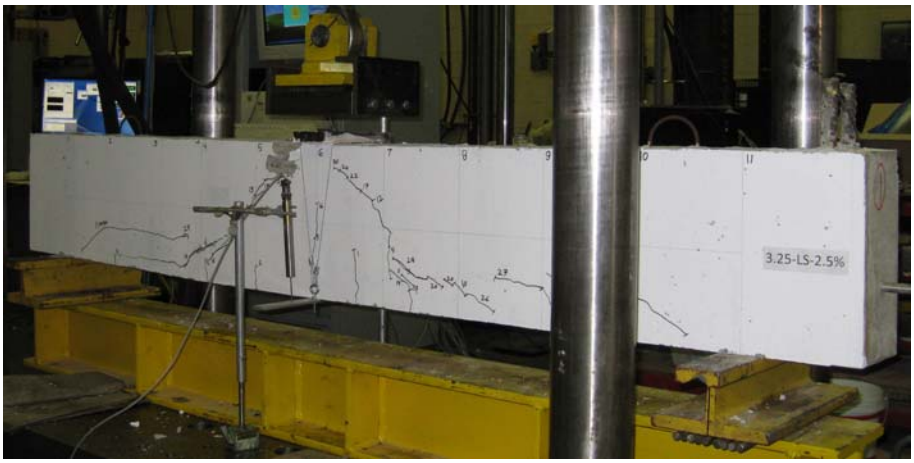

(a)

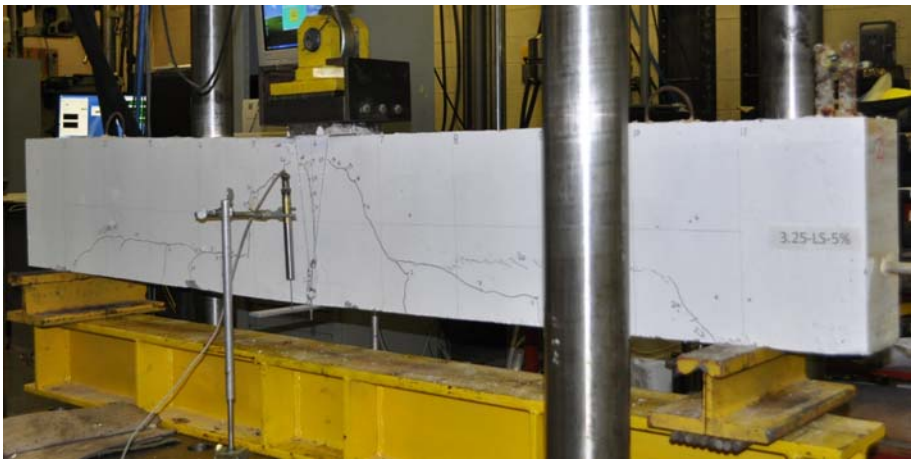

(b)

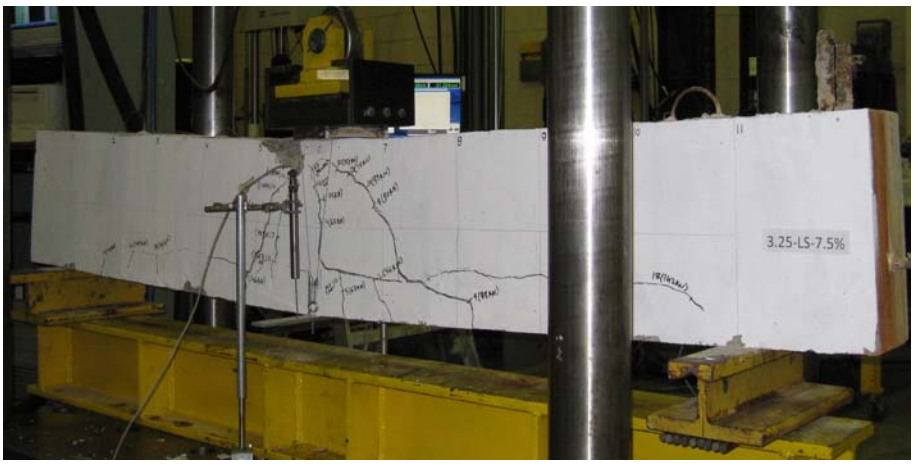

(c)

Figure 4.41: Failure modes of corroded beams (a) (3.25-LS-2.5%), (b) (3.25-LS-5.0%) and (c) (3.25-LS-7.5%)

The beam with medium corrosion level (3.25-LS-2.5%) behaved similarly as the beam with low corrosion level. The beam with medium corrosion also had two main flexural-shear cracks near mid span, which progressed upwards towards the compression zone and laterally towards the supports with increasing load. The beam continued to carry load until yielding of the longitudinal bar at a load of 241 kN load and a deflection of 11.5 mm. After yielding of the longitudinal bar, load was maintained approximately constant but the deflection continued to increase until crushing of the concrete occurs at a load of 235 kN load and a deflection of 23.5 mm.

The beam with high corrosion level (1.63-L-7.5%) behaved similarly as the other two corroded beams. The yield load of the beam was 239 kN at a deflection of 11.0 mm. The load at concrete crushing was 231 kN at a deflection of 30 mm.

4.4.2.3 FRP Repaired Corroded Beam

The load-deflection response and failure mode of the FRP repaired corroded beam (3.25-LS-7.5%-R) are shown in Figure 4.42 and Figure 4.43, respectively. Figure 4.42 shows three stages in the load deflection curve; beam behaviour before flexural cracking, beam behaviour after flexural cracking until yielding and the beam behaviour after yielding until failure by crushing of concrete. The post peak stage clearly shows a ductile response that is different from the control un-corroded but similar to the corroded beams. The FRP-repaired corroded beam failed in a similar manner as corroded beams except due to confinement of the bond between steel and concrete provided by the FRP U-wrap, crushing of concrete occurred earlier than the corroded beam. The yield load was 239 kN at a deflection of 8.8 mm. The load at concrete crushing was 243 kN at a deflection of 22.5 mm.

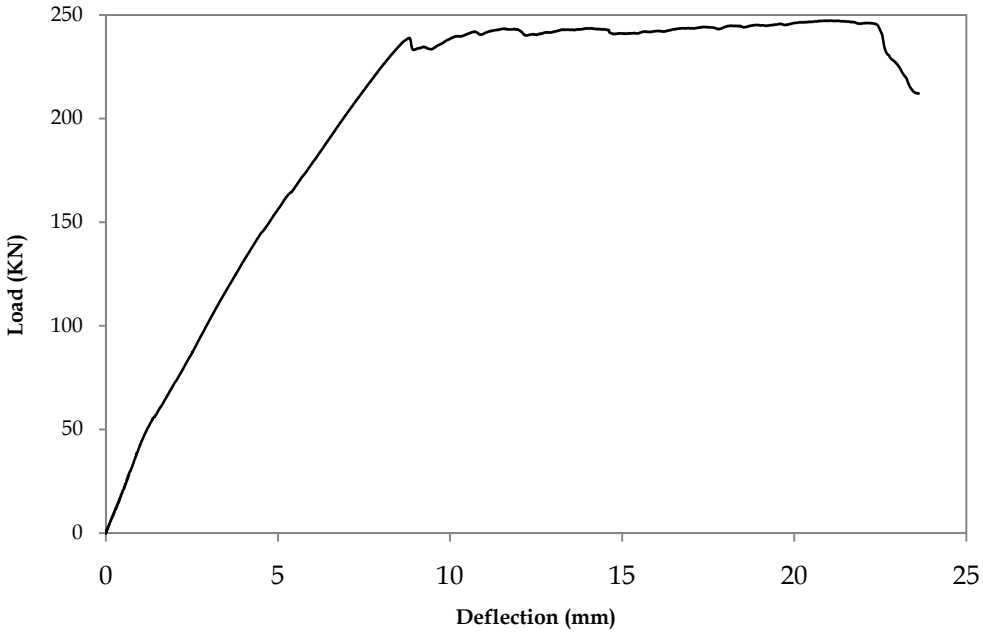

Figure 4.42: Load vs. deflection curve of FRP repaired corroded beam (series B-2)

Figure 4.43: Failure mode of FRP repaired corroded beam (3.25-LS-7.5%-R)

Chapter 5:Discussion of Results

5.1 General

This chapter presents the discussion of the experimental results of shear-critical beams with corroded longitudinal steel reinforcement. The effect of corrosion on the behaviour of the beams is discussed in Section 5.2. The effect of the stirrups on the control and corroded beams is discussed in Section 5.3. Section 5.4 discusses the effect of FRP repair on the behaviour of corroded shear critical beams.

5.2 Effect of Corrosion

Corrosion of the longitudinal reinforcement changed the load transfer mechanism of the beams from beam action (control slender beams) or combination of beam and arch action (control deep beams) to pure arch action (corroded slender and deep beams). As discussed in Section 2.1.1, shear force in RC beams can be transferred by beam action or arch action depending on whether the reinforcing steel is bonded or unbonded. The reinforcement in the control (un-corroded) beams was bonded along the beam length while that in the corroded beams was debonded from the concrete due to corrosion. The debonding of the reinforcement led to change in the load transfer mechanism to pure arch action in corroded beams.

Corrosion of the longitudinal reinforcement altered the shear cracking behaviour of the tested beams; the control un-corroded beams experienced inclined cracking, while the corroded beams did not have inclined cracking. This phenomenon resulted in load being transferred directly from the load point to the support through arch action.

Corrosion of the longitudinal steel also changed the failure mode in the corroded beams as compared to the control un-corroded beams. The control un-corroded deep beams (with and without stirrups) failed in shear compression whereas the corroded deep beams failed in splitting of the compression struts. The control un-corroded slender beams failed in diagonal tension failure while the corroded beams failed in anchorage or flexural failure (anchorage failure in slender beams without stirrups and flexural yielding and crushing failure in slender beams with stirrups).

A summary of the experimental results of the corroded beams is presented in Table 5.1. The following sections present the effect of corrosion on different test series in this study.

Table 5.1: Summary of corrosion effect on deep and slender beams with/without stirrups

Beam			Tested fc′ (MPa)	Measured Mass Loss (%)	Inclined Cracking Load (KN)	Ultimate Load (KN)	Deflection at Ultimate Load (mm)	Failure Mode
Deep Beams	Series-A1	1.63-L-0%	47.3	-	127	191.63	2.0	Shear-Compression
		1.63-L-2.5%	47.3	3.15	-	459.26	3.71	Splitting of Strut
		1.63-L-5%	47.3	4.38	-	476.4	3.90	Splitting of Strut
		1.63-L-7.5%	47.3	4.64	-	476.17	3.88	Splitting of Strut
	Series-A2	1.63-LS-0%	47.3	-	124	418.41	3.85	Shear-Compression
		1.63-LS-5%	47.3	3.85	-	386.17	2.74	Splitting of Strut
		1.63-LS-7.5%	47.3	4.49	-	422.85	3.22	Splitting of Strut
Slender Beams	Series-B1	3.25-L-0%	47.3	-	109	109.5	3.72	Diagonal Tension
		3.25-L-2.5%	47.3	4.0	-	206.17	11.96	Anchorage Failure
		3.25-L-5%	47.3	5.18	-	221.51	11.40	Anchorage Failure
		3.25-L-7.5%	47.3	5.78	-	225.21	12.87	Anchorage Failure
	Series-B2	3.25-LS-0%	46.3	-	128	132.36	6.6	Diagonal Tension
		3.25-LS-2.5%	47.3	3.28	-	238*	15.0	Yielding and crushing
		3.25-LS-5%	47.3	4.39	-	235**	23.5	Yielding and crushing
		3.25-LS-7.5%	47.3	5.22	-	231.1***	29.7	Yielding and crushing

*Yielding load for this beam was 248 KN at 12.5 mm deflection

**Yielding load for this beam was 241 KN at 11.5 mm deflection

***Yielding load for this beam was 239 KN at 11.3 mm deflection

5.2.1 Deep Beams without Stirrups

Figure 5.1 briefly illustrates the effect of corrosion on deep beams without stirrups. All beams were shear critical and expected to fail in shear. The control un-corroded and corroded beams failed in shear as expected. However, there was a significant change in the overall behaviour of corroded beams compared to the control un-corroded beam. The control un-corroded beam failed in shear compression failure at a load of 192 kN. The beams that were corroded to 3.2%, 4.4% and 4.6% mass loss experienced significant increase in ultimate load and failed by splitting of the compression strut at a load of 459 kN, 476 kN and 476 kN, respectively (Table 5.1). All three corroded beams failed at similar load levels, demonstrating an average increase of 150% in the ultimate load of the corroded beams compared to the control un-corroded beam. The slight

variation in the ultimate strength of the corroded beams may be attributed to the variation in the concrete strength. The increase in deflection at the ultimate load in the corroded beams was on average 100% from 2.0 mm in the un-corroded beam (beam with 0% mass loss) to an average of 3.8 mm for the corroded beams.

The stiffness reduction in control beam occurred at the onset of the inclined cracking while the stiffness reduction in the corroded beam occurred at onset of the flexural cracking. The corroded beams exhibited the same post-cracking stiffness which was close to the stiffness of the control beam.

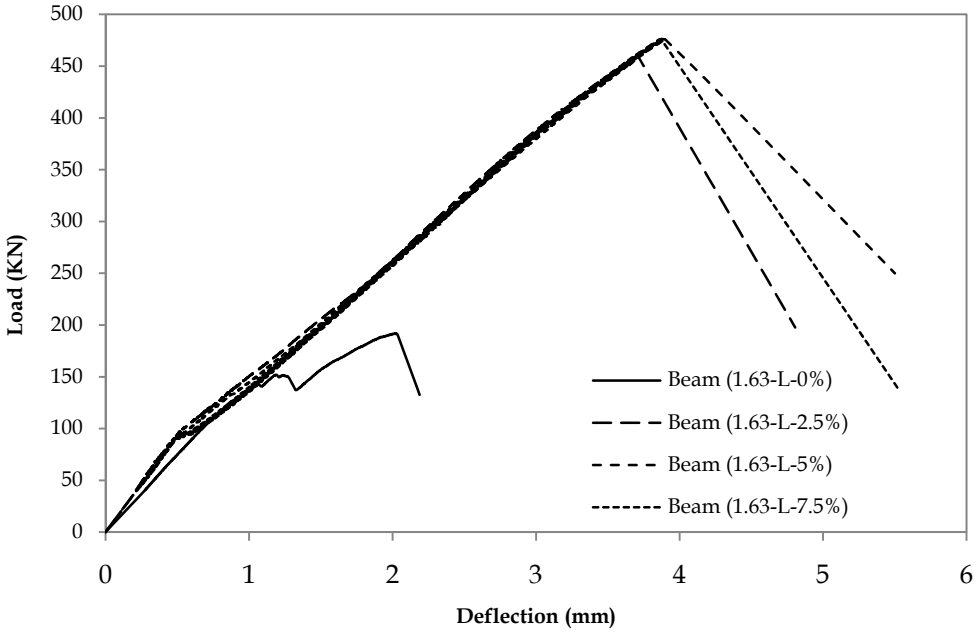

Figure 5.1: Load vs deflection curves for control and corroded deep beams without stirrups (series A-1)

The failure modes and the crack patterns at failure of the corroded beams were shown in Chapter-4. The crack patterns at failure showed that the longitudinal reinforcement was de-bonded due to corrosion along the length of the beam and no inclined crack appeared in the corroded beams. This allowed arch action to develop and the load was transferred directly from the load point to the support as shown in Figure 5.2.

The change of failure mode in the corroded beams is mainly attributed to the change in load transfer mechanism. The control un-corroded beam carried almost 70% of the ultimate load by beam action before the appearance of the main shear crack. Once the inclined/shear crack appeared, the beam carried the remainder 30% of the ultimate load by arch action. The occurrence of shear cracks in the control beam before the beam started carrying load by arch

action weakens the compression strut. The inclined cracks progressed rapidly towards the compression zone leaving only a small nodal zone area. The nodal zone was unable to carry these compressive stresses and the beam failed due to crushing of the concrete. The corroded beams carried 100% load by arch action as the longitudinal reinforcement was debonded prior to the load testing. The corrosion of longitudinal reinforcement prevented the inclined cracking which resulted in direct load transfer from the load point to the support resulting in pure arch action until the compression strut was split due to transverse tensile stresses.

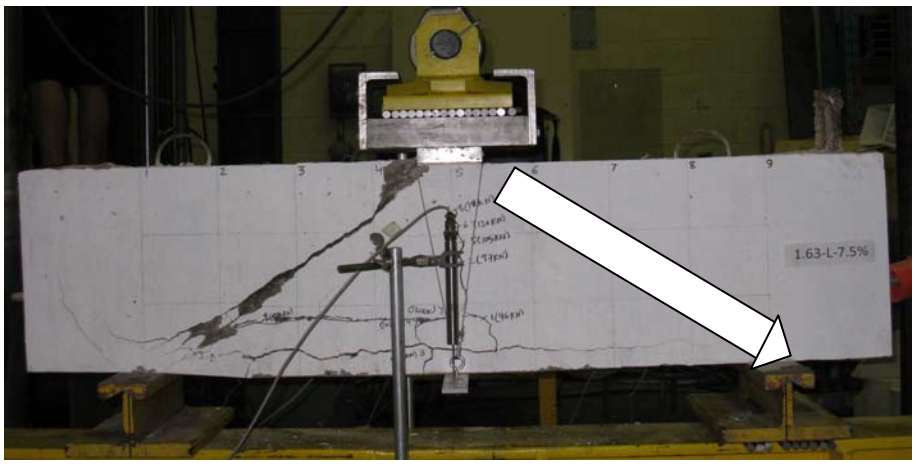

Figure 5.2: Arch action in corroded deep beams

This series showed that the performance of deep beams without stirrups improved when subjected to corrosion as compared to the control beams as a result in change in load transfer from beam action (control beam) to arch action (corroded beams).

5.2.2 Deep Beams with Stirrups

Figure 5.3 illustrates the effect of corrosion on deep beams with stirrups. All beams (the control un-corroded and corroded beams) failed in shear as expected. However, the failure mode of the corroded beams changed. The control un-corroded beam failed in shear compression at a load of 418 kN. The beams that were corroded to a mass loss of 3.9% and 4.5% failed by splitting of compression strut at loads of 386 kN and 423 kN, respectively (Table 5.1). The corroded beams failed at similar load level which was also close to the failure load of the control un-corroded beam. This demonstrates that there was minimal effect of corrosion on the ultimate load of the beams. The slight variation in the ultimate strength may be attributed to the variation in concrete strength.

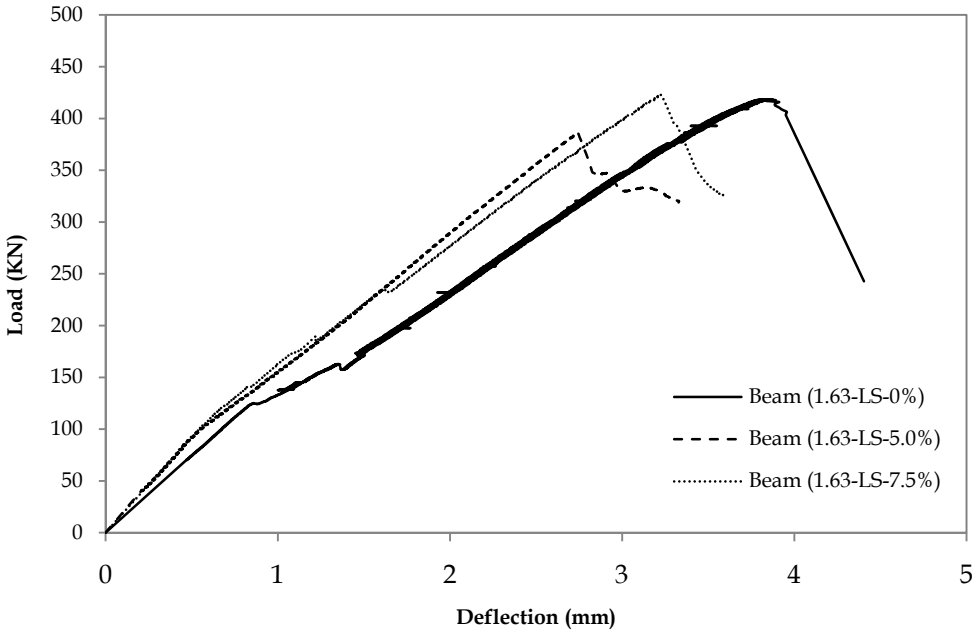

Figure 5.3: Load vs. deflection curves of control and corroded deep beams with stirrups (series A-2)

The load transfer mechanism changed from a combination of beam and arch action to pure arch action as a result of debonding of the longitudinal reinforcement. The control un-corroded beam carried 30% load by beam action and 70% load by arch action. The change in load transfer mechanism occurred at the onset of the main shear crack. The propagation of the inclined crack towards the compression zone was stopped by the stirrups, which helped in the development of arch action to carry the additional load until failure. The de-bonding of the longitudinal reinforcement due to corrosion prior to loading changed the load transfer mechanism and the beam carried 100% load by arch action. In contrast, the control un-corroded beam carried 70% of the load by arch action and as such the load was not affected by corrosion.

The deflection at the ultimate load in the corroded beams was lower compared to the control un-corroded beam. The higher deflection in the control beam is mainly attributed to the shear deformation due to the inclined cracking that was observed.

The stiffness reduction in the control beam occurred at the onset of the inclined cracking whereas the stiffness reduction in the corroded beams occurred at the onset of flexural cracking. The corroded beam exhibited the same post-cracking stiffness as the control beam.

The results of this series showed that deep beams with stirrups subjected to corrosion of the longitudinal reinforcement behaved almost similar to the control un-corroded beam and there was almost no effect of corrosion on such beams.

5.2.3 Slender Beams without Stirrups

Figure 5.4 illustrates the effect of corrosion on slender beams without stirrups. All beams were designed to fail in shear. The control un-corroded beam failed suddenly in shear as expected by diagonal tension failure at load of 109 kN. However, the failure mode of the corroded beams was changed to tensile anchorage failure. The ultimate load for beams corroded to 4.0%, 5.2% and 5.8% mass loss increased to 206 kN, 222 kN and 225 kN, respectively (Table 5.1). The increase in ultimate load of the corroded beams was on average 100% greater than that of the control beam.

The failure mode in the corroded beams changed mainly because of the change in load transfer mechanism from beam action (control un-corroded beam) to arch action (corroded beams). The control un-corroded beam carried 100% of the load by beam action as per measured strains in the beam. The corrosion of the reinforcing bars forced the corroded beams to transfer the load by arch action. The corroded beam carried 100% of the load by arch action until the beams experienced an anchorage failure at the support. The cracking at the top surface of the corroded beams near anchorage zone can be explained as follows: close to failure, the bond of longitudinal reinforcement was lost within the clear span causing very high tensile forces in the bar near the support. This force was resisted by the 90˚ hook provided at the end of the longitudinal bar. Since, the stiffness of the anchorage zone which was highly reinforced was relatively high, cracking occurred just beside the anchorage zone where there was an abrupt change in stiffness.

As shown in Figure 5.4, the corroded beams experienced higher deflections at ultimate load with a 200% increase in the deflection over the control un-corroded beam. This increase in deflection is associated with a change of failure mode.

Figure 5.4 shows that the corroded beams experienced a significant loss of stiffness after cracking, which was on average equal to 30% as compared to the stiffness of control beam.

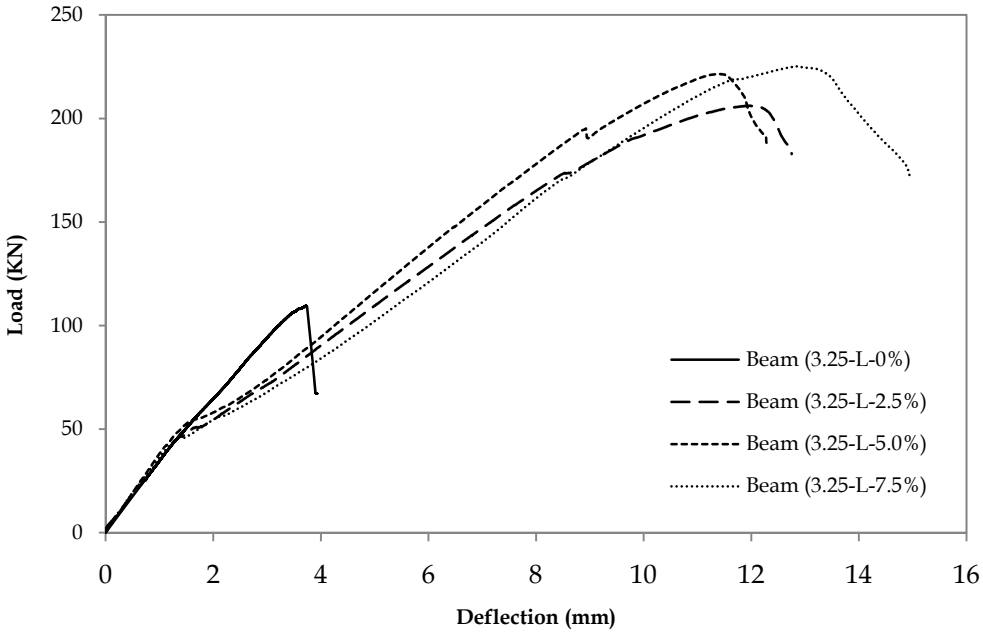

Figure 5.4: Load vs. deflection curves of control and corroded slender beams without stirrups (series B-1)

5.2.4 Slender Beams with Stirrups

Figure 5.5 illustrates the effect of corrosion on slender beams with stirrups. All slender beams with stirrups were designed to fail in shear. The control beam failed in shear by diagonal tension failure at a load of 132 kN. The failure mode of the corroded beams was changed from the expected shear failure to a flexural failure (yielding and then crushing of concrete), which resulted in an increase in the ultimate load of the corroded beams compared to the control un-corroded beam. The yield load of the corroded beams was 248 kN, 241 kN and 239 kN with mass loss of 3.3%, 4.4% and 5.2%, respectively (Table 5.1). All corroded beams experienced an average increase in ultimate load equal to 84%. The reduction in the yield strength of corroded beams was directly proportional to the mass loss of the reinforcing steel.

The corrosion of the longitudinal steel changed the load transfer mechanism from beam action in the control beam and forced the corroded beams to carry the load by arch action.

The corroded beams exhibited very ductile behaviour compared to the control un-corroded beam as shown in Figure 5.5. The ductility of the corroded beams increased with an increase in corrosion level. The deflection at ultimate load in the corroded beams ranged between 15 mm to 30 mm compared to the deflection of 6.6 mm in control un-corroded beam representing an increase of 125 to 350%. Figure 5.5 shows that there was no stiffness loss in the corroded beams compared to the stiffness in control beam.

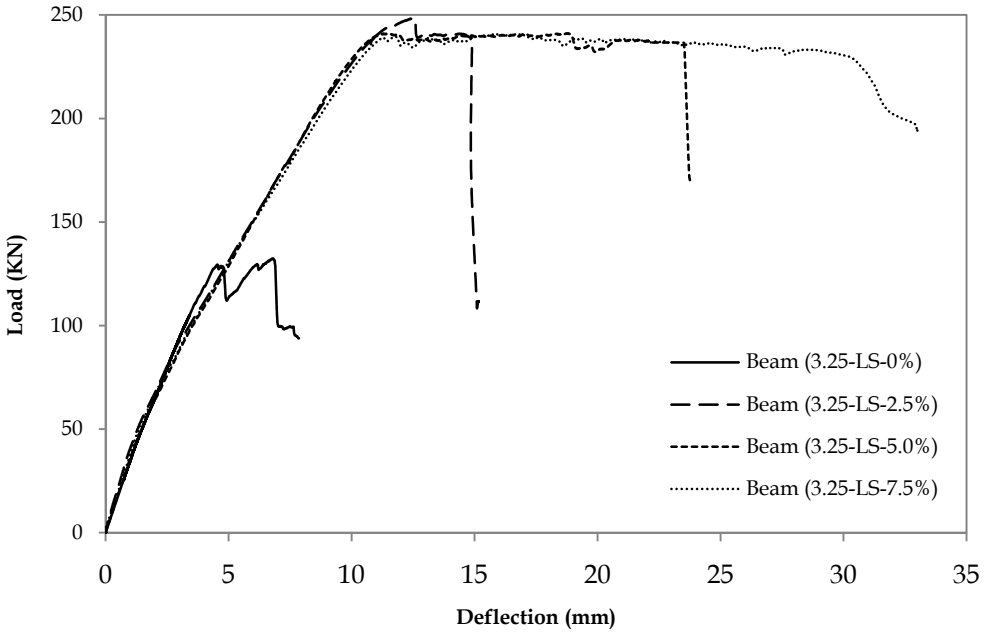

Figure 5.5: Load vs. deflection curves of control and corroded slender beams with stirrups (series B-2)

5.3 Effect of Stirrups

5.3.1 Deep Beams

The effect of stirrups on the behaviour of control and corroded deep beams is presented in Figure 5.6 and Figure 5.7, respectively.

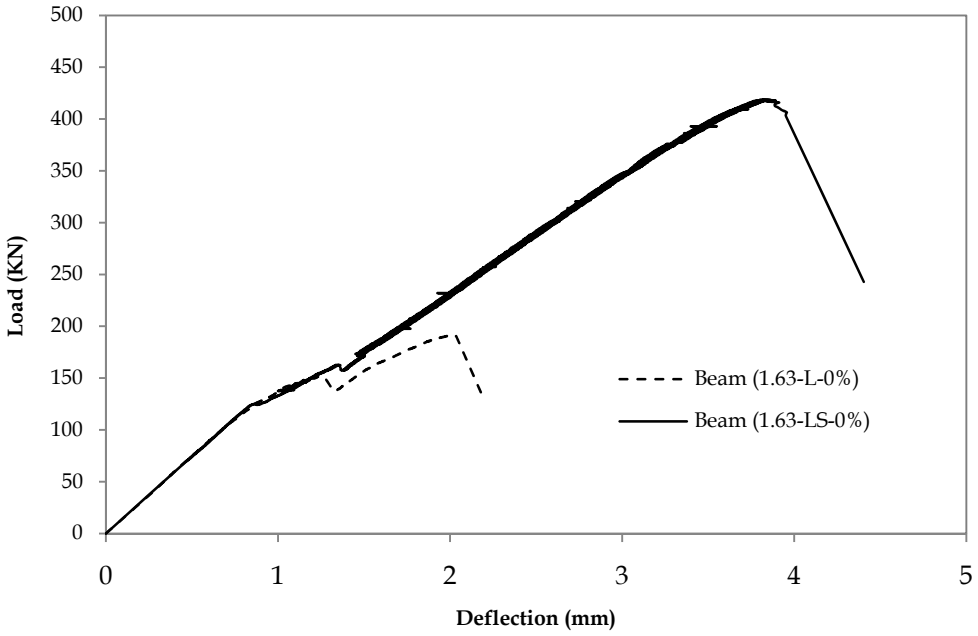

Figure 5.6: Load vs. deflection curves of control deep beams with and without stirrups

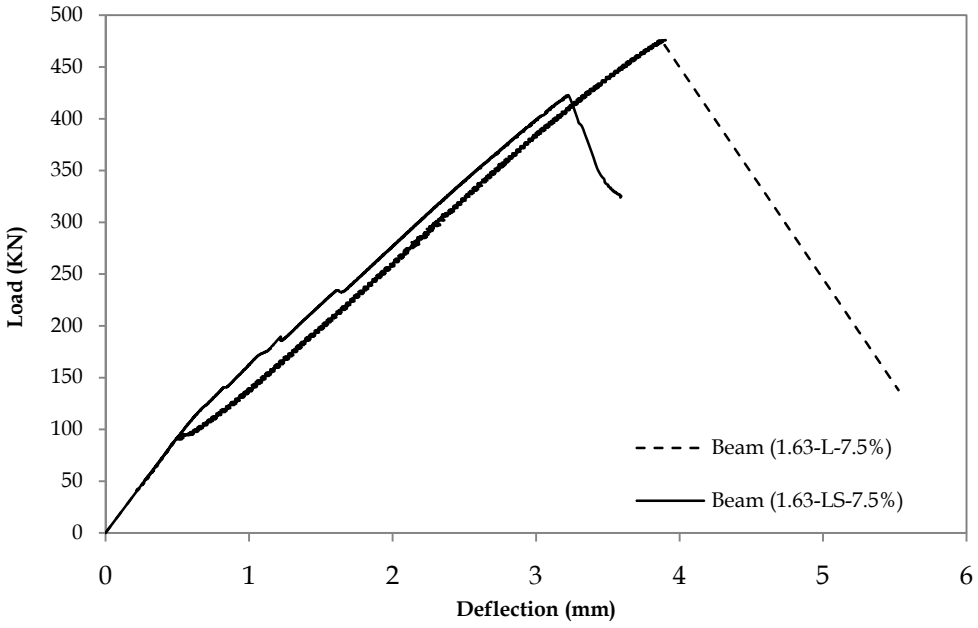

Figure 5.7: Load vs. deflection curves of corroded deep beams with and without stirrups

The presence of shear stirrups significantly increased the ultimate load of the control un-corroded beams. The control beam without stirrups failed at a load of 191 kN while the control beam with stirrups failed at a load of 418 kN, which is more than a 100% increase in the capacity (Table 5.1).

Once the inclined crack appeared in the control beam without stirrups, it quickly progressed towards the compression zone before the beam started carrying load by arch action, leaving a small nodal zone area to carry the concentrated compressive forces in the strut. This caused the beam to fail quickly by crushing of the concrete under the concentrated load. Conversely, in the control beam with stirrups the propagation of inclined cracks was prevented leaving a relatively greater nodal zone area. As a result, crushing of the nodal zone was delayed and the beam with stirrups sustained higher failure load through arch action as compared to the beam without stirrups.

The corroded beam without stirrups (1.63-L-7.5%) failed at a load of 476 kN while the corroded beam with stirrups (1.63-LS-7.5%) failed at a load of 422 kN showing a 13% decrease in the capacity (Table 5.1). Similar results were found in other corroded beams (1.63-L-5% and 1.63-LS-5%). The beam with stirrups contained 2-10M bar as compression reinforcement. The trend may be attributed to the fact that the beam with compression reinforcement have smaller strut as compared to beams without stirrups which will result in earlier failure of strut in beam with stirrups. Hence, beam with stirrups (which contained compression reinforcement) will fail at lower load as compared to beams without stirrups as observed in experimental results.

5.3.2 Slender Beams

The effect of stirrups on the behaviour of the control and corroded slender beams is presented in Figure 5.8 and Figure 5.9, respectively.

The control beam without stirrups failed at a load of 109 kN while the control beam with stirrups failed at a load of 132 kN (Table 5.1). It was expected that the control beam with stirrups will sustain higher load and be more ductile but it behaved differently and it failed suddenly after the appearance of diagonal crack causing diagonal tension failure. Figure 5.8 shows that the beam with stirrups did show relatively ductile behaviour and a slight increase in the ultimate strength, but it was considerably lower than expected. The analysis of the strain gauges mounted on the stirrups also indicated that the stirrups were ineffective to control the crack width which led to premature failure. The reason for this may the spacing of stirrups, as the spacing provided was the maximum spacing allowed by CSA A23.3-94, which may not be adequate for such beams. The other reason may be the smoothness of stirrups, as the stirrups were made from smooth bars and smooth bars may not be as effective at controlling crack widths.

The existence of stirrups changed the failure mode of corroded beams: the beams without stirrups failed by anchorage while the beams with stirrups failed by yielding and then by crushing of concrete. The beams with stirrups contained stirrups throughout the beam resulting in similar stiffness in the span and the anchorage zone whereas the beams without stirrups have stirrups only in the anchorage zone resulting in a change of stiffness at the end of the anchorage zone. This change in stiffness in beams without stirrups caused anchorage failure at location where stiffness changes.

The existence of stirrups increased the deflection at ultimate load by 130% and stiffness by 5% of the corroded beams. The increase in ultimate deflection was due to the different failure modes observed. The increase in stiffness was mainly due to the effect of the stirrups on bond.

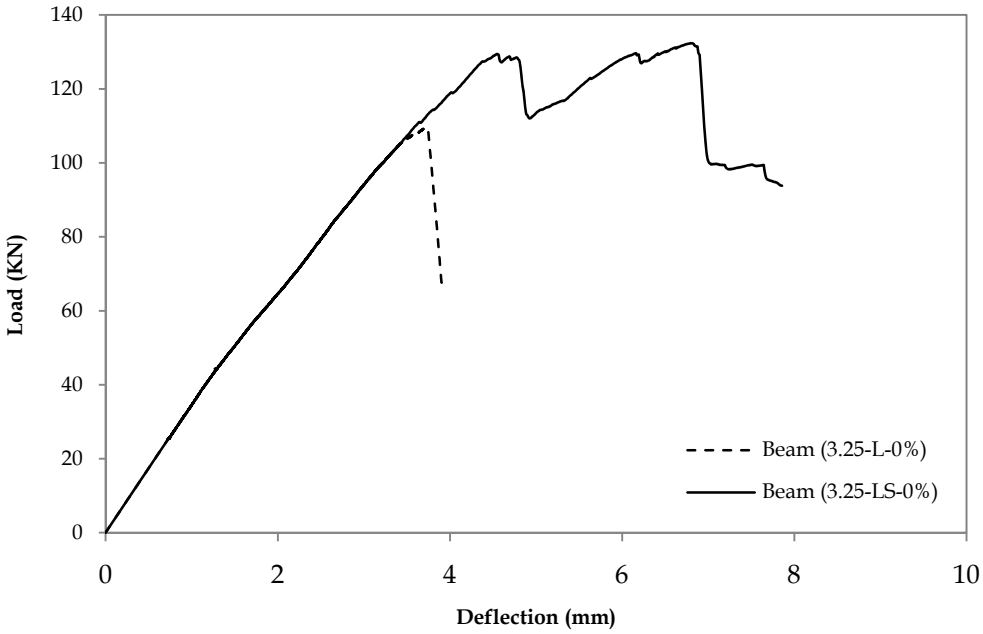

Figure 5.8: Load vs. deflection curves of control slender beams with and without stirrups

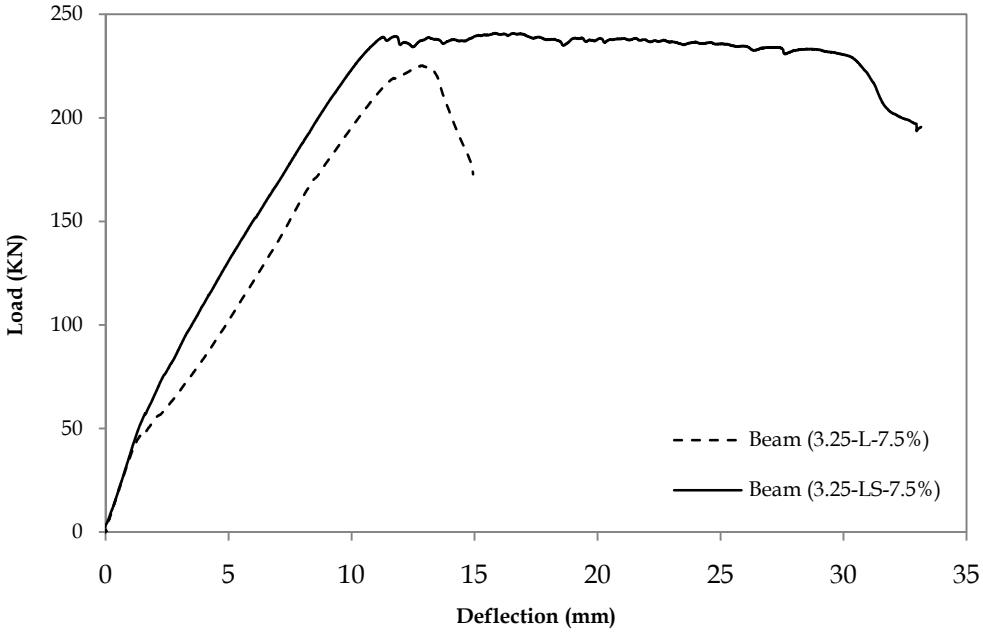

Figure 5.9: Load vs. deflection curves of slender beams with and without stirrups

5.4 Effect of FRP Repair

A summary of test results for the FRP repair on corroded beams is presented in Table 5.2.

Table 5.2: Summary of FRP repair effect on corroded beams

Beam		Ultimate Load (KN)	Deflection at Ultimate Load (mm)	Post Cracking Stiffness (KN/mm)	Failure Mode
Series A-1	1.63-L-7.5%	476.16	3.88	124.93	Splitting of Strut
	1.63-L-7.5%(R)	497.13	3.37	137.74	Splitting of Strut
Series A-2	1.63-LS-7.5%	422.85	3.22	119.47	Splitting of Strut
	1.63-LS-7.5%(R)	447.44	3.54	143.68	Splitting of Strut
Series B-1	3.25-L-7.5%	225.21	12.87	18.53	Anchorage Failure
	3.25-L-7.5%(R)	224.49*	12.42	24.31	Yielding and Crushing
Series B-2	3.25-LS-7.5%	231.1**	29.7	19.44	Yielding and Crushing
	3.25-LS-7.5%(R)	247.44***	3.54	25.14	Yielding and Crushing

*Yielding load for this beam was 236.36 KN at 9.35 mm deflection

**Yielding load for this beam was 239.02 KN at 11.28 mm deflection

***Yielding load for this beam was 238.90 KN at 8.82 mm deflection

5.4.1 Deep Beams without Stirrups

Figure 5.10 illustrates the effect of FRP repair on the corroded deep beam without stirrups. The load deflection response of the corroded and FRP repaired beam was similar to that of the corroded beam. The failure modes of corroded and FRP repaired beam was also similar to that of corroded beam. However, FRP confinement delayed the failure crack until the FRP sheets debonded. The FRP repair of corroded beam slightly increased its ultimate strength and stiffness in comparison to the corroded beam. The increase in strength and stiffness was only 4% and 10%, respectively (Table 5.2). The FRP U-wrap delayed the occurrence of the initial flexural cracking which led to attaining a higher load in the FRP repaired beam. The increase in stiffness is possibly due to increased bond strength resulting from FRP confinement.

The results of this series show that the FRP U-wrap was not effective in preventing the shear failure of the corroded deep beams. Full FRP wrapping may prove to be a better alternative.

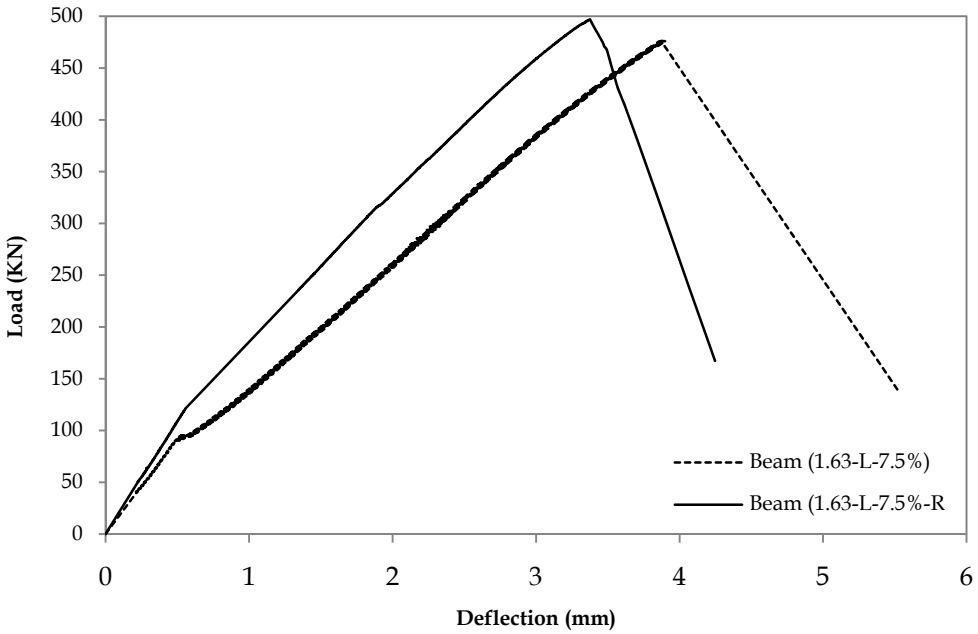

Figure 5.10: Load vs. deflection curves of corroded and FRP repaired deep beams without stirrups

5.4.2 Deep Beams with Stirrups

Figure 5.11 illustrates the effect of FRP repair on corroded deep beams with stirrups. The load deflection response of the corroded beam and FRP-repaired corroded beams were very similar up to the splitting of the diagonal strut. The corroded beam failed suddenly after splitting of the diagonal strut. The FRP repaired corroded beam showed a sudden drop in the load deflection curve at splitting of the strut but kept carrying load until the FRP wrap debonded. The FRP repaired corroded beam exhibited limited ductility in comparison to the corroded beam that failed with no ductility.

The FRP repair of the corroded beams increased the ultimate strength and stiffness of the beam compared to the corroded beams. The increase in strength and stiffness was 6% and 20%, respectively (Table 5.2). The increase in stiffness is possibly due to increased bond strength as a result of the confinement provided by the FRP U-wrap.

The results of this series show that the FRP U-wrap of the corroded deep with stirrups was insufficient to prevent the shear failure. Future studies should consider full wrapping to repair such beams.

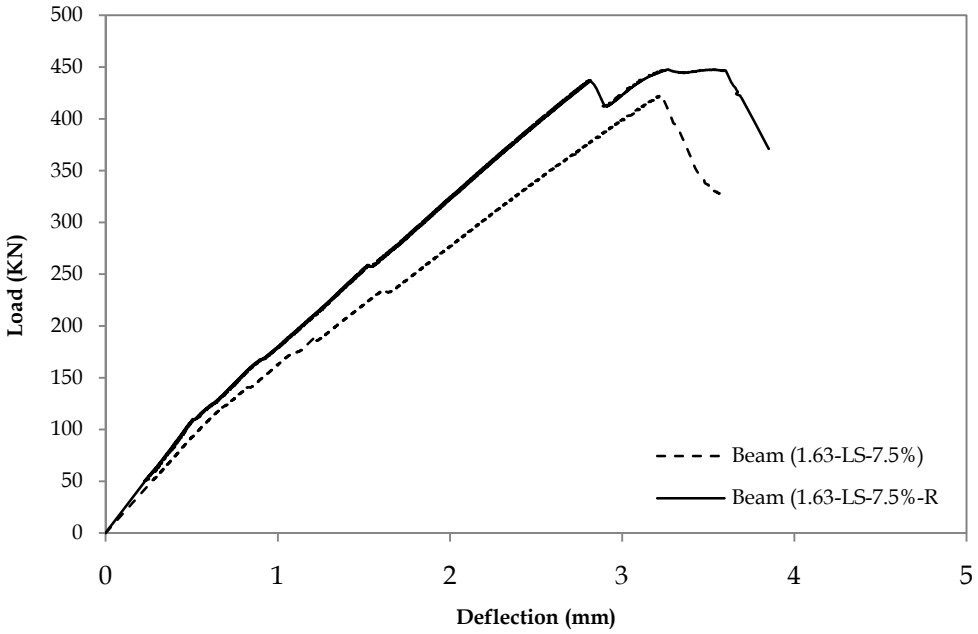

Figure 5.11: Load vs. deflection curves of corroded and FRP repaired deep beams with stirrups

5.4.3 Slender Beams without Stirrups

Figure 5.12 illustrates the effect of FRP repair on the corroded slender beams without stirrups. It is evident that the FRP repaired corroded beam failed in a different manner compared to corroded beam. The post peak stage in FRP repaired corroded beam showed a ductile response which is different from the corroded beam that failed in a brittle manner.

The FRP repair of the corroded beam increased its stiffness post cracking stiffness by around 30% (Table 5.2). The increase in stiffness may be attributed to the increased bond strength due to confinement provided by the FRP U-wrap.

The results of this series show that the FRP U-wrap of the corroded slender beams without stirrups was sufficient to prevent the anchorage failure.

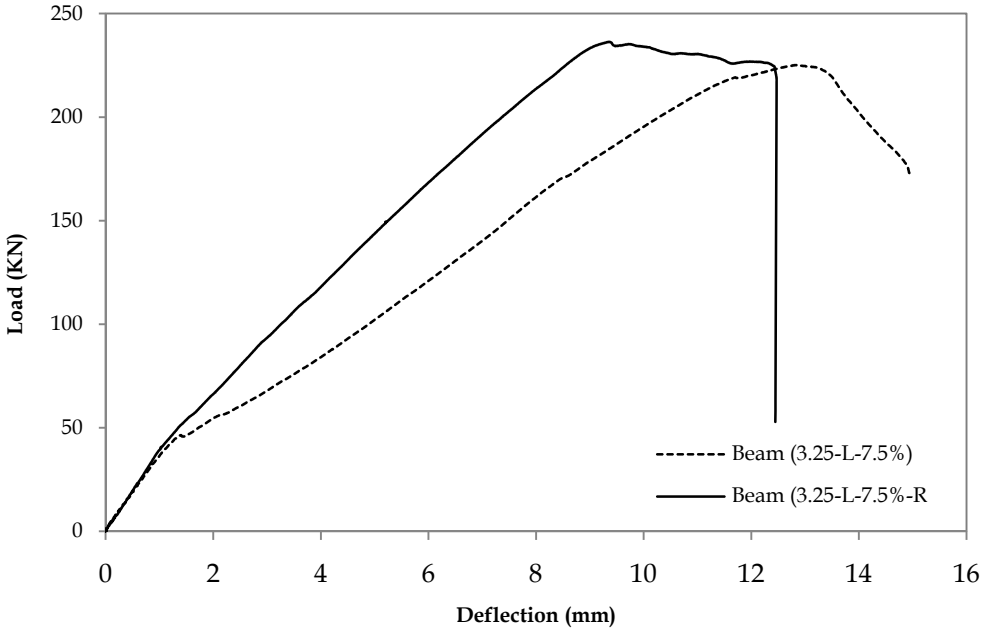

Figure 5.12: Load vs. deflection curves of corroded and FRP repaired slender beams without stirrups

5.4.4 Slender Beams with Stirrups

Figure 5.13 illustrates the effect of FRP repair on the corroded slender beams with stirrups. The corroded beam and FRP repaired corroded beams behaved similarly. The failure mode of FRP repaired beam was similar to that of the corroded beam; due to FRP confinement the crushing of concrete occurred earlier as compared to corroded beam. The FRP repair of the corroded beam also increased the post cracking stiffness about around 30% over the corroded beam (Table 5.2). The increase in stiffness may be attributed to the increased bond strength due to confinement provided by the FRP U-wrap.

The results of this series show that the FRP U-wrap of the corroded slender with stirrups did not significantly affect the behaviour of such beams.

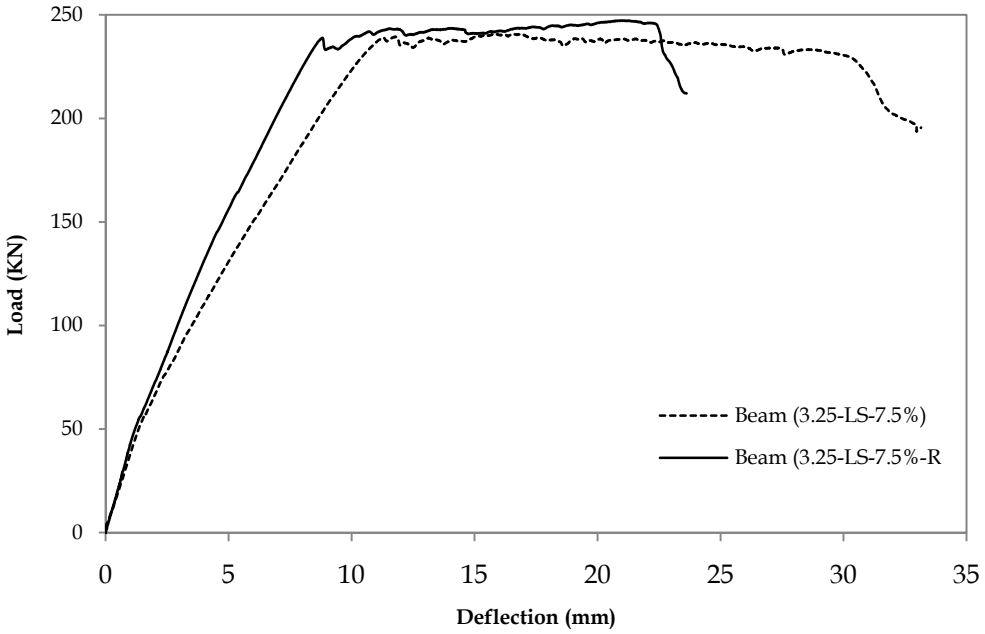

Figure 5.13: Load vs. deflection curves of corroded and FRP repaired slender beams with stirrups

Chapter 6: Analytical Modeling

6.1 General

The shear strengths of the control beams were predicted using analytical procedures in CSA A23.3-04. The shear strengths of the corroded beams were predicted using proposed strut and tie models. The following sections present the models used and a comparison of the predicted versus experimental results for the control and corroded beams.

6.2 Strength Predictions of Control Beams

Most building codes use different shear design procedures for deep and slender beams. CSA A23.3 04 uses the strut and tie model approach for deep beams and modified compression field theory (MCFT) for slender beams.

The ultimate strength of the control beams are predicted using the analytical procedures in CSA A23.3-04. The strut and tie model given in clause 11.4 is used to predict the ultimate shear strength of the control deep beams and the general method for shear given in clause 11.3 (which is based on the modified compression field theory) is used to predict the shear capacity of the control slender beams. The iterative procedure developed based on the strut and tie model (clause 11.4) is presented in Figure 6.1 and the iterative procedure based on the general method (clause 11.3) is presented in Figure 6.2.

All resistance factors are taken as unity while predicting the experimental results. Table 6.1 gives a comparison of the predicted and experimental ultimate loads.

Table 6.1: Experimental and predicted ultimate loads for control beams

Beam	Experimental Ultimate Load (kN)	Predicted Ultimate Load (kN)	Experimental/Predicted
1.63-L-0%	191.63	330.0*	0.58
1.63-LS-0%	418.41	330.0*	1.27
3.25-L-0%	109.5	125.0**	0.88
3.25-LS-0%	132.36	192.8**	0.69

*Predicted by strut and tie model given in CSA A23.3-04

** Predicted by general method given in CSA A23.3-04

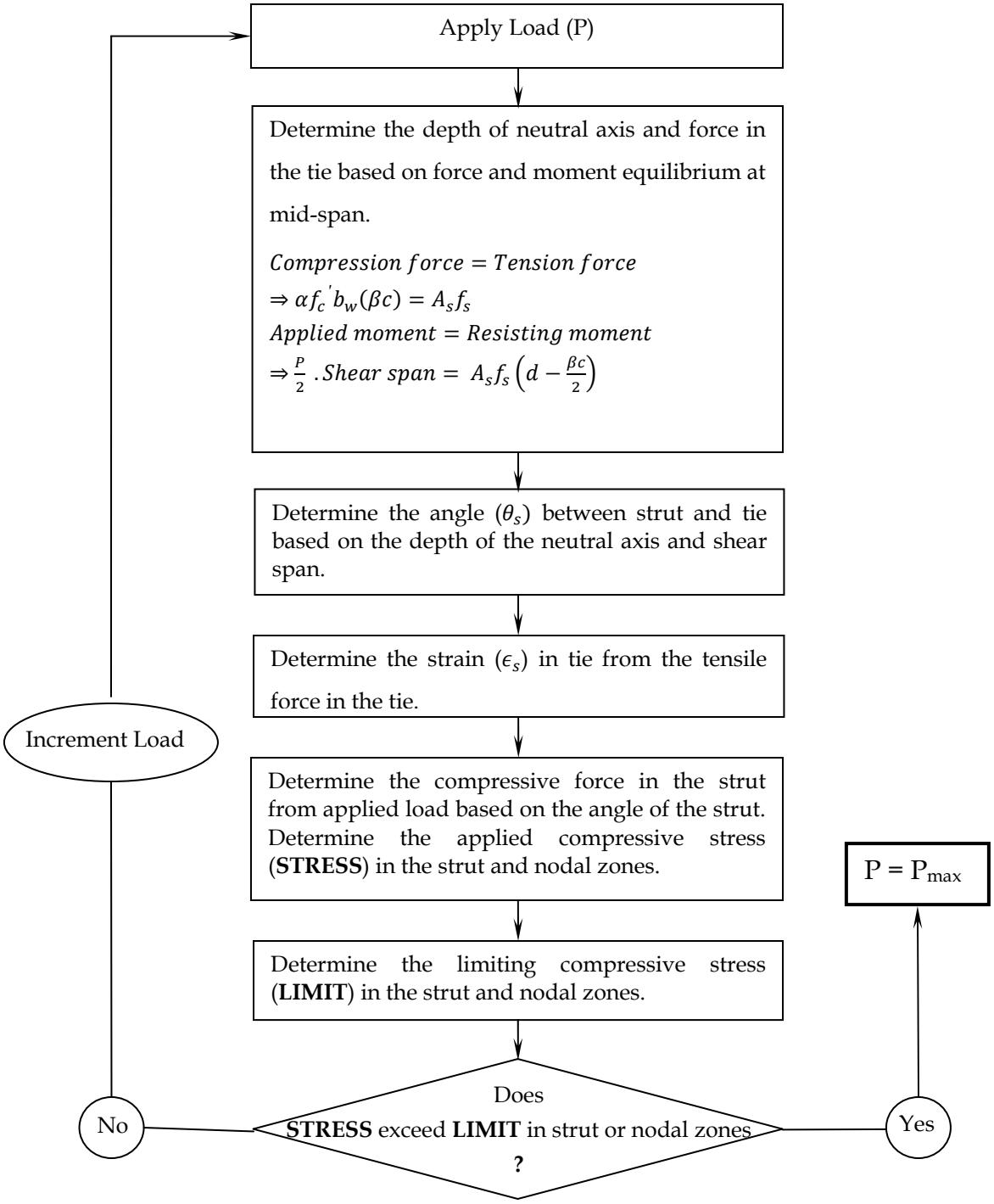

Figure 6.1: Iterative procedure developed for the struts and tie model given in CSA A23.3-04

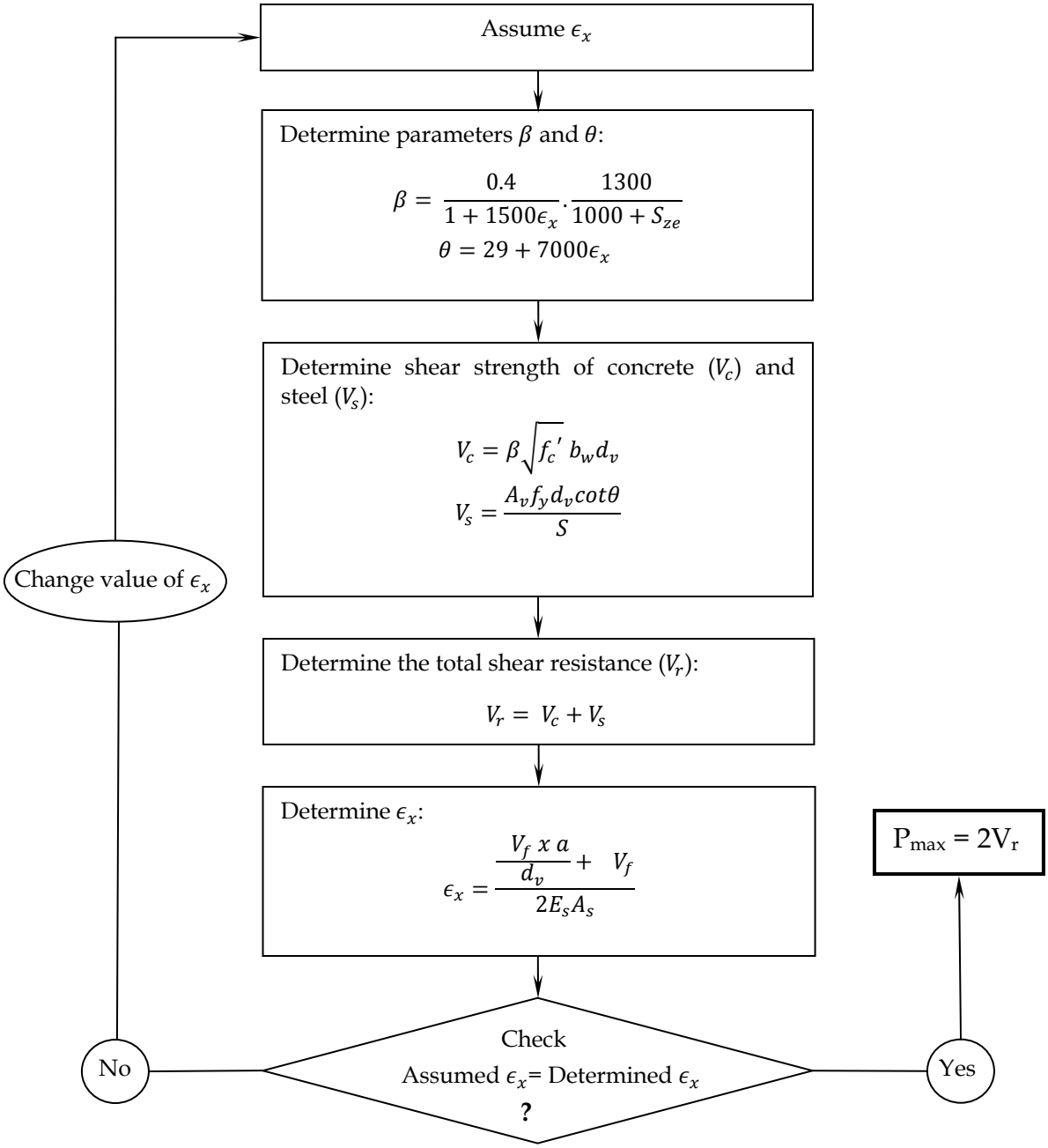

Figure 6.2: Iterative procedure developed for the general method given in CSA A23.3-04

The predicted failure load of the deep beam without stirrups (10.63-L-0%) is higher than the experimentally observed load. This difference is mainly due to the fact that the design procedure given in the struts and tie model (CSA A23.3-04) require an orthogonal grid of reinforcing bars near each face and the beam without stirrups does not satisfy this condition. The predicted failure load of the deep beam with stirrups is reasonably close to the experimental failure load as it contains the compression bars as well as the stirrups which make the design of this beam quite close to the recommended design in CSA A23.3-04. The predicted failure load of the slender beam without stirrup (3.25-L-0%) is close to the experimentally observed failure load. However, the predicted failure load of the slender beam with stirrups is higher than the experimentally observed failure load. The reason for this difference is because the stirrups were ineffective controlling the crack widths and the beam failed at the lower load. The reason for ineffectiveness of the stirrups may the spacing of stirrups, as the spacing provided was the maximum spacing allowed by CSA A23.3-94, which may not be adequate for such beams. The other reason may be the surface texture of the stirrups, as they were made from smooth bars and smooth bars may not be as effective controlling the crack width as deformed bars.

6.3 Strength Predictions of Corroded Beams

The general method (presented in section 6.2) given in CSA A23.3-04 for shear strength prediction of slender beams assumes that a perfect bond exists between the reinforcing bar and the concrete. This assumption is not valid for corroded beams since the reinforcing bar becomes unbonded as a result of corrosion.

The strut and tie model given in CSA A23.3-04 (presented in section 6.2) for shear strength prediction of deep beams does not include the effect of corrosion. The corroded deep beams failed differently in comparison to the control deep beams. The control deep beams experienced shear cracking whereas the corroded beams did not.

Therefore, for the corroded beams, two simplified strut and tie models are proposed: one for deep beams and one for slender beams.

6.3.1 Proposed Strut and Tie Model for Corroded Deep Beams

The first step is to establish the geometry of the strut and tie model. The width of the strut is based on the width of the bearing plate (loading plate and reaction plate), the neutral axis depth

and the height of the centroid of the tension reinforcement. The upper end of the strut starts from one end of the loading plate and ends at double the height of the centroid of the tension reinforcement above the reaction plate. The lower end of the strut starts from the neutral axis under the loading plate (determined from the flexural analysis) and ends at the other end of the reaction plate.

The capacity of deep beams can be determined by performing two checks using the proposed model in Figure 6.3:

- Failure due to splitting of the strut
- Failure due to yielding of the longitudinal steel reinforcement

6.3.1.1 Failure due to Splitting of the Strut

In a strut and tie model, the struts are subjected to compressive stress. The compression in the diagonal struts spread out to maintain the compatibility of the concrete causing transverse tension near the mid height of the strut. If appropriate reinforcement is not provided, the beam will fail by splitting of the strut. Failure by splitting of the strut is observed in pile caps, which act as deep beams and are typically constructed without any transverse or longitudinal reinforcement distributed over the member height (Adebar and Zhou, 1993). Adebar and Zhou (1993) recommended a stress limit of 0.6 f_c' for beams with no bearing confinement to the struts, in order to avoid the failure in deep beams by splitting of the strut. Therefore, a compressive stress limit of 0.6 f_c' is used in this study.

6.3.1.2 Failure due to Yielding of Longitudinal Steel Reinforcement

In a strut and tie model, the tie is subjected to tension. When the beam capacity is governed by the yield strength of their reinforcement, the tension force in the tie is determined by multiplying the yield stress in the reinforcing steel by the cross sectional area of reinforcing bar. Then the capacity of the beam is calculated based on equilibrium using the procedure shown in Figure 6.3. The effect of corrosion is included by reducing the area of the reinforcing bar depending on the actual mass loss. The procedure used to determine the reduced area based on actual mass loss is presented in sample calculations for proposed models in appendix-B.

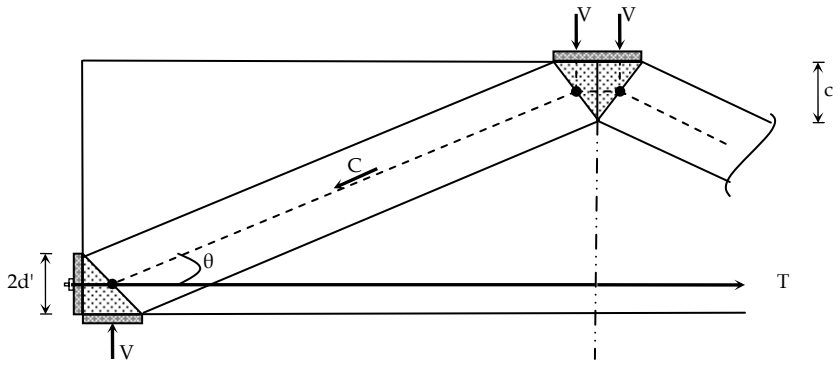

$P = 2.V$

$V = Lesser\ of \begin{cases} C\ sin\theta \\ T\ tan\theta \end{cases}$

Check-1 (Capacity based on splitting strength of concrete)

$V = C\ sin\theta$ $\qquad$ $C = (Limiting\ stress\ in\ a\ strut).(Area\ of\ strut)$

$C = \left(0.6f_c^{'}\right).(w_c\ x\ b)$

Check-2(Capacity based on yield strength of steel)

$V = T\ tan\theta$ $\qquad$ $T = A_s^{*}.F_y$

$Where$

$P = Failure\ Load$
$V = Shear\ force$
$T = Tension\ force\ in\ tie$
$C = Compression\ force\ in\ the\ strut$
$\theta = Angle\ between\ strut\ and\ Tie$
$A_s^{*} = Reduced\ cros\ sectional\ area\ of\ steel$
$F_y = Yield\ strength\ of\ steel$
$f_c^{'} = Compressive\ strength\ of\ concrete$
$w_c = Width\ of\ strut$
$b = Width\ of\ beam$
$c = Neutral\ axis\ depth$
$d^{'} = Concrete\ cover\ to\ center\ of\ the\ longitudinal\ bar$

Figure 6.3: Proposed strut and tie model for deep beams

6.3.2 Proposed Strut and Tie Model for Corroded Slender Beams

In this model, the direct strut is replaced by an arch band unlike deep beams. The first step is to establish the arch band of the tied arch. The arch trajectory, z, can be determined based on a study by Kim et al. (1998) using equation 6.1 given below:

$$z(x) = \left(\frac{x}{a}\right)^{r} jd \qquad Eq.(6.1)$$

$$r = k\left(\frac{d}{a}\right)^{n1}(\rho)^{n2} \leq 1$$

$$with\ k = 1.0\ , n1 = 0.6, and\ n2 = -0.1\ for\ beams\ with\ no\ stirrups$$

$$with\ k = 0.6\ , n1 = 1.4, and\ n2 = -0.2\ for\ beams\ with\ stirrups$$

Where x is the distance from the support; a is the shear span; r is the empirical constant; jd is the internal moment arm length based on beam theory; ρ is the steel reinforcement ratio. Equation 6.1 can be used to establish the arch band (defined by z_{upper} and z_{lower}) with known starting and ending heights. The starting height for z_{upper} at the beam end is assumed twice the height of the centroid of the tension reinforcement while the ending height under point load is assumed equal to the neutral axis depth based on flexural capacity.

The capacity of corroded slender beams is determined based on the yielding of the tie (check-1) and comparing the concrete capacity in the arch to code limits (check-2). The details of the proposed model are presented in Figure 6.4.

6.3.2.1 Check 1- Yielding of the Tie

The corrosion of longitudinal reinforcement in this study forced the slender beams to behave as a tied arch as observed in the experimental results. The load transfer in the arch was such that it caused failure by yielding of the tie. The beam failure load is determined based on the failure of the tie using the procedure given in Figure 6.4. The effect of corrosion is included by reducing the area of the reinforcing bar depending on the actual mass loss. The procedure used to determine the reduced area based on actual mass loss is presented in sample calculations for proposed models in appendix-B.

6.3.2.2 Check 2-Crushing of Concrete Arch

The capacity of the concrete arch is checked using the failure load determined based on yielding of the tie (check-1). The capacity of the concrete under the point load and the support nodes is compared with the stress limits of 0.85fc′ and 0.75 fc′ (the compressive stress limits in nodal

zones as specified in CSA A23.3-04. It is expected that the arch will not fail in the web if checks are satisfied in the nodal zone; however the capacity of the arch in the web can be checked based on the procedure developed by Ng (Ng, 2005).

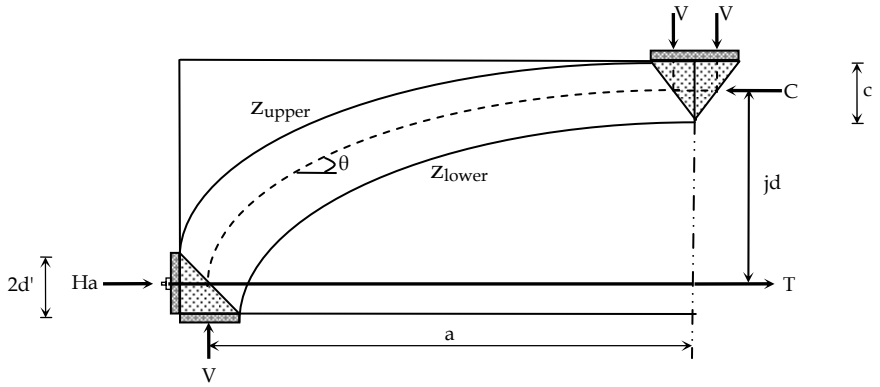

$P = 2.V$

Check-1 (Yielding of the tie):

$$H_a = \frac{V.a}{jd}$$

$$V = \frac{H_a.jd}{a} \qquad Beam\ behaving\ in\ pure\ arch,\ H_a = T$$

$$T = yield\ strength\ of\ steel\ x\ Reduced\ cross\ sectional\ area\ of\ steel$$

Check-2(Crushing of concrete arch):

Compressive stress limits in the nodal zones:

$Under\ point\ load = 0.85f_c{}'$
$Under\ support = 0.75f_c{}'$
$Where$
$P = Failure\ Load$
$V = Shear\ force$
$Ha = horizental\ thrust = T\ (for\ pure\ arch\ action)$
$T = Tension\ force\ in\ tie$
$jd = moment\ arm\ betwwen\ tension\ and\ compression$
$a = shear\ span$
$f_c{}' = Compressive\ strength\ of\ concrete$
$\theta = Angle\ of\ the\ arch\ tracjectory$
$C = Compression\ force$
$c = Neutral\ axis\ depth$
$d' = Concrete\ cover\ to\ center\ of\ the\ longitudinal\ bar$

Figure 6.4: Proposed strut and tie model for slender beams

6.3.3 Predicted Results of Corroded Beams

The ultimate strengths of the corroded beams were predicted using the proposed strut and tie models presented in Section 6.3.1 and 6.3.2. The predicted and experimental ultimate loads of the corroded beams are given in Table 6.2. The detailed calculations based on proposed models are presented in Appendix-B.

Table 6.2: Experimental and predicted ultimate loads for corroded beams

Beam		Experimental Ultimate Load (KN)	Predicted Ultimate Load (KN)	Experimental/Predicted
Series A-1	1.63-L-2.5%	459.26	404.5	1.14
	1.63-L-5.0%	476.4	404.5	1.18
	1.63-L-7.5%	476.17	404.5	1.18
Series A-2	1.63-LS-5.0%	386.17	361.1	1.07
	1.63-LS-7.5%	422.85	361.1	1.17
Series B-1	3.25-L-2.5%	206.17*	204.1	1.01
	3.25-L-5.0%	221.51*	201.6	1.10
	3.25-L-7.5%	225.21*	200.3	1.12
Series B-2	3.25-LS-2.5%	248.41	211.3	1.17
	3.25-LS-5.0%	240.51	208.8	1.15
	3.25-LS-7.5%	239.02	207.0	1.15

*beams failed by anchorage failure

The capacity of the beams that failed by anchorage was calculated assuming the anchorage was properly designed. It is evident from Table 6.2 that the predicted failure loads correlate very well with the experimental failure loads with the average correlation ratio of 1.13.

Chapter 7: Conclusions and Recommendations

7.1 General

An experimental and analytical study was performed to investigate the effect of corrosion on the behaviour of shear critical reinforced concrete deep and slender beams. The variables studied included; the level of corrosion, the existence of stirrups and FRP repair. The results demonstrated that corrosion of properly anchored longitudinal steel reinforcement does not have any adverse effect on the behaviour of shear critical reinforced concrete beams; rather it improves their behaviour. Strut and tie models were proposed to predict the ultimate load of corroded shear critical reinforced concrete deep and slender beams. The predicted results of these models correlated very well with the experimental results. The major conclusions from this study and recommendation for future work are presented in the following sections.

7.2 Experimental Conclusions

The following conclusions are made based on the experimental results.

7.2.1 Effect of Corrosion

- Corrosion of the longitudinal reinforcement changed the load transfer mechanism in shear-critical reinforced concrete beams; the corroded deep beams transferred the load from load point to the supports by pure arch action compared to a combination of beam and arch action in the control un-corroded deep beams. The corroded slender beams transferred the load from load point to support by pure arch action compared to pure beam action in the control un-corroded slender beams.
- The change in load transfer mechanism changed the failure mode of the corroded beams. The corroded deep beams failed by splitting of a compression strut compared to shear compression failure in the control un-corroded beams. The corroded slender beams failed in flexure (yielding and crushing in slender beams with stirrups and anchorage failure in slender beams without stirrups) compared to shear failure (diagonal tension failure) in the control un-corroded slender beams.
- An increase in ultimate strength was observed in all corroded beams except the deep beams with stirrups. The average increase in the ultimate strength was 150%, 100% and 84% in

deep beams without stirrups, slender beams without stirrups and slender beams with stirrups, respectively.

- Higher deflections at ultimate load in corroded beams were observed compared to the control un-corroded beams.
- Different corrosion levels had no significant effect on deep beams while an increase in ductility with increasing corrosion level was observed in corroded slender beams with stirrups.

7.2.2 Effect of Stirrups

- The existence of stirrups increased the ultimate load and deflection at ultimate load in control deep beams. No significant effect due to stirrups in corroded deep beams was observed.
- The existence of stirrups had no effect on control slender beams, but it changed the behaviour of the corroded slender beams: beams with stirrups failed by yielding of longitudinal steel compared to anchorage failure in beams without stirrups, which resulted in a higher ultimate load, higher deflection at ultimate load and higher stiffness in corroded beams.

7.2.3 Effect of FRP Repair

- The FRP repair of corroded deep beams (with and without stirrups) increased their ultimate failure load and stiffness.
- The FRP repair of corroded slender beams (without stirrups) changed the failure mode from anchorage failure in the corroded beams to yielding of longitudinal steel, which resulted in a relatively higher ultimate load, higher deflection at ultimate load and higher stiffness.
- The FRP repair of corroded slender beams (with stirrups) had no significant effect on the behaviour of these beams.

7.3 Analytical Conclusions

- The ultimate strengths of corroded shear-critical reinforced concrete deep and slender beams are predicted using proposed strut and tie models. The predicted results from these models had reasonable correlation in comparison to experimental results.

- At present, the models are only applicable to shear critical deep and slender beam (with and without stirrups) with corrosion over the full span of the beam and no corrosion in the anchorage zones.

7.4 Recommendations for Future Work

- Experimental work is needed to examine the behaviour of RC beams with corrosion of their longitudinal reinforcement in the anchorage zones, shear stirrups and combined longitudinal and shear stirrups.
- To validate the proposed models, a wide range of experimental data is needed, including the effect of different a/d ratios and corrosion induced over part of the span.
- In this study the feasibility of FRP repair of corroded beams was investigated using U-wraps. It is recommended for future studies to use full FRP wraps especially for deep beams.

Bibliography

ACI Committee 440, (2006) "State-of–the-art report on fibre reinforced polymer (FRP) reinforcement for concrete structures" ACI 440R-06, American Concrete Institute, Farmington Hills, MI., 228p.

ACI Committee 318, (2008) "Building code requirements for structural concrete" ACI 318M-08, American Concrete Institute, Farmington Hills, MI., U.S.A.

Adebar, P., and Zhou, Z., (1993) "Bearing strength of compressive struts confined by plain concrete" ACI Structural Journal, 90 (5), 534-541.

Al-Hammoud, R., (2006) " Fatique flexural behaviour of corroded reinforced concrete beams repaired with CFRP sheets" MASc Thesis, University of Waterloo, Waterloo, Ontario, Canada.

Almusallam, A. A.; Al-Gahtani, A. S.; Aziz, A. R.; and Rasheeduzzafar, (1996) "Effect of reinforcement corrosion on bond strength" Construction and Building Materials, 10(2), 123-129.

Al-Sulaimani, G. J.; Kaleemullah, M.; Basunbul, I. A.; and Rasheeduzzafar,(1990) "Influence of corrosion and cracking on bond behaviour and strength of reinforced concrete members" ACI Structural Journal, 87(2), 220-231.

ASTM G1. (1990) "Standard practice for preparing, cleaning and evaluating test specimens" ASTM International, West Conshohocken, Pa.

Azad, A.K.; Ahmad, S.; and Azher, S.A.; (2007) "Residual strength of corrosion damaged reinforced concrete beams" ACI Material Journal, 104(1), 40–47.

Bhargava, K.; Ghosh, A.K.; Mori, Y.; and Ramanujam, S., (2007) "Models for corrosion-induced bond strength degradation in reinforced concrete" ACI Structural Journal, 104 (6), 594-603.

CAN/CSA-A23.3-04, (2004)"Design of concrete structures" Canadian Standard Association, Rexdale, Ontario, Canada, 240p.

Cairns, J., (1995)"Strength in shear of concrete beams with exposed reinforcement" Proceedings of the Institution of Civil Engineers: Structures and Buildings, 110(2), 176-185.

Collins, M.P., Bentz E.C., and Sherwood, E.G., (2008) "Where is shear reinforcement required? A review of research results and design procedures" ACI Structural Journal, 105(5), 590-600.

EL Maaddawy, T. A., and Soudki, K. A., (2003) "Effectiveness of impressed current technique to simulate corrosion of steel reinforcement in concrete" Journal of Materials in Civil Engineering, ASCE, 15(3), 41-47.

EL Maaddawy, T. A., (2004) "Performance of corrosion-damaged reinforced concrete beams repaired with CFRP laminates" PhD Thesis, University of Waterloo, Waterloo, Ontario, Canada.

El-Sayed, A.K., (2006) "Concrete contribution to the shear resistance of FRP-reinforced concrete beams" PhD Thesis, University of Sherbrooke, Sherbrooke, Quebec, Canada

Fang, C.; Lundgren, K.; Chen, L.; and Zhu, C., (2004) "Corrosion influence on bond in reinforced concrete" Cement and Concrete Research, 34(11), 2159-2167

Federation Internation du Beton (fib), (2000) "Bond of Reinforcement in Concrete, State-of-Art Report" International Federation for Structural Concrete, Switzerland.

Higgins, C., and Farrow, W. C., (2006) " Tests of reinforced concrete beams with corrosion-damaged stirrups" ACI Structural Journal, 103(1),133-41.

Jeppsson, J., and Thelandersson, S., (2003)"Behavior of reinforced concrete beams with loss of bond at longitudinal reinforcement" Journal of Structural Engineering, 129(10), 1376-1383.

Kim, D., Kim, W., and White, R. N., (1998) "Prediction of reinforcement tension produced by arch action in RC beams," Journal of Structural Engineering., 124(6), 611-622.

Lee, J., and Kim, U., (2008)"Effect of longitudinal tensile reinforcement ratio and shear span to depth ratio on minimum reinforcement in beams" ACI Structural Journal, 105(2),134-144.

MacGregor, J.G., (1997) "Reinforced Concrete-Mechanics and Design" Prentice Hall International Series.

Mangat, P.S., and Elgarf, M.S., (1999) "Flexural strength of concrete beams with corroding reinforcement" ACI Structural Journal, 96(1), 149–158.

Newman, J., and Chow, B. S., (2003) "Advanced Concrete Technology: Concrete Properties, Butterworth-Heinemann" pp. 9/11.

Ouglova, A.; Berthaud, Y.; Foct, F.; Francois, M.; Ragueneau, F.; and Petre-Lazar, I., (2008) "The influence of corrosion on bond properties between concrete and reinforcement in concrete structures" Materials and Structures, 41, 969-980.

Raoof, M.,and Lin, Z., (1997)"Structural characteristics of RC beams with exposed main steel" Proceedings of the Institution of Civil Engineers: Structures and Buildings, 122(1),35-51

Regan, P. E., and Kennedy Reid, I. L., (2004)"Shear strength of RC beams with defective stirrup anchorages" Magazine of Concrete Research, 56(3),159-166.

ISIS Canada, (2007) "Reinforced concrete structures with fibre reinforced polymers" Design Manual No. 4.

Ritter, W., (1899)"Die bauweise hennebique." Schweizerische Bauzeitung, 33(7),59-61.

Rodriguez, J., Ortega, L. M., and Casal, J., (1997)"Load carrying capacity of concrete structures with corroded reinforcement" Construction and Building Materials, 11(4), 239-248.

Sherwood, E.G.; Lubell A.S.; Bentz E.C.; and Collins, M.P., (2006) "One way shear strength of thick slabs and wide beams" ACI Structural Journal, 103(6), 180-190.

Sneed, L.H., (2007) "Influence of member depth on shear strength of concrete beams" PhD Thesis, Purdue University, West Lafayette, Indiana, USA.

Ng, S., (2005) "Shear behaviour of RC beams externally prestressed with CFRP rods" MASc Thesis, University of Waterloo, Waterloo, Ontario, Canada.

Suffern, C.A., (2008) "Shear behaviour of disturbed regions in reinforced concrete beams with corrosion damaged Stirrups" MASc Thesis, University of Waterloo, Waterloo, Ontario, Canada.

Toongoenthong, K., and Maekawa, K., (2004) "Interaction of pre-induced damages along main reinforcement and diagonal shear in RC members" Journal of Advanced Concrete Technology, 2(3), 431-443.

Toongoenthong, K., and Maekawa, K., (2005)"Multi-mechanical approach to structural performance assessment of corroded RC members in shear" Journal of Advanced Concrete Technology, 3(1), 107-122.

Val, D, V., (2007)"Deterioration of strength of RC beams due to corrosion and its influence on beam reliability" Journal of Structural Engineering, 133(9), 1297-1306.

Wang, X., and Liu, X., (2003) "Bond strength modeling for corroded reinforcements" Construction and Building Material, 20, 177-186.

West, J., (1999) "Durability design of post-tensioned bridge substructures" PhD Thesis, University of Texas at Austin, Texas, USA.

Xiao-Hui, W., and Xia-La, L., (2008) "Modelling the flexural carrying capacity of corroded RC beam" Journal of Shanghai Jiaotong University, 13(2), 129–135.

Xu, S., Niu, D., (2003)"The shear behavior of corroded reinforced concrete beam" International Conference on Advances in Concrete and Structures.

Zhao, Y., Chen, J., and Jin, W., (2009)"Design of shear strengths of corroded reinforced concrete beams" International Journal of Modeling, Identification and Control,7(2),190-198.

Appendix A: Experimental Calculations

A.1 Impressed Current Calculations

The time required to corrode the reinforcing steel bars, using accelerated corrosion technique, was calculated based on Faraday's law. Faraday's law along with sample induced current calculations is presented in the following:

$$m_l = \frac{MIT}{zF}$$

$Where$

$m_l = Weight\ of\ Steel\ consumed\ (g)$

$M = The\ atomic\ weight\ of\ metal\ (56\ g\ for\ Fe)$

$I = Current\ (\ Ampares)$

$T = time\ (\ Seconds)$

$z = Inonic\ Charge\ (\ Fe \longrightarrow Fe^{+2} + 2e^{-}) = 2$

$F = Faraday's\ Constant\ = 96500\ Ampares.second$

$For\ Practical\ Purposes\ , the\ current\ density, i\ is\ used\ insted\ of\ current, I$:

$$\Rightarrow m_l = \frac{M.i.S_a.T}{zF}$$

$Where\ S_a\ is\ the\ surface\ area\ of\ the\ corroded\ steel\ and\ i\ is\ the\ current\ density\ level.$

Example:

Calculate the time required to obtain 5% mass loss in 25M bar of 1600 mm length using Faraday's law. The current density to be used is 150 $\mu A/cm^2$.

Solution:

Mass loss of the steel reinforcement:

$$m_l = \frac{M.i.S_a.T}{zF}$$

$M = 56g$

$i = 150\mu A/cm^2$

$T = time\ (\ Seconds) =?$

$z = 2$

$F = = 96500\ Ampares.second$

$S_a = \pi \; x \; D \; x \; L$

$Diameter \; of \; 25M \; bar = 25.2mm = 2.52 \; cm$

$Area \; of \; 25M \; bar = 500 \; mm^2 = 5 \; cm^2$

$S_a = \pi \; x \; D \; x \; L = \pi \; x \; 2.52 \; x \; 160 = 1266.7 \; cm^2$

Also we know

$$\%age \; Mass \; loss = \frac{Mass \; Loss \; (g)}{Original \; Mass}$$

$Mass \; Loss \; (g) = \; \%Mass \; loss \; x \; Initial \; Mass$

$Where$

$$\%\; Mass \; loss = \frac{5}{100} = 5\%$$

$$Initial \; Mass \; = Density \; x \; Volume = Density \; x \; A \; x \; L = \frac{7.85g}{cm^3} x \; 5cm^2 \; x \; 160cm = 6280 \; g$$

$$\Rightarrow \; Mass \; Loss \; (g) = m_l = \; \%\; Mass \; loss \; x \; Initial \; Mass = 0.05 \; x \; 6280 = 314 \; g$$

$Finally, substituting \; all \; values \; in \; the \; mass \; loss \; equation$:

$$m_l = \frac{M.i.S_a.T}{zF}$$

$$314 = \frac{56 \; x150 \; x \; 10^{-6} \; x \; 1267 \; x \; T}{2 \; x \; 96500}$$

$$T = 5694178 \; Seconds = 151.7 \; Hours = 65.9 \; Days$$

Appendix B: Sample Calculation for Proposed Models

B.1 Proposed Strut and Tie Model for Deep Beams

B.1.1 Deep Beams without Stirrups (1.65-L-7.5%)

The properties of deep beam without stirrups (1.65-L-7.5%) are given in Table B.1. This beam was corroded to 7.5% mass loss but actual mass loss was 4.64%.

Table B.1: Properties of beam (1.63-L-7.5%)

Cross sectional properties	Width of beam	b	150 mm
	Height of beam	H	350 mm
	Length of beam	L	1400 mm
	Depth of tension steel	d	307.5
	Depth of neutral axis	c	83.5
Material properties	Tension steel area	A_s	1000 mm^2
	Density of steel bar	ρ	7.85 g/cm^3
	Yield strength	f_y	400 MPa
	Compressive strength	f_c'	47.3 MPa

Reduction in cross sectional area of the tie due to corrosion

Tension tie is 2-25M longitudinal bars (A_s = 2 x 500 = 1000 mm^2)

$$Mass\ loss\ \ in\ one\ \ steel\ bar\ (g) = Percentage\ mass\ loss\ x\ original\ mass$$

$$= Percentage\ mass\ loss\ x\ (density\ of\ \ bar\ x\ area\ of\ \ bar\ x\ \ length)$$

$$Mass\ loss\ \ of\ one\ steel\ bar\ per\ unit\ length\ (g) = \frac{4.64}{100}\ \ x\ 7.85\ x\ 5\ x1 = 1.82g$$

$$Reduced\ mass\ \ of\ one\ bar\ per\ unit\ length(g) = Original\ mass - Mass\ loss$$

$$= (7.85\ x\ 5\ x\ 1) - 1.82 =\ \ 37.43g$$

$$Reduced\ mass\ \ of\ one\ bar\ per\ unit\ length\ (g) = Density\ of\ \ bar\ x\ reduced\ area\ x\ unit\ length$$

$$37.43 = 7.85x\ reduced\ area\ x\ 1$$

$Reduced\ area = 4.77\ cm^2 = 477\ mm^2$

$Reduced\ area\ of\ two\ steel\ bars\ acting\ as\ tie, \qquad A_s^* = 2\ x\ 477\ = 954\ mm^2$

The strut and tie for deep beams without stirrups is shown in Figure B.1.

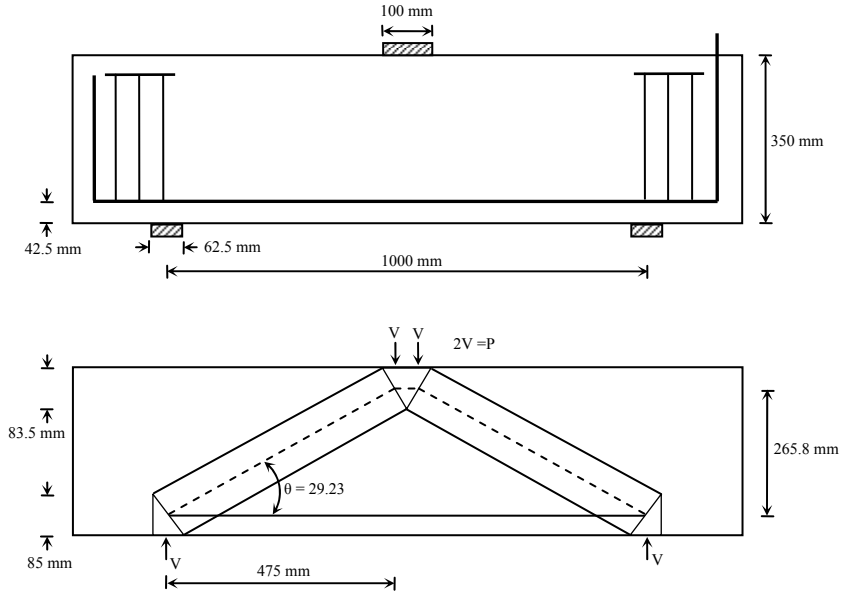

Figure B.1: Strut and Tie Model for beam 1.65-L-7.5%

The capacity of deep beams is determined by performing two checks:

Check-1: Failure due to splitting of the strut

Check-2: Failure due to yielding of the longitudinal steel reinforcement

Check-1: Capacity based on splitting strength of concrete

$V = C\ sin\theta$

$C = compressive\ force\ in\ strut = (Limiting\ stress\ in\ a\ strut)x\ (Area\ of\ strut)$

$Limiting\ stress\ in\ a\ strut = 0.6f_c^{'}$

$where\ f_c^{'} = 47.3\ MPa$

$Limiting\ stress\ in\ a\ strut = 0.6x\ 47.3 = 28.38\ MPa$

$Area\ of\ strut = \ Width\ of\ strut\ x\ width\ of\ beam$

$Where\ Width\ of\ the\ strut\ near\ load\ point = \sqrt{50^2 + 83.5^2} = 97.3\ mm$

$Width\ of\ the\ strut\ near\ reaction\ point = \sqrt{62.5^2 + 85^2} = 105.5\ mm$

$Limiting\ width\ of\ strut\ = 97.3\ mm$ and $Width\ of\ beam\ = 150\ mm$

$Area\ of\ strut = 97.3\ x\ 150 = 14595\ mm^2$

$C = 28.38x\ 14595 = 414206.1\ N = 414.2kN$

$V = C\ sin\theta\ = 414.2 \sin 29.23 = 202.26\ kN$

$Failure\ Load = P_1 = 2V = 2\ x\ 202.26 = 404.52\ kN$

Check-2: Capacity based on yield strength of concrete

$V = T\ tan\theta$

$T = Tensile\ force\ in\ tie = A_s^*.F_y$

$Where\ Fy = Yield\ strength\ of\ tie = 400\ MPa$

$A_s^* = Reduced$ cross sectional area of tie $= 954\ mm^2$

$T = 400\ x\ 954 = 381{,}600\ N = 381.6\ kN$

$V = T\ tan\theta = 381.6\ tan\ 29.23 = 213.53\ kN$

$Failure\ Load = P_2 = 2V = 2\ x\ 213.98 = 427.06\ kN$

The beam failure load is the smaller of P_1 or P_2 and is equal to 404.52 kN.

B.1.2 Deep Beams with Stirrups (1.65-LS-7.5%)

The properties of deep beam with stirrups (1.65-LS-7.5%) are given in Table B.2. This beam was corroded to 7.5% mass loss but actual mass loss was 4.49%.

Table B.2: Properties of beam (1.63-LS-7.5%)

Cross sectional properties	Width of beam	b	150 mm
	Height of beam	H	350 mm
	Length of beam	L	1400 mm
	Depth of tension steel	d	307.5 mm
	Depth of neutral axis	c	68.9* mm
Material properties	Tension steel area	A_s	1000 mm^2
	Density of steel bar	ρ	7.85 g/cm^3
	Yield strength	f_y	400 MPa
	Compressive strength	f_c'	47.3 MPa

*Depth of neutral axis is calculated including the effect 2-10M compression bars.

Reduction in cross sectional area of the tie due to corrosion

Tension tie is 2-25M longitudinal bars (A_s = 2 x 500 = 1000 mm^2)

$$Mass\ loss\ \ in\ one\ \ steel\ bar\ (g) = Percentage\ mass\ loss\ x\ original\ mass$$

$$= Percentage\ mass\ loss\ x\ (density\ of\ bar\ x\ area\ of\ bar\ x\ \ length)$$

$$Mass\ loss\ \ of\ one\ steel\ bar\ per\ unit\ length\ (g) = \frac{4.49}{100}\ \ x\ 7.85\ x\ 5\ x1 = 1.76\ g$$

$$Reduced\ mass\ \ of\ one\ bar\ per\ unit\ length(g) = Original\ mass - Mass\ loss$$

$$= (7.85\ x\ 5\ x\ 1) - 1.76 = \ 37.5g$$

$$Reduced\ mass\ \ of\ one\ bar\ per\ unit\ length\ (g) = Density\ of\ bar\ x\ reduced\ area\ x\ unit\ length$$

$$37.5 = 7.85x\ reduced\ area\ x\ 1$$

$$Reduced\ area = 4.78\ cm^2 = 478\ mm^2$$

$$Reduced\ area\ of\ two\ steel\ bars\ acting\ as\ tie = \ A_s{}^* = 2\ x\ 478\ = 956\ mm^2$$

The strut and tie for deep beams with stirrups is shown in Figure B.2.

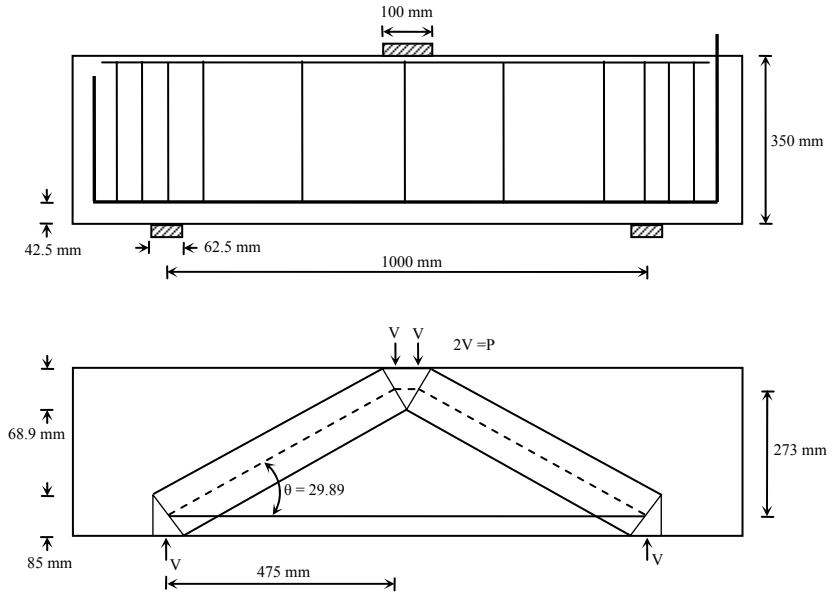

Figure B.2: Strut and Tie Model for beam 1.65-LS-7.5%

The capacity of deep beams is determined by performing two checks:

Check-1: Failure due to Splitting of the Strut

Check-2: Failure due to Yielding of the Longitudinal Steel Reinforcement

Check-1: Capacity based on splitting strength of concrete

$V = C\ sin\theta$

$C = compressive\ force\ in\ strut = (Limiting\ stress\ in\ a\ strut) x\ (Area\ of\ strut)$

$Limiting\ stress\ in\ a\ strut = 0.6 f_c{}'$

$Where\ f_c{}' = 47.3\ MPa$

$Limiting\ stress\ in\ a\ strut = 0.6x\ 47.3 = 28.38\ MPa$

$Area\ of\ strut = \ Width\ of\ strut\ x\ width\ of\ beam$

$Where\ Width\ of\ the\ strut\ near\ load\ point = \sqrt{50^2 + 68.9^2} = 85.1\ mm$

$Width\ of\ the\ strut\ near\ reaction\ point = \sqrt{62.5^2 + 85^2} = 105.5\ mm$

$Limiting\ width\ of\ strut\ = 85.1\ mm$

$Width\ of\ beam\ = 150\ mm$

$Area\ of\ strut = \ 85.1\ x\ 150 = 12765\ mm^2$

$C = 28.38x\ 12765 = 362{,}270.7\ N = 362.27kN$

$V = C\ sin\theta\ = 362.3 \sin 29.89 = 180.55\ kN$

$Failure\ Load = P_1 = 2V = 2\ x\ 180.55 = 361.1$ kN

Check-2: Capacity based on yield strength of concrete

$V = T\ tan\theta$

$T = Tensile\ force\ in\ tie = A_s^*.F_y$

$Where\ Fy = Yield\ strength\ of\ tie = 400\ MPa$

A_s^* = $Reduced$ cross sectional area of tie $= 956\ mm^2$

$T = 400\ x\ 956 = 382{,}000\ N = 382.4\ kN$

$V = T\ tan\theta = 382.4\ tan\ 29.89 = 219.80\ kN$

$Failure\ Load = P_2 = 2V = 2\ x\ 219.80 = 439.6$

The beam failure load is the smaller of P_1 or P_2 and is equal to 361.1 kN

B.2 Proposed Strut and Tie Model for Slender Beams

B.2.1 Slender Beams without Stirrups (3.25-L-7.5%)

The properties of slender beam without stirrups (3.25-L-7.5%) are given in Table B.3. This beam was corroded to 7.5% mass loss but actual mass loss was 5.78%.

Table B.3: Properties of beam (3.25-L-7.5%)

Cross sectional properties	Width of beam	b	150 mm
	Height of beam	H	350 mm
	Length of beam	L	2400 mm
	Depth of tension steel	d	307.5 mm
	Depth of neutral axis	c	83.5 mm
	Shear Span	a	1000 mm
Material properties	Tension steel area	A_s	1000 mm^2
	Density of steel bar	ρ	7.85 g/cm^3
	Yield strength	f_y	400 MPa
	Compressive strength	f_c'	47.3 MPa

Reduction in cross sectional area of the tie due to corrosion

Tension tie is 2-25M longitudinal bars (A_s = 2 x 500 = 1000 mm^2)

$$Mass\ loss\ \ in\ one\ \ steel\ bar\ (g) = Percentage\ mass\ loss\ x\ original\ mass$$

$$= Percentage\ mass\ loss\ x\ (density\ of\ bar\ x\ area\ of\ bar\ x\ \ length)$$

$$Mass\ loss\ \ of\ one\ steel\ bar\ per\ unit\ length\ (g) = \frac{5.78}{100}\ \ x\ 7.85\ x\ 5\ x1 = 2.27\ g$$

$$Reduced\ mass\ \ of\ one\ bar\ per\ unit\ length(g) = Original\ mass - Mass\ loss$$

$$= (7.85\ x\ 5\ x\ 1) - 2.27 = \ 36.98 = 37g$$

$$Reduced\ mass\ \ of\ one\ bar\ per\ unit\ length\ (g) = Density\ of\ bar\ x\ reduced\ area\ x\ unit\ length$$

$$37 = 7.85x\ reduced\ area\ x\ 1$$

$$Reduced\ area = 4.71\ cm^2 = 471\ mm^2$$

$$Reduced\ area\ of\ two\ steel\ bars\ acting\ as\ tie = \ A_s{}^* = 2\ x\ 471\ \ = 942\ mm^2$$

The strut and tie for slender beams without stirrups is shown in Figure B.3.

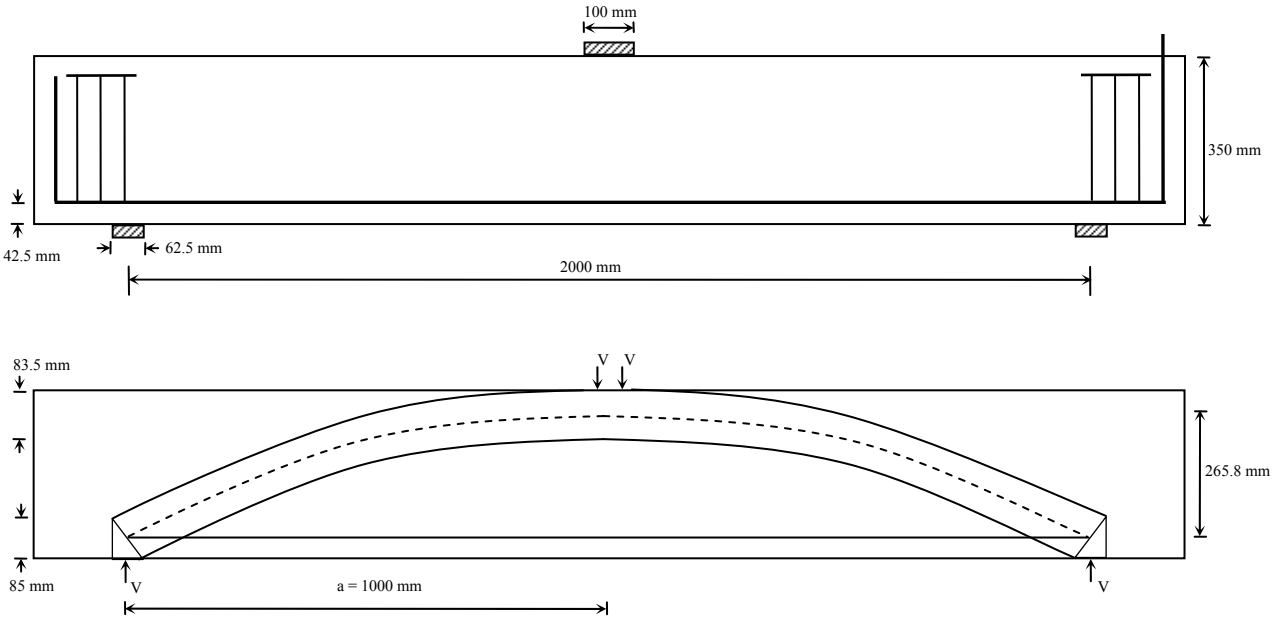

Figure B.3: Strut and Tie Model for beam 3.25-L-7.5%

The capacity of corroded slender beams is determined based on the yielding of the tie (check-1) and ensuring that the concrete capacity in the arch is below the specified code limits (check-2).

Check-1: Yielding of the tie

$$H_a = \frac{V.a}{jd} \Rightarrow V = \frac{H_a.jd}{a}$$

$jd = 265.8mm$, $a = 1000\ mm$ and $H_a = T = A_s{}^* F_y$

$Where\ F_y = Yield\ strength\ of\ tie = 400\ MPa$

$A_s{}^* =$ Reduced cross sectional area of tie $= 942\ mm^2$

$H_a = T = 400\ x\ 942 = 376{,}800\ N = 376.8\ kN$

$$V = \frac{H_a.jd}{a} = \frac{376.8\ x\ 265.8}{1000} = 100.15\ kN$$

$Failure\ Load = P = 2V = 2\ x\ 100.13 = 200.3\ kN$

Check-2: Crushing of concrete arch

The crushing of the concrete in nodal zones is checked for failure load (P) (calculated based on check-1) against the specified code limits.

Applied stress under point load = $\frac{H_a}{area\ of\ strut} = \frac{H_a}{width\ of\ beam\ x\ depth\ of\ strut} = \frac{376.8\ x\ 10^3}{150\ x\ 83.5}$

$$= 30.0\ MPa$$

Stress Limit = $0.85 f_c{}' = 0.85\ x\ 47.3 = 40.2\ MPa$

Applied Stress ≤ Limiting Stress OK

Applied stress in nodal zones at support = $\frac{\sqrt{{H_a}^2+V^2}}{area\ of\ strut} = \frac{\sqrt{(376.8\ x\ 10^3)^2+(100.15\ x\ 10^3)^2}}{150\ x\ \sqrt{62.5^2+85^2}}$

$$= \frac{389.88\ x\ 10^3}{150\ x\ 105.5} = 24.6\ MPa$$

Stress Limit = $0.85 f_c{}' = 0.75\ x\ 47.3 = 35.4\ MPa$

Applied Stress ≤ Limiting Stress OK

The capacity of the concrete arch is lower than the specified code limits and the beam failure is due to yielding of the tie with a failure load of 200.3 kN.

B.2.2 Slender Beams with Stirrups (3.25-LS-7.5%)

The properties of slender beam with stirrups (3.25-LS-7.5%) are given in Table B.4. This beam was corroded to 7.5% mass loss but actual mass loss was 5.22%.

Table B.4: Properties of beam (3.25-LS-7.5%)

Cross sectional properties	Width of beam	b	150 mm
	Height of beam	H	350 mm
	Length of beam	L	2400 mm
	Depth of tension steel	d	307.5 mm
	Depth of neutral axis	c	68.9* mm
	Shear Span	a	1000 mm
Material properties	Tension steel area	A_s	1000 mm^2
	Density of steel bar	ρ	7.85 g/cm^3
	Yield strength	f_y	400 MPa
	Compressive strength	f_c'	47.3 MPa

* Depth of neutral axis is calculated including the effect 2-10M compression bars.

Reduction in cross sectional area of the tie due to corrosion

Tension tie is 2-25M longitudinal bars (A_s = 2 x 500 = 1000 mm^2)

$$Mass\ loss\ \ in\ one\ \ steel\ bar\ (g) = Percentage\ mass\ loss\ x\ original\ mass$$

$$= Percentage\ mass\ loss\ x\ (density\ of\ bar\ x\ area\ of\ bar\ x\ \ length)$$

$$Mass\ loss\ \ of\ one\ steel\ bar\ per\ unit\ length\ (g) = \frac{5.22}{100}\ \ x\ 7.85\ x\ 5\ x1 = 2.05\ g$$

$$Reduced\ mass\ \ of\ one\ bar\ per\ unit\ length(g) = Original\ mass - Mass\ loss$$

$$= (7.85\ x\ 5\ x\ 1) - 2.05 = \ 37.2\ g$$

$$Reduced\ mass\ \ of\ one\ bar\ per\ unit\ length\ (g) = Density\ of\ bar\ x\ reduced\ area\ x\ unit\ length$$

$$37.2 = 7.85x\ reduced\ area\ x\ 1$$

$$Reduced\ area = 4.74\ cm^2 = 474\ mm^2$$

$$Reduced\ area\ of\ two\ steel\ bars\ acting\ as\ tie = \ A_s{}^* = 2\ x\ 474\ \ = 948\ mm^2$$

The strut and tie for slender beams with stirrups is shown in Figure B.4.

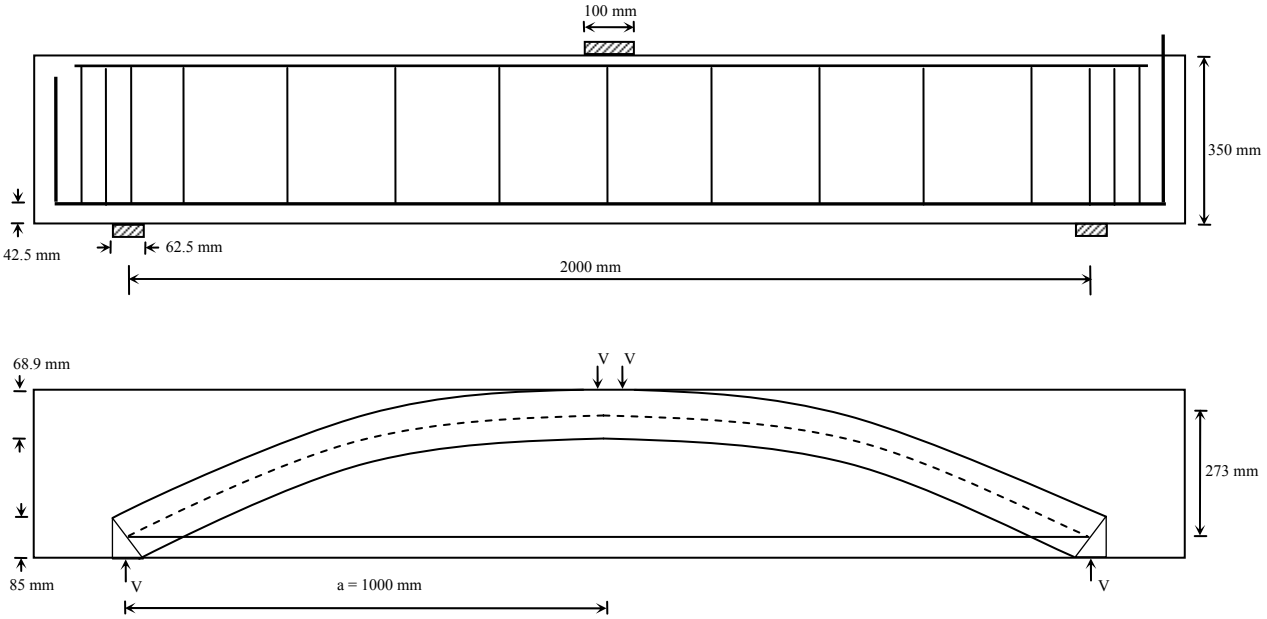

Figure B.4: Strut and Tie Model for beam 3.25-LS-7.5%

The capacity of corroded slender beams is determined based on the yielding of the tie (check-1) and ensuring that the concrete capacity in the arch is below the specified code limits (check-2).

Check-1: Yielding of the tie

$$H_a = \frac{V.a}{jd} \Rightarrow V = \frac{H_a.jd}{a}$$

$$jd = 273\ mm\ , a = 1000\ mm\ and\ H_a = T = \mathrm{A_s}^{*}\ F_y$$

$$Where\ F_y = Yield\ strength\ of\ tie = 400\ MPa$$

$\mathrm{A_s}^{*} =$ *reduced* cross sectional area of tie $= 948\ mm^2$

$$H_a = T = 400\ x\ 948 = 379{,}200\ N = 379.2\ kN$$

$$V = \frac{H_a.jd}{a} = \frac{379.2\ x\ 273}{1000} = 103.52\ kN$$

$$Failure\ Load = P_1 = 2V = 2\ x\ 103.52 = 207.04\ kN$$

Check-2: Crushing of concrete arch

The crushing of the concrete in nodal zones is checked for failure load (P) (calculated based on check-1) against the specified code limits.

Applied stress under point load = $\frac{H_a}{area\ of\ strut} = \frac{H_a}{width\ of\ beam\ x\ depth\ of\ strut} = \frac{379.2\ x\ 10^3}{150\ x\ 68.9}$

$$= 36.69\ MPa$$

Stress Limit = $0.85 f_c{}' = 0.85\ x\ 47.3 = 40.2\ MPa$

Applied Stress ≤ Limiting Stress OK

Applied stress in nodal zones at support = $\frac{\sqrt{{H_a}^2+V^2}}{area\ of\ strut} = \frac{\sqrt{(379.2\ x\ 10^3)^2+(103.52\ x\ 10^3)^2}}{150\ x\ \sqrt{62.5^2+85^2}}$

$$= \frac{393.08\ x\ 10^3}{150\ x\ 105.5} = 24.84\ MPa$$

Stress Limit = $0.85 f_c{}' = 0.75\ x\ 47.3 = 35.475\ MPa$

Applied Stress ≤ Limiting Stress OK

The capacity of the concrete arch is lower than the specified code limits and the beam failure is due to yielding of tie with a failure load of 207.04 kN.